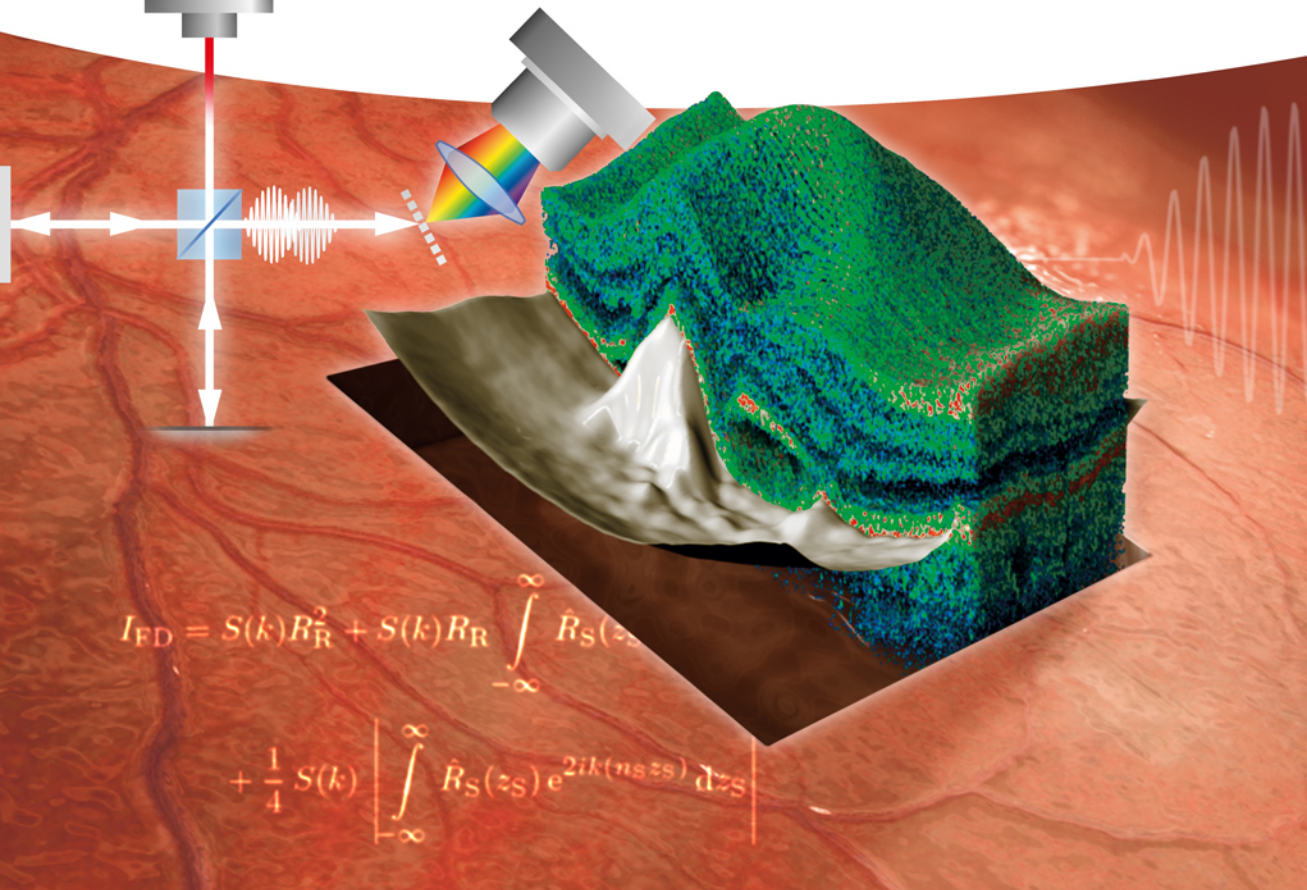


Michael Kaschke, Karl-Heinz Donnerhacke  
and Michael Stefan Rill

Layout by Kerstin Willnauer

# Optical Coherence Methods for Three-Dimensional Visualization and Structural Analysis



## Contents

### **P7 Optical Coherence Methods for 3D Visualization and Structural Analysis** 1

- P7.1 Coherence time 1
- P7.2 Autocorrelation function, spectral density, and coherence length 3
- P7.3 Swept-source OCT 28
- P7.4 Group velocity delay 30
- P7.5 Theory of TD-OCT 32
- P7.6 Theory of FD-OCT 34
- P7.7 Theory of FD-OCT 36
- P7.8 Theory of SS-OCT 45
- P7.9 Group velocity dispersion in OCT 56
- P7.10 Signal-to-noise ratio 64
- P7.11 Light sources for OCT 70
- P7.12 Optical and acoustic biometry 75
- P7.13 Intraocular lens formula 78
- P7.14 Intraocular lens power determination with biometry 79
- P7.15 Polarization-sensitive OCT 81
- P7.16 Doppler OCT 81
- P7.17 Spectroscopic OCT 83

**P7.1**
**Coherence time**

Derive the coherence length of a Gaussian pulse of spectral bandwidth  $\Delta\omega$ . Express it also in terms of  $\lambda_0$  and  $\Delta\lambda$ . Compare this to the pulse duration or the product of pulse duration and speed of light. Use the coherence length of a superluminescence diode (see e.g. [30, 32]). What differences do you notice?

**Solution:**

The intensity of a Gaussian spectrum reads

$$\sigma(\omega) = \sigma_0 \exp\left(-4 \ln(2) \left(\frac{\omega - \omega_0}{\Delta\omega_{\text{FWHM}}}\right)^2\right). \quad (7.35)$$

At the spectral width  $\omega = \Delta\omega_{\text{FWHM}}/2 \pm \omega_0$ , the intensity is reduced by half of its maximum value. For simplicity, we set  $\omega_0 = 0$  and obtain the autocorrelation function as the inverse Fourier transform of the intensity spectrum of the pulse given by

$$\begin{aligned} \mathcal{G}(\Delta t) &= \frac{1}{2\pi} \int_{-\infty}^{+\infty} \sigma_0 \exp\left(-4 \ln(2) \left(\frac{\omega}{\Delta\omega_{\text{FWHM}}}\right)^2\right) e^{-i\omega\Delta t} d\omega \\ &= \frac{1}{2\pi} \int_{-\infty}^{+\infty} \sigma_0 \exp\left(-\frac{4 \ln(2)}{\Delta\omega_{\text{FWHM}}^2} \left(\omega + i \frac{\Delta\omega_{\text{FWHM}}^2 \Delta t}{8 \ln(2)}\right)^2\right) \\ &\quad \cdot \exp\left(-\frac{\Delta\omega_{\text{FWHM}}^2 \Delta t^2}{16 \ln(2)}\right) d\omega \\ &= \frac{\Delta\omega_{\text{FWHM}}}{4\sqrt{\pi \ln(2)}} \mathcal{S}_0 \exp\left(-\frac{\Delta\omega_{\text{FWHM}}^2 \Delta t^2}{16 \ln(2)}\right). \end{aligned}$$

In the last step, we used the relation

$$\int_{-\infty}^{+\infty} e^{-a^2 x^2} dx = \frac{\sqrt{\pi}}{a} \quad \text{with}$$

$$a^2 = \frac{4 \ln(2)}{\Delta\omega_{\text{FWHM}}^2}.$$

The autocorrelation function is thus also a Gaussian function. The coherence time is defined as the time within which the autocorrelation function is reduced to half of its

maximum value, that is, for

$$\Delta t = \frac{t_c}{2} ,$$

$$\mathcal{G}\left(\frac{t_c}{2}\right) = \frac{1}{2}\mathcal{G}_0 = \frac{1}{2}\left(\frac{\Delta\omega_{\text{FWHM}}}{\sqrt{4\pi\ln(2)}}\sigma_0\right) .$$

Accordingly, we have

$$\begin{aligned} \exp\left(-\frac{\Delta\omega_{\text{FWHM}}^2 t_c^2}{4 \cdot 16 \ln(2)}\right) &= \frac{1}{2} & (S7.1) \\ \Rightarrow \frac{\Delta\omega_{\text{FWHM}}^2 t_c^2}{4 \cdot 16 \ln(2)} &= \ln(2) \\ \Rightarrow t_c &= \frac{8 \ln(2)}{\Delta\omega_{\text{FWHM}}} . \end{aligned}$$

With  $\omega_0 = 2\pi c/\lambda_0$  and  $|\Delta\omega_{\text{FWHM}}| = 2\pi c\lambda_{\text{FWHM}}/\lambda_0^2$ , the coherence length thus follows as

$$L_c = ct_c = \frac{8 \ln(2) c}{\Delta\omega_{\text{FWHM}}} = \frac{4 \ln(2)}{\pi} \frac{\lambda_0^2}{\Delta\lambda_{\text{FWHM}}} . \quad (S7.2)$$

The intensity of a Gaussian bandwidth-limited pulse is given by the squared inverse Fourier transform of the amplitude spectrum of the pulse. Thus, it is similar (but not identical) to the autocorrelation function and given by

$$I(t) = I_0 \exp\left(-\frac{\Delta\omega_{\text{FWHM}}^2 t^2}{4 \ln(2)}\right) .$$

The pulse duration again is defined by  $I(t_p) = I_0/2$  at its full width at half maximum (FWHM). In analogy to the above consideration in Eq. (S7.1), we have

$$\begin{aligned} \exp\left(-\frac{\Delta\omega_{\text{FWHM}}^2 t_p^2}{4 \cdot 4 \ln(2)}\right) &= \frac{1}{2} \\ \Rightarrow t_p &= \frac{4 \ln(2)}{\Delta\omega_{\text{FWHM}}} . \end{aligned}$$

This shows that for Gaussian pulses the pulse duration is half the coherence length.

Next, we want to calculate the values for a specific source. In Figure S7.1, the data sheet and the intensity spectrum of the superluminescence diode SLD1325 (<http://www.thorlabs.de>) are shown. From the application sheet we can calculate a specified coherence length of 20  $\mu\text{m}$ .

If we use Eq. (7.2) to calculate the coherence length (assuming a Gaussian shape of the spectrum), we obtain with  $\lambda_0 = 1325 \text{ nm}$  and  $\Delta\lambda_{\text{FWHM}} = 100 \text{ nm}$

$$L_c = ct_c = \frac{4 \ln(2)}{\pi} \frac{\lambda_0^2}{\Delta\lambda_{\text{FWHM}}} = 16 \mu\text{m}$$

which comes pretty close to the specified value.

SPECIFICATIONS	
Central Wavelength	1325 nm
Bandwidth (FWHM)	>100 nm
Fiber-Coupled Power	>10 mW
SLD Injection Current (Max)	780 mA
Voltage (Max)	4 V
Operating Temperature Range	0 – 40 °C
Isolation of Integrated Isolator	>30 dB
Fiber Pigtail	SMF-28e+
Fiber Length	-1 m
Fiber Connector	FC/APC
Return Loss of FC/APC Connector	>50 dB
Thermoelectric Cooler Current (Max)	4 A
Thermoelectric Cooler Voltage (Max)	4 V
Thermistor Resistance*	10 kΩ

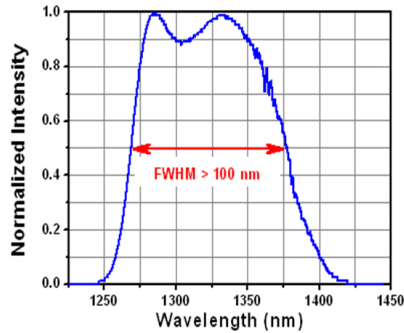


**Figure S7.1** Data sheet and intensity spectrum for the superluminescence diode SLD1325.

## P7.2

### Autocorrelation function, spectral density, and coherence length

Calculate the autocorrelation function  $\mathcal{G}$ , the spectral density  $\sigma(\omega)$ , and coherence length  $L_c$  for various pulse forms and spectral distributions:

1. Gaussian pulse
2. Rectangle pulse
3. Lorentz spectrum
4.  $\text{sech}^2$  pulse

Use the definitions for  $\mathcal{G}(\Delta t)$  and  $\sigma(\omega)$  as given in Eqs. (A111) and (A109), respectively. For the coherence length as well as the spectral density use appropriate definitions, such as the full width at half maximum (FWHM), second momentum of a normalized function, or second momentum of a squared normalized function.

### Solution:

#### a) Basic understanding of coherence length:

Before we discuss the various pulse shapes, we take a look at the possible definitions for the coherence length. The same various definitions can be applied to the pulse duration. Typically, one uses the definition of full width at half maximum (FWHM), a concept which works well if the pulse's energy distribution is fairly "localized" around a maximum. The concept fails for instance in cases where the pulses have substructures and/or substantial energy lies in the outside "wings" of the pulse. For this, other definitions need to be considered.

A simple picture for the definition of the axial length of coherence can be derived from Figure S7.2. Here, two monochromatic plane waves are considered with slightly different wavelengths  $\lambda_1$  and  $\lambda_2$ , where  $\Delta\lambda = \lambda_1 - \lambda_2 \ll \lambda_{1,2}$ . The resulting

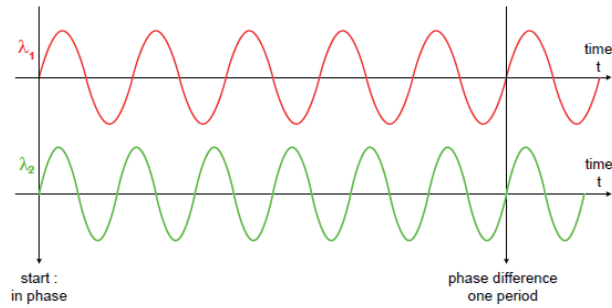


**Figure S7.2** Two waves with different wavelengths. The time after which the phase difference corresponds to one period is marked.

modulation of the superposition has a characteristic length  $L_c$  if one of the waves has exactly one more period. The traveling time for this distance corresponds to the time of axial coherence  $t_c$ . We have

$$\begin{aligned}
 L_c &= N_1 \lambda_1 = N_2 \lambda_2 = (N_1 + 1) \lambda_2 \\
 \Rightarrow N_1 (\lambda_1 - \lambda_2) &= \lambda_2, \\
 N &= \frac{\lambda}{\Delta \lambda}, \\
 \Delta \nu &= \frac{c}{\lambda^2} \Delta \lambda, \\
 L_c = N \lambda &= \frac{\lambda^2}{\Delta \lambda} = \frac{c}{\Delta \nu},
 \end{aligned}$$

where  $N$  is the number of periods. Hence, our main finding is that the coherence time is inverse to the spectral width:

$$t_c = \frac{L_c}{c} = \frac{1}{\Delta \nu}.$$

In a generalization of the above picture, we can write

$$t_c = \text{bwp} \cdot \frac{1}{\Delta \nu},$$

in which the proportionality factor  $\text{bwp}$  is called the coherence time-bandwidth product. This factor depends on the shape/spectral distribution (width) of the pulse and is of the order of 1.

**b) Definitions of the coherence time:**

Next, we want to calculate the coherence time of a Gaussian pulse. For this purpose, let us consider a Gaussian pulse with some temporal width  $t_p$ . It can be described by a (complex) field amplitude

$$E(t, t_p) = E_0 \cdot e^{-\left(\frac{t}{t_p}\right)^2 - i\omega t - i\varphi(t)}$$

or by the intensity

$$I(t, t_p) = I_0 \cdot e^{-2\left(\frac{t}{t_p}\right)^2} .$$

Note that the temporal width  $t_p$  is not the pulse duration at FWHM. We will address the difference later. According to Eq. (A111), the normalized coherence function then becomes

$$\mathcal{G}(\Delta t) = \langle E^*(t) \cdot E(t + \Delta t) \rangle_\tau = e^{-\frac{1}{2}\left(\frac{\Delta t}{t_p}\right)^2} .$$

in the case of  $\varphi(t) = \text{const.}$  With Eq. (A112), the normalized power spectral density can be determined via

$$\sigma(\nu) = \int_{-\infty}^{+\infty} \mathcal{G}(\Delta t) \cdot e^{i2\pi\nu\Delta t} d\Delta t = e^{-2\pi^2\nu^2 t_p^2} .$$

The coherence time of a pulse can now be defined in several ways. All of these definitions apply different criteria and deliver results with considerably different absolute values corresponding to the criterion.

1. Mean value of the normalized coherence function<sup>1)2)3)</sup>:

$$t_c = \int_{-\infty}^{+\infty} |\mathcal{G}(\Delta t)|^2 d\Delta t = \sqrt{\pi} \cdot t_p = 1.772 \cdot t_p .$$

2. Second momentum of the square of the normalized coherence function<sup>2)3)4)</sup>:

$$t_c = \sqrt{\frac{\int_{-\infty}^{+\infty} \Delta t^2 \cdot |\mathcal{G}(\Delta t)|^2 d\Delta t}{\int_{-\infty}^{+\infty} |\mathcal{G}(\Delta t)|^2 d\Delta t}} = \frac{t_p}{\sqrt{2}} = 0.707 \cdot t_p .$$

3. Second momentum of the absolute value of the normalized coherence function<sup>2)</sup>:

$$t_c = \sqrt{\frac{\int_{-\infty}^{+\infty} \Delta t^2 \cdot |\mathcal{G}(\Delta t)| d\Delta t}{\int_{-\infty}^{+\infty} |\mathcal{G}(\Delta t)| d\Delta t}} = t_p .$$

4. FWHM of the normalized coherence function:

$$\exp\left(-\frac{1}{2}\left(\frac{t_c}{2t_p}\right)^2\right) = \frac{1}{2}$$

$$\Rightarrow t_c = 2\sqrt{2\ln 2} \cdot t_p = 2.354 \cdot t_p .$$

1) Saleh, B.E.A and Teich, M.C. (2007) *Fundamentals of Photonics*, John Wiley & Sons, Inc.

2) Mandel, L. and Wolf, E. (1995) *Optical Coherence and Quantum Optics*, Cambridge University Press.

3) Perina, J. (1971) *Coherence of Light*, Van Nostrand Reinhold.

5. FWHM of the squared normalized coherence function<sup>4)</sup>:

$$\exp\left(-\left(\frac{t_c}{2t_p}\right)^2\right) = \frac{1}{2}$$

$$\Rightarrow t_c = 2\sqrt{\ln 2} \cdot t_p = 1.662 \cdot t_p .$$

6. First momentum / average of the normalized coherence function<sup>5)</sup> (notice the begin of the integration interval in comparison to the other definitions):

$$t_c = \frac{\int_0^{+\infty} \Delta t \cdot |\mathcal{G}(\Delta t)| d\Delta t}{\int_0^{+\infty} |\mathcal{G}(\Delta t)| d\Delta t} = \sqrt{\frac{2}{\pi}} \cdot t_p = 0.798 \cdot t_p .$$

**c) Definitions of the spectral width:**

In an analogous way, it is possible to define the spectral width. This is also somewhat arbitrary and can be formulated in different ways via the power spectral density.

A.  $1/e^2$  threshold of power spectral density:

$$\exp\left(-2\pi^2 t_p^2 \left(\frac{\Delta\nu}{2}\right)^2\right) = e^{-2}$$

$$\Rightarrow \Delta\nu = \frac{2}{\pi} \cdot \frac{1}{t_p} = 0.637 \cdot \frac{1}{t_p} .$$

B. FWHM threshold of power spectral density<sup>5)</sup>:

$$\exp\left(-2\pi^2 t_p^2 \left(\frac{\Delta\nu}{2}\right)^2\right) = \frac{1}{2}$$

$$\Rightarrow \Delta\nu = \frac{\sqrt{2\ln 2}}{\pi} \cdot \frac{1}{t_p} = 0.3748 \cdot \frac{1}{t_p} .$$

C. Definition as second momentum<sup>2)3)</sup>:

$$\Delta\nu = \sqrt{\frac{\int_{-\infty}^{+\infty} \nu^2 \cdot |\sigma(\nu)|^2 d\nu}{\int_{-\infty}^{+\infty} |\sigma(\nu)|^2 d\nu}} = \frac{1}{2\pi\sqrt{2}t_p} = \frac{0.133}{t_p} .$$

4) Diels, J.-C. and Rudolph, W. (2006) *Ultrashort Laser Pulse Phenomena: Fundamentals, Techniques, and Applications on a Femtosecond Time Scale*, Academic Press, 2nd edn.

5) Weiner, A.M. (2009) *Ultrafast Optics*, John Wiley & Sons Inc.

#### d) The bandwidth product:

Corresponding to the above definitions of the coherence time and spectral width, the bandwidth product  $\Delta\nu t_c$  can take the values listed in Table S7.1. The bandwidth products for all pulse shapes are obtained by eliminating the arbitrarily chosen temporal width  $t_p$  from the expressions for the spectral width and the coherence time. The bandwidth product is thus a characteristic value for each pulse shape. In Table S7.1, we highlight the most commonly used combination, that is, the FWHM definition for both coherence time and bandwidth. We will also apply this in the following considerations of various pulse shapes.

**Table S7.1** Various definitions of the coherence time  $t_c$  and the spectral width  $\Delta\nu$ .

	Definition of spectral width	A	B	C
Def. of coher. time		$\Delta\nu = \frac{2}{\pi} \frac{1}{t_p}$	$\Delta\nu = \frac{\sqrt{2\ln 2}}{\pi t_p}$	$\Delta\nu = \frac{1}{2\pi\sqrt{2} t_p}$
1	$t_c = \sqrt{\pi} t_p$	$2\sqrt{\pi} = 3.545$	$\sqrt{2\pi \ln 2} = 2.087$	$\frac{1}{2\sqrt{2\pi}} = 0.199$
2	$t_c = t_p/\sqrt{2}$	$\sqrt{2}/\pi = 0.450$	$\sqrt{\ln 2}/\pi = 0.265$	$\frac{1}{4\pi} = 0.0796$
3	$t_c = t_p$	$2/\pi = 0.637$	$\frac{\sqrt{2\ln 2}}{\pi} = 0.375$	$\frac{1}{2\pi\sqrt{2}} = 0.113$
4	$t_c = 2\sqrt{2\ln 2} t_p$	$\frac{4\sqrt{2\ln 2}}{\pi} = 1.499$	$\frac{4\ln 2}{\pi} = 0.883$	$\frac{1}{\pi} \sqrt{\ln 2} = 0.265$
5	$t_c = 2\sqrt{\ln 2} t_p$	$\frac{2\sqrt{\ln 2}}{\pi} = 0.530$	$\frac{2\sqrt{2}\ln 2}{\pi} = 0.624$	$\frac{1}{\pi} \sqrt{\frac{\ln 2}{2}} = 0.187$
6	$t_c = \sqrt{\frac{2}{\pi}} t_p$	$(2/\pi)^{\frac{3}{2}} = 0.508$	$\frac{2\sqrt{\ln 2}}{\pi\sqrt{\pi}} = 0.299$	$\frac{1}{2\pi\sqrt{\pi}} = 0.0598$

We now look at the influence of the pulse shape on the coherence time and the bandwidth product. For this purpose, we only use the definitions 4 and B (FWHM), as this is most commonly used and most convenient. It is also sufficient for the applications dealt within in the book. In the following, we sketch the calculation of the autocorrelation function  $\mathcal{G}(\Delta t)$  and the spectral density  $\sigma(\omega)$  of various functions (Figure S7.3) as given in Eqs. (A111) and (A109).

#### 1. Gaussian pulse envelope:

The field of a Gaussian pulse (blue curve in Figure S7.3a) is given by

$$E(t) = E_0 \exp\left(-2\ln(2) \left(\frac{t}{\Delta\tau_{\text{FWHM}}}\right)^2\right) = E_0 \exp\left(-\left(\frac{t}{t_p}\right)^2\right) \quad (\text{S7.3a})$$

and its intensity (Figure S7.3b) by

$$I(t) = I_0 \exp\left(-4\ln(2) \left(\frac{t}{\Delta\tau_{\text{FWHM}}}\right)^2\right) = I_0 \exp\left(-2 \left(\frac{t}{t_p}\right)^2\right) . \quad (\text{S7.3b})$$

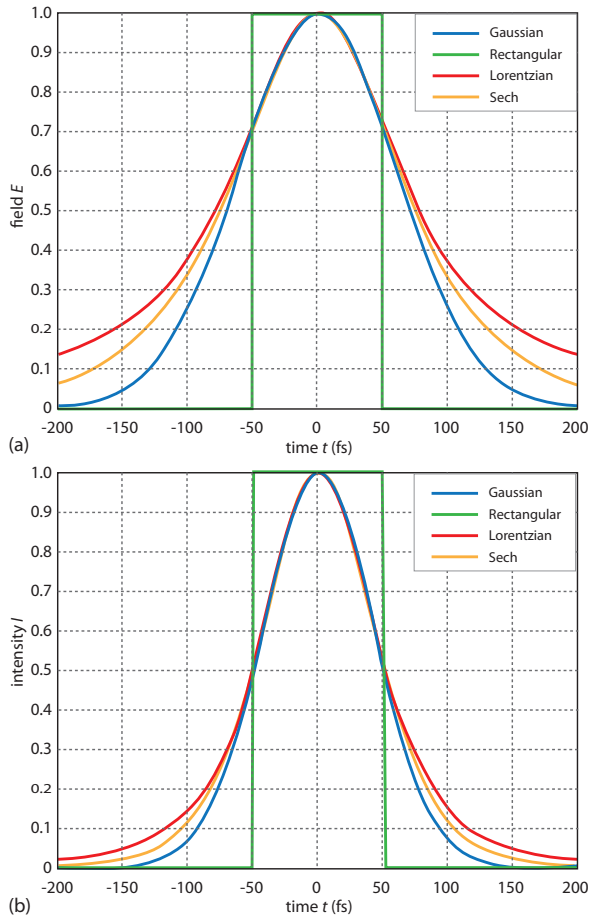


Figure S7.3 (a) Field plots and (b) intensity plots for various pulse shapes.

From Eq. (S7.3), we obtain  $\Delta\tau_{\text{FWHM}} = \sqrt{2 \ln 2} t_p = 1.1774 t_p$ . For the auto-correlation function<sup>6)</sup>, we then find

$$\begin{aligned}
 \mathcal{G}(\Delta t) &= \int_{-\infty}^{+\infty} E(t)E(t + \Delta t)dt \\
 &= E_0^2 \int_{-\infty}^{+\infty} \exp \left[ -2 \ln(2) \left( \frac{t}{\Delta\tau_{\text{FWHM}}} \right)^2 \right] \exp \left[ -2 \ln(2) \left( \frac{t + \Delta t}{\Delta\tau_{\text{FWHM}}} \right)^2 \right] dt \\
 &= E_0^2 \int_{-\infty}^{+\infty} \exp \left[ -\frac{2 \ln(2)}{\Delta\tau_{\text{FWHM}}^2} (t^2 + (t + \Delta t)^2) \right] dt \\
 &= E_0^2 \exp \left( -\frac{\ln(2)}{\Delta\tau_{\text{FWHM}}^2} \Delta t^2 \right) \int_{-\infty}^{+\infty} \exp \left( -\frac{4 \ln(2)}{\Delta\tau_{\text{FWHM}}^2} \left( t + \frac{1}{2} \Delta t \right)^2 \right) dt \\
 &= \frac{\Delta\tau_{\text{FWHM}}}{2} \sqrt{\frac{\pi}{\ln(2)}} E_0^2 \exp \left( -\frac{\ln(2)}{\Delta\tau_{\text{FWHM}}^2} \Delta t^2 \right) \\
 &= \mathcal{G}_0 \exp \left( -\frac{\ln(2)}{\Delta\tau_{\text{FWHM}}^2} \Delta t^2 \right) . \tag{S7.4}
 \end{aligned}$$

The autocorrelation function of a Gaussian function (Figure S7.4a), also called the temporal coherence function, is still a Gaussian. For a temporal width  $t_c$  (full width at half maximum of the autocorrelation; also called the coherence time), the intensity decreases to half of its maximum value. Accordingly, we have

$$-\ln(2) = -\frac{\ln(2)}{\Delta\tau_{\text{FWHM}}^2} \left( \frac{t_c}{2} \right)^2 . \tag{S7.5}$$

This implies that

$$\frac{1}{\Delta\tau_{\text{FWHM}}^2} = \frac{4}{t_c^2}$$

and that the coherence time and coherence length are given by

$$\begin{aligned}
 t_c &= 2 \Delta\tau_{\text{FWHM}} \quad \text{and} \\
 L_c &= ct_c = 2c \Delta\tau_{\text{FWHM}} ,
 \end{aligned}$$

respectively. The spectral density is defined as the Fourier transform of the intensity autocorrelation  $\mathcal{G}(\Delta t)$  as has been used in Problem P7.1 and which holds in

- 6) Please note that we consider the autocorrelation function of the field and *not* the intensity autocorrelation, which is often confused in literature:

$$\mathcal{G}(\Delta t) = \int_{-\infty}^{+\infty} E(t)E(t + \Delta t)dt \quad \text{versus} \quad \text{IAC}(\Delta t) = \int_{-\infty}^{+\infty} I(t)I(t + \Delta t)dt .$$

. For further information, we refer to Appendix 5.

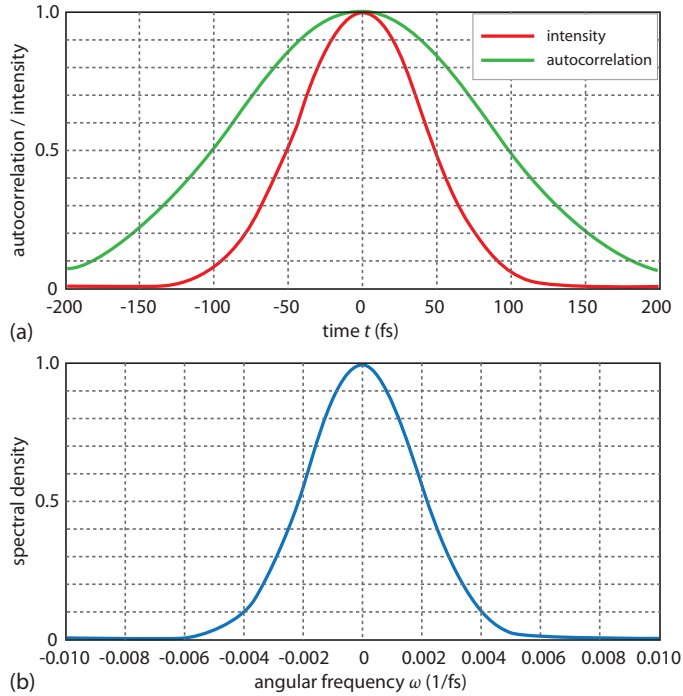


**Figure S7.4** (a) Intensity (red), autocorrelation (green) function and (b) spectral density (blue) for a Gaussian pulse with  $\Delta\tau_{\text{FWHM}} = 100$  fs.

general (Wiener–Khinchin theorem). Hence, it is given by (Figure S7.4b)

$$\begin{aligned}
 \sigma(\omega) &= \int_{-\infty}^{+\infty} \mathcal{G}(\Delta t) e^{-i\omega\Delta t} d\Delta t \\
 &= \mathcal{G}_0 \int_{-\infty}^{+\infty} \exp\left(-\frac{4\ln(2)}{t_c^2} \Delta t^2\right) \exp(-i\omega\Delta t) d\Delta t \\
 &= \mathcal{G}_0 \exp\left(-\frac{t_c^2}{16\ln(2)} \omega^2\right) \int_{-\infty}^{+\infty} \exp\left[-\frac{4\ln(2)}{t_c^2} \left(\Delta t + \frac{it_c^2}{2\ln(2)}\right)^2\right] d\Delta t \\
 &= \sqrt{\frac{\pi}{\ln(2)}} \frac{t_c}{2} \mathcal{G}_0 \exp\left(-\frac{t_c^2}{16\ln(2)} \omega^2\right) \\
 &= \sigma_{\text{max}} \exp\left(-\frac{1}{\ln 2} \left(\frac{\Delta\tau_{\text{FWHM}} \omega}{4}\right)^2\right) .
 \end{aligned}$$

As before, we have

$$-\ln 2 = -\frac{1}{\ln 2} \left( \frac{\Delta\tau_{\text{FWHM}} \Delta\omega_{\text{FWHM}}}{4} \right)^2$$

which yields a spectral width of

$$\begin{aligned} \Delta\omega_{\text{FWHM}} &= \frac{4 \ln 2}{\Delta\tau_{\text{FWHM}}} \quad \text{or} \\ \Delta\nu_{\text{FWHM}} &= \frac{2 \ln 2}{\pi} \frac{1}{\Delta\tau_{\text{FWHM}}} = \frac{0.4413}{\Delta\tau_{\text{FWHM}}} = \frac{0.8826}{t_c} = \frac{\sqrt{2 \ln 2}}{\pi t_p} = \frac{0.3748}{t_p} . \end{aligned}$$

For a Gaussian pulse, the bandwidth product becomes

$$\Delta\nu_{\text{FWHM}} \Delta\tau_{\text{FWHM}} = \frac{1}{2} \Delta\nu_{\text{FWHM}} t_c = 0.4413 .$$

In a similar way, the autocorrelation functions and spectral densities for the other pulse shapes can be obtained. It should be noted that the spectral densities can also be calculated (often more conveniently) directly from the Fourier transform of the temporal profile of the field according to

$$\sigma(\omega) = \tilde{E}(\omega) \cdot \tilde{E}(\omega)^* = |\tilde{E}(\omega)|^2 .$$

Here,  $\tilde{E}(\omega) = \mathcal{F}[E](\omega/(2\pi))$  is the Fourier transform of  $E(t)$  with respect to  $\omega/(2\pi)$ . The equivalence of this method is shown in Appendix 4. We will use one or the other in the following calculations for the spectral densities.

## 2. Rectangular pulse envelope:

In the following, we provide the results for the rectangular pulse (green curve in Figure S7.3). Here, the field amplitude reads

$$E(t) = \begin{cases} E_0; & |t| \leq \frac{\Delta\tau_{\text{FWHM}}}{2} \\ 0; & |t| \geq \frac{\Delta\tau_{\text{FWHM}}}{2} \end{cases} \quad (\text{S7.6a})$$

and the intensity

$$I(t) = \begin{cases} I_0; & |t| \leq \frac{\Delta\tau_{\text{FWHM}}}{2} \\ 0; & |t| \geq \frac{\Delta\tau_{\text{FWHM}}}{2} \end{cases} \quad (\text{S7.6b})$$

The autocorrelation function is generally given by

$$\mathcal{G}(\Delta t) = \int_{-\infty}^{+\infty} E(t)E(t + \Delta t)dt .$$

which then yields (green curve in Figure S7.5a)

$$\mathcal{G}(\Delta t) = E_0^2 \Delta\tau_{\text{FWHM}} \begin{cases} 1 - \left| \frac{\Delta t}{\Delta\tau_{\text{FWHM}}} \right|; & |\Delta t| \leq \Delta\tau_{\text{FWHM}} \\ 0; & \text{elsewhere} \end{cases}$$

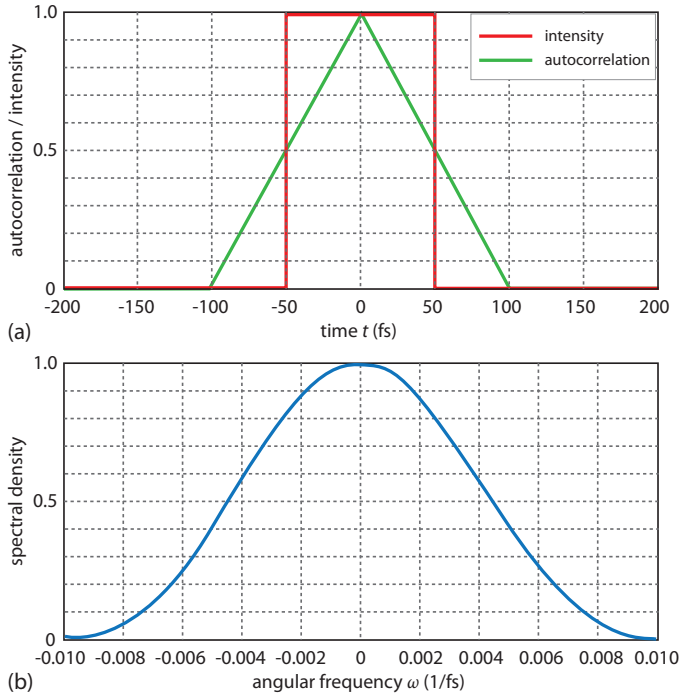


**Figure S7.5** (a) Intensity (red), autocorrelation (green) function and (b) spectral density (blue) for a rectangular pulse with  $\Delta\tau_{\text{FWHM}} = 100$  fs.

For the temporal width  $t_c$  (full width at half maximum coherence time), the autocorrelation function decreases to half of its maximum, that is,

$$t_c = \Delta\tau_{\text{FWHM}} ,$$

The coherence length is given by

$$L_c = c t_c = c \Delta\tau_{\text{FWHM}} ,$$

which is half the value for the Gaussian pulse envelope. Consequently, the spectral density curve must be much broader. The spectral density is obtained either by the Fourier transform of the autocorrelation function or, more conveniently, via the absolute square of the Fourier transform of the field (Appendix 4). Thus, it

reads (Figure S7.5b)

$$\begin{aligned}
 \sigma(\omega) &= \int_{-\infty}^{+\infty} \mathcal{G}(\Delta t) e^{-i\omega\Delta t} d\Delta t = |\tilde{E}(\omega)|^2 \\
 &= E_0^2 \Delta\tau_{\text{FWHM}}^2 \text{sinc}^2\left(\frac{\omega \Delta\tau_{\text{FWHM}}}{2\pi}\right) \\
 &= E_0^2 \Delta\tau_{\text{FWHM}}^2 \text{sinc}^2(\nu \Delta\tau_{\text{FWHM}}) ,
 \end{aligned}$$

in which  $\text{sinc}(x) = \sin(\pi x)/(\pi x)$  and  $\omega = 2\pi\nu$ . A more detailed derivation of the autocorrelation function  $\mathcal{G}(\Delta t)$  and spectral density  $\sigma(\omega)$  of a rectangular pulse can be found in Appendix 1.

### 3. $\text{Sech}^2$ pulse envelope:

The field amplitude and the pulse intensity (orange functions in Figure S7.3) are

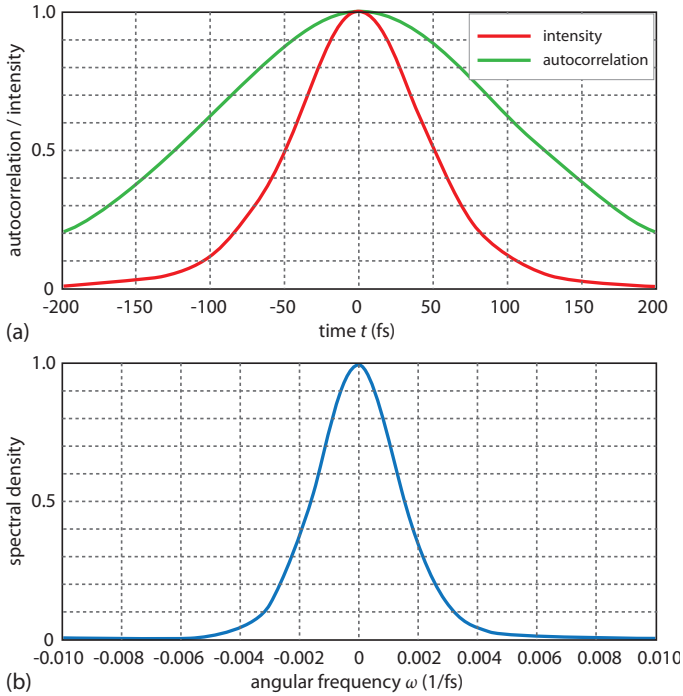


**Figure S7.6** (a) Intensity, autocorrelation function and (b) spectral density for a  $\text{sech}^2$  pulse with  $\Delta\tau_{\text{FWHM}} = 100$  fs.

given by

$$\begin{aligned} E(t) &= E_0 \operatorname{sech} \left( 2 \ln(1 + \sqrt{2})t / \Delta\tau_{\text{FWHM}} \right) \\ &= \sqrt{I_0} \operatorname{sech} \left( 1.7627 \frac{t}{\Delta\tau_{\text{FWHM}}} \right), \end{aligned} \quad (\text{S7.7a})$$

$$\begin{aligned} I(t) &= I_0 \operatorname{sech}^2 \left( 2 \ln(1 + \sqrt{2})t / \Delta\tau_{\text{FWHM}} \right) \\ &= I_0 \operatorname{sech}^2 \left( 1.7627 \frac{t}{\Delta\tau_{\text{FWHM}}} \right), \end{aligned} \quad (\text{S7.7b})$$

respectively. The autocorrelation function is then determined by (Figure S7.6; Appendix 3)

$$\begin{aligned} \mathcal{G}(\Delta t) &= \int_{-\infty}^{+\infty} E(t)E(t + \Delta t)dt \\ &= I_0 \int_{-\infty}^{+\infty} \operatorname{sech} \left( 1.7627 \frac{t}{\Delta\tau_{\text{FWHM}}} \right) \operatorname{sech} \left( 1.7627 \frac{t + \Delta t}{\Delta\tau_{\text{FWHM}}} \right) dt \\ &= I_0 \Delta t \cdot \left( \frac{1}{\sinh \left( \frac{1.7627 \Delta t}{\Delta\tau_{\text{FWHM}}} \right)} \right). \end{aligned}$$

By Fourier transformation and with  $\omega = 2\pi\nu$ , we obtain the spectral density (Figure S7.6b; Appendix 3)

$$\begin{aligned} \sigma(\omega) &= I_0 \left( \frac{\pi \Delta\tau_{\text{FWHM}}}{1.7627} \right)^2 \operatorname{sech}^2 \left( \frac{\pi \Delta\tau_{\text{FWHM}} \omega}{2 \cdot 1.7627} \right) \\ &= I_0 \left( \frac{\pi \Delta\tau_{\text{FWHM}}}{1.7627} \right)^2 \operatorname{sech}^2 \left( \frac{\pi^2 \Delta\tau_{\text{FWHM}} \nu}{1.7627} \right). \end{aligned}$$

#### 4. Lorentzian pulse envelope:

The field of the Lorentzian pulse is given by (red curve in Figure 7.3)

$$\begin{aligned} E(t) &= E_0 \cdot \left( 1 + \frac{4}{1 + \sqrt{2}} \left( \frac{t}{\Delta\tau_{\text{FWHM}}} \right)^2 \right)^{-1} \\ &= \frac{E_0}{1 + \left( \frac{1.2872 t}{\Delta\tau_{\text{FWHM}}} \right)^2} \end{aligned} \quad (\text{S7.8a})$$

and the intensity by

$$\begin{aligned} I(t) &= I_0 \cdot \left( 1 + \frac{4}{1 + \sqrt{2}} \left( \frac{t}{\Delta\tau_{\text{FWHM}}} \right)^2 \right)^{-2} \\ &= \frac{I_0}{\left( 1 + \left( \frac{1.2872 t}{\Delta\tau_{\text{FWHM}}} \right)^2 \right)^2}. \end{aligned} \quad (\text{S7.8b})$$

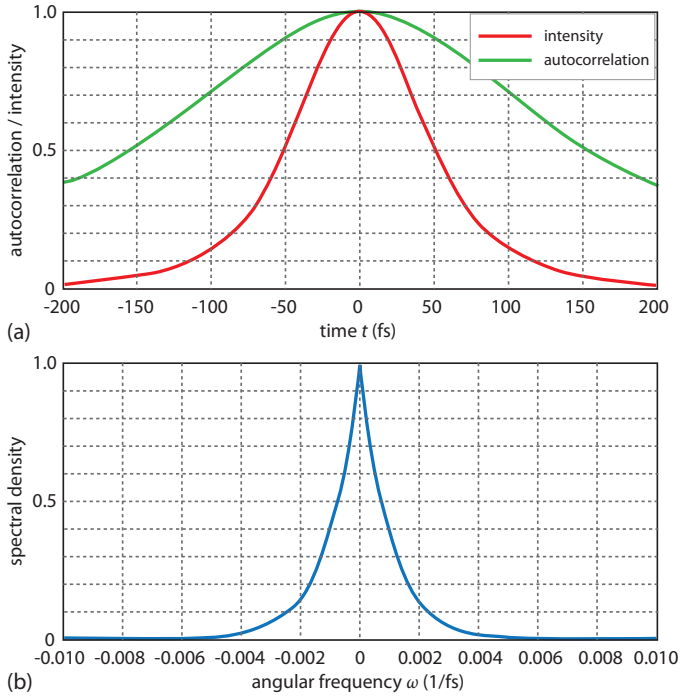


**Figure S7.7** (a) Intensity, autocorrelation function and (b) spectral density for a Lorentzian pulse with  $\Delta\tau_{\text{FWHM}} = 100$  fs.

The autocorrelation function reads (Figure S7.7a; Appendix 2)

$$\begin{aligned} \mathcal{G}(\Delta t) &= \int_{-\infty}^{+\infty} E(t)E(t + \Delta t)dt \\ &= \frac{1}{2} \cdot \frac{\pi\tau E_0^2}{1 + \left(\frac{\Delta t}{2\tau}\right)^2} \end{aligned}$$

from which we obtain with  $\tau = \Delta\tau_{\text{FWHM}}/1.2872$  and via Fourier transformation the spectral density (Figure S7.7b; Appendix 2)

$$\begin{aligned} \sigma(\omega) &= (E_0\pi\tau)^2 e^{-2\tau|\omega|} \\ &= (E_0\pi\tau)^2 e^{-4\pi\tau|\nu|} . \end{aligned}$$

Finally, in Figure S7.8, a comparison of spectral densities is shown for various pulse shapes with equal  $\Delta\tau_{\text{FWHM}} = 100$  fs. As one can see, different spectral widths  $\Delta\omega_{\text{FWHM}}$  are obtained which depend on the pulse shape.

The so-called pulse duration – bandwidth product (see also part b) of this Problem) is a characteristic of the pulse shape. The values of the pulse duration – bandwidth

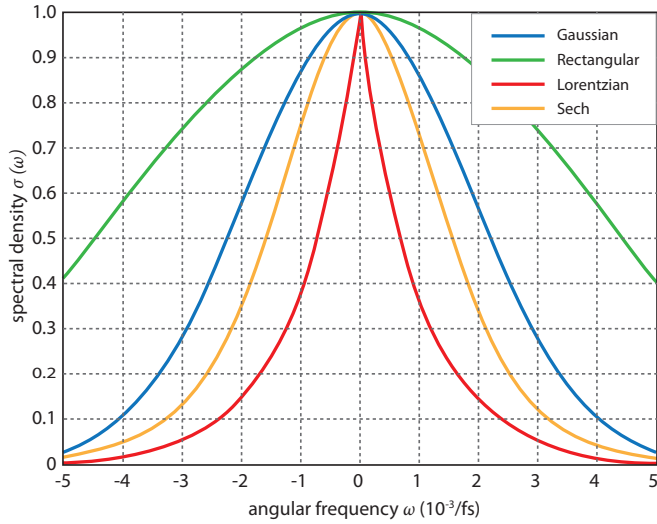


**Figure S7.8** Comparison of the spectral density  $\sigma(\omega)$  for various pulse shapes each with  $\Delta\tau_{FWHM} = 100$  fs.

product can be derived from Figure S7.8 and yield

$$\frac{\Delta\tau_{FWHM}\Delta\omega_{FWHM}}{2\pi} = \Delta\tau_{FWHM}\Delta\nu_{FWHM} = \begin{cases} 0.441; & \text{Gaussian pulse} \\ 0.886; & \text{Rectangular pulse} \\ 0.142; & \text{Lorentzian pulse} \\ 0.315 = 1/\pi; & \text{Sech}^2\text{ pulse} \end{cases}$$

One can very nicely see the Wiener-Khinchin theorem in Figure S7.8. A relatively narrow autocorrelation function like for the rectangular pulse leads to a broad spectrum. And vice versa a broad correlation function like for the Lorentzian pulse (with its broad “wings”) leads to a relatively narrow spectrum.

## Appendix to Problem P7.2

In this appendix<sup>7)</sup>, we provide some lengthy derivations and conceptual considerations mentioned in the discussion of Problem P7.2.

### Appendix 1: Derivation of the autocorrelation function and spectral density for a rectangular pulse shape

At first, let us consider the autocorrelation function. For this purpose, we start from

$$E(t) = E_0 \Theta \left( \frac{\Delta\tau_{\text{FWHM}}}{2} - |t| \right) \quad (\text{AP.1})$$

with  $\Delta\tau_{\text{FWHM}} > 0$  and the Heaviside function

$$\Theta(x) = \begin{cases} 1, & \text{for } x > 0 \\ 0, & \text{for } x < 0 \end{cases} \quad (\text{AP.2})$$

In this case, the autocorrelation function reads

$$\begin{aligned} \mathcal{G}(\Delta t) &= \int_{-\infty}^{\infty} E(t)E(t + \Delta t) dt \quad (\text{AP.3}) \\ &= E_0^2 \int_{-\infty}^{\infty} \Theta \left( \frac{\Delta\tau_{\text{FWHM}}}{2} - |t| \right) \Theta \left( \frac{\Delta\tau_{\text{FWHM}}}{2} - |t + \Delta t| \right) dt \\ &= E_0^2 \int_{-\infty}^{\infty} \Theta \left( \frac{\Delta\tau_{\text{FWHM}}}{2} - \left| t - \frac{\Delta t}{2} \right| \right) \Theta \left( \frac{\Delta\tau_{\text{FWHM}}}{2} - \left| t + \frac{\Delta t}{2} \right| \right) dt \\ &= E_0^2 \int_{-\infty}^{\infty} \Theta(\Delta\tau_{\text{FWHM}} - |\Delta t|) \Theta \left( \frac{\Delta\tau_{\text{FWHM}} - \Delta t}{2} - |t| \right) dt . \quad (\text{AP.4}) \end{aligned}$$

The product of the two Heaviside functions only becomes zero, if the condition

$$-\frac{\Delta\tau_{\text{FWHM}}}{2} \leq t \pm \frac{\Delta t}{2} \leq \frac{\Delta\tau_{\text{FWHM}}}{2}$$

is valid. This can be rewritten according to

$$\max \left\{ -\frac{\Delta\tau_{\text{FWHM}} - \Delta t}{2}, -\frac{\Delta\tau_{\text{FWHM}} + \Delta t}{2} \right\} \leq t \leq \min \left\{ \frac{\Delta\tau_{\text{FWHM}} - \Delta t}{2}, \frac{\Delta\tau_{\text{FWHM}} + \Delta t}{2} \right\} .$$

7) Provided by J.-M. Kaltenbach (Carl Zeiss AG, Oberkochen, Germany).

This means that the conditions  $\Delta\tau_{\text{FWHM}} \geq |\Delta t|$  and  $(\Delta\tau_{\text{FWHM}} + |\Delta t|)/2 \geq |t|$  are true. Knowing this, we may continue with Eq. (AP.4) as follows:

$$\begin{aligned}
 \mathcal{G}(\Delta t) &= E_0^2 \Theta(\Delta\tau_{\text{FWHM}} - |\Delta t|) \int_{-\frac{\Delta\tau_{\text{FWHM}} - \Delta t}{2}}^{\frac{\Delta\tau_{\text{FWHM}} - \Delta t}{2}} dt \\
 &= E_0^2 (\Delta\tau_{\text{FWHM}} - |\Delta t|) \Theta(\Delta\tau_{\text{FWHM}} - |\Delta t|) \\
 &= E_0^2 \Delta\tau_{\text{FWHM}} \left(1 - \left|\frac{\Delta t}{\Delta\tau_{\text{FWHM}}}\right|\right) \Theta\left(1 - \left|\frac{\Delta t}{\Delta\tau_{\text{FWHM}}}\right|\right) \\
 &= E_0^2 \Lambda\left(\frac{\Delta t}{\Delta\tau_{\text{FWHM}}}\right), \tag{AP.5}
 \end{aligned}$$

where  $\Lambda(x) = (1 - |x|) \Theta(1 - |x|)$  is the so-called triangle function.

Next, we have a look at the spectral density, which reads

$$\begin{aligned}
 \sigma(\omega) &= \int_{-\infty}^{\infty} \mathcal{G}(\Delta t) e^{-i\omega\Delta t} d\Delta t \tag{AP.6} \\
 &= E_0^2 \int_{-\infty}^{\infty} \Lambda\left(\frac{\Delta t}{\Delta\tau_{\text{FWHM}}}\right) e^{-i\omega\Delta t} d\Delta t \\
 &= E_0^2 \int_{-\Delta\tau_{\text{FWHM}}}^{\Delta\tau_{\text{FWHM}}} (\Delta\tau_{\text{FWHM}} - |\Delta t|) e^{-i\omega\Delta t} d\Delta t \\
 &= 2E_0^2 \int_0^{\Delta\tau_{\text{FWHM}}} (\Delta\tau_{\text{FWHM}} - \Delta t) \cos(\omega \Delta t) d\Delta t \\
 &= 2E_0^2 \int_0^{\Delta\tau_{\text{FWHM}}} \left(\Delta\tau_{\text{FWHM}} \cos(\omega \Delta t) - \frac{\partial}{\partial\omega} \sin(\omega \Delta t)\right) d\Delta t \\
 &= 2E_0^2 \left(\frac{\Delta\tau_{\text{FWHM}}}{\omega} \sin(\omega\Delta\tau_{\text{FWHM}}) - \frac{\partial}{\partial\omega} \frac{1 - \cos(\omega \Delta\tau_{\text{FWHM}})}{\omega}\right) \\
 &= \frac{2E_0^2}{\omega^2} (1 - \cos(\omega \Delta\tau_{\text{FWHM}})) \\
 &= \frac{4E_0^2}{\omega^2} \sin\left(\frac{\omega \Delta\tau_{\text{FWHM}}}{2}\right)^2 \\
 &= (E_0 \Delta\tau_{\text{FWHM}})^2 \left(\frac{\sin(\omega \Delta\tau_{\text{FWHM}}/2)}{\omega \Delta\tau_{\text{FWHM}}/2}\right)^2 \\
 &= \left(E_0 \Delta\tau_{\text{FWHM}} \text{sinc}\left(\frac{\omega \Delta\tau_{\text{FWHM}}}{2\pi}\right)\right)^2 \\
 &= \left(E_0 \Delta\tau_{\text{FWHM}} \mathcal{J}\left(\frac{\omega \Delta\tau_{\text{FWHM}}}{2}\right)\right)^2 \tag{AP.7}
 \end{aligned}$$

with  $\text{sinc}(x) = \sin(\pi x)/(\pi x)$  and the spherical Bessel function  $\mathcal{J} = \sin(x)/x$ .

## Appendix 2:

### Derivation of the autocorrelation function and spectral density for a Lorentzian pulse shape

The Lorentzian pulse shape is generally determined by the function

$$f(x) = \frac{1}{1+x^2} .$$

The autocorrelation function is again given by Eq. (AP.3) and the spectral density by Eq. (AP.6), whereas

$$E(t) = E_0 f(t/\tau) \equiv E_0 f_\tau(t) . \quad (\text{AP.8})$$

For the calculation of  $\mathcal{G}(\Delta t)$ , we would like to follow here a different approach. We use the convolution theorem and the Fourier transform (see also Info Box A.2 in Section A.2.4) of  $E(t)$ . In mathematical standard literature, it can be found that the Fourier transform of a Lorentzian function  $f(t)$  is proportional to  $\exp(-a|\omega|)$ . In the following, we define the Fourier transformation<sup>8)</sup> as

$$\mathcal{F}\{f(t)\} = \int_{-\infty}^{\infty} f(t) e^{2\pi i \nu t} dt \quad (\text{AP.9})$$

and the inverse Fourier transformation as

$$\mathcal{F}^{-1}\{f(\nu)\} = \int_{-\infty}^{\infty} f(\nu) e^{-2\pi i \nu t} d\nu . \quad (\text{AP.10})$$

Next, we define a function

$$g_a(\nu) = e^{-a|\nu|}$$

8) Please note that, in contrast to Chapter A, the definition of the Fourier transform has a factor  $2\pi$  in the exponent. This is indeed the simplest choice, as it allows us to decide whether to use  $2\pi$  or  $\sqrt{2\pi}$  as pre-factors in both transform and inverse transform or not. In addition, this definition simplifies the convolution theorem. Hence, the Fourier transform and the inverse Fourier transform now only differ in the sign of the exponent, and Eqs. (AP.9) and (AP.10) are written such that  $\sigma(2\pi\nu) = \mathcal{F}\{g\}(\nu)$ .

with  $a > 0$  and calculate its inverse Fourier transform, that is,

$$\begin{aligned}
 \mathcal{F}^{-1}\{g_a(\nu)\} &= \int_{-\infty}^{\infty} e^{-2\pi i\nu t - a|\nu|} d\nu \\
 &= \int_0^{\infty} e^{-(2\pi i\nu t + a)\nu} d\nu + \int_0^{\infty} e^{+(2\pi i\nu t - a)\nu} d\nu \\
 &= \frac{1}{2\pi i t + a} - \frac{1}{2\pi i t - a} \\
 &= \frac{2a}{a^2 + (2\pi t)^2} \\
 &= \frac{2/a}{1 + (2\pi t/a)^2} \\
 &= \frac{2}{a} f_{\frac{a}{2\pi}}(t)
 \end{aligned}$$

or

$$\begin{aligned}
 \mathcal{F}^{-1}\{\pi\tau g_{2\pi\tau}\}(t) &= f_{\tau}(t) = \frac{1}{1 + (t/\tau)^2} \quad , \\
 \mathcal{F}\{f_{\tau}\}(\nu) &= \pi\tau g_{2\pi\tau}(\nu) = \pi\tau e^{-2\pi\tau|\nu|} = \pi\tau e^{-\tau|\omega|} \quad . \quad (\text{AP.11})
 \end{aligned}$$

For the calculation of  $\mathcal{G}$ , we now substitute  $t$  by  $t - \Delta t$  and use the fact that the Lorentzian function is an even function. Hence, we have

$$\begin{aligned}
 \mathcal{G}(\Delta t) &= E_0^2 \int_{-\infty}^{\infty} f_{\tau}(t) f_{\tau}(t + \Delta t) dt \\
 &= E_0^2 \int_{-\infty}^{\infty} f_{\tau}(t - \Delta t) f_{\tau}(t) dt \\
 &= E_0^2 \int_{-\infty}^{\infty} f_{\tau}(\Delta t - t) f_{\tau}(t) dt \\
 &= E_0^2 (f_{\tau} * f_{\tau})(\Delta t) \quad (\text{AP.12}) \\
 &= E_0^2 \mathcal{F}^{-1}\{\mathcal{F}\{f_{\tau}\} \cdot \mathcal{F}\{f_{\tau}\}\}(\Delta t) \quad , \quad (\text{AP.13})
 \end{aligned}$$

where  $*$  denotes the convolution. For the transition from Eq. (AP.12) to Eq. (AP.13), we used the convolution theorem. From Eq. (AP.11), we derive

$$(\mathcal{F}\{f_{\tau}\}(\nu))^2 = \frac{\pi\tau}{2} \mathcal{F}\{f_{2\tau}\}(\nu)$$

and thus

$$\begin{aligned}
 \mathcal{G}(\Delta t) &= \frac{\pi\tau E_0^2}{2} \mathcal{F}^{-1}\{\mathcal{F}\{f_{2\tau}\}\}(\Delta t) \\
 &= \frac{\pi\tau E_0^2}{2} f_{2\tau}(\Delta t) \\
 &= \frac{1}{2} \frac{\pi\tau E_0^2}{1 + \left(\frac{\Delta t}{2\tau}\right)^2} .
 \end{aligned}$$

As we can see, the autocorrelation of a Lorentzian function is again a Lorentzian. For the spectral density, we consequently derive from Eqs. (AP.11) and (AP.13)

$$\begin{aligned}
 \sigma(\omega) &= (\pi\tau E_0)^2 e^{-2\tau|\omega|} \\
 &= \left(\pi\tau E_0 e^{-\tau|\omega|}\right)^2 .
 \end{aligned}$$

### Appendix 3: Derivation of the autocorrelation function and spectral density for a sech pulse shape

The field of a sech pulse is given by

$$E(t) = \sqrt{I_0} \operatorname{sech}\left(\frac{t}{\tau}\right) = \sqrt{I_0} \frac{1}{\cosh\left(\frac{t}{\tau}\right)}$$

with  $\tau = \Delta\tau_{\text{FWHM}}/1.7627$ . The autocorrelation function then becomes

$$\begin{aligned}
 \mathcal{G}(\Delta t) &= I_0 \int_{-\infty}^{\infty} \left( \cosh\left(\frac{t}{\tau}\right) \cosh\left(\frac{t+\Delta t}{\tau}\right) \right)^{-1} dt \\
 &= I_0 \int_{-\infty}^{\infty} \left( \cosh\left(\frac{t-\Delta t/2}{\tau}\right) \cosh\left(\frac{t+\Delta t/2}{\tau}\right) \right)^{-1} dt \\
 &= 2I_0 \int_{-\infty}^{\infty} \left( \cosh\left(\frac{2t}{\tau}\right) + \cosh\left(\frac{\Delta t}{\tau}\right) \right)^{-1} dt \\
 &= 4I_0 \int_0^{\infty} \left( \cosh\left(\frac{2t}{\tau}\right) + \cosh\left(\frac{\Delta t}{\tau}\right) \right)^{-1} dt . \tag{AP.14}
 \end{aligned}$$

Here, we have used the theorems of the hyperbolic functions

$$\cosh(x \pm y) = \cosh(x) \cosh(y) \pm \sinh(x) \sinh(y) , \tag{AP.15}$$

$$\sinh(x \pm y) = \sinh(x) \cosh(y) \pm \cosh(x) \sinh(y) , \tag{AP.16}$$

and in particular

$$\cosh^2(x) - \sinh^2(x) = 1 . \tag{AP.17}$$

From Eq. (AP.15), we directly obtain

$$\begin{aligned} \cosh(x + y) + \cosh(x - y) &= 2 \cosh(x) \cosh(y) , \\ 1 + \cosh(2x) &= 2 \cosh^2(x) \end{aligned}$$

and from Eq. (AP.16)

$$\frac{\sinh(2x)}{1 + \cosh(2x)} = \frac{2 \sinh(x) \cosh(x)}{2 \cosh^2(x)} = \tanh(x) , \text{ with} \quad (\text{AP.18})$$

$$\tanh(x) = \frac{e^x - e^{-x}}{e^x + e^{-x}} = \frac{e^{2x} - 1}{e^{2x} + 1} = y . \quad (\text{AP.19})$$

When we solve Eq. (AP.19) for  $x$ , it follows that

$$x = \operatorname{arctanh}(y) = \frac{1}{2} \log \left( \frac{1 + y}{1 - y} \right) . \quad (\text{AP.20})$$

For the integral in Eq. (AP.14), we need to consider the term

$$\int (p + q \cosh(ax))^{-1} dx$$

for  $p \neq q$ . Substituting  $\xi = \exp(ax)$  yields  $\cosh(ax) = (\xi^2 + 1)/(2\xi)$  and  $dx = d\xi/(a\xi)$ . Consequently, we obtain

$$\begin{aligned} &\int (p + q \cosh(ax))^{-1} dx \\ &= \begin{cases} \frac{2}{a\sqrt{q^2 - p^2}} \operatorname{arctan} \left( \frac{q e^{ax} + p}{\sqrt{q^2 - p^2}} \right), & \text{for } q^2 - p^2 > 0 \\ \frac{1}{a\sqrt{p^2 - q^2}} \log \left( \frac{q e^{ax} + p - \sqrt{p^2 - q^2}}{q e^{ax} + p + \sqrt{p^2 - q^2}} \right), & \text{for } p^2 - q^2 > 0 \end{cases} \end{aligned}$$

We now evaluate the case  $p^2 > q^2$ , as it is the only relevant one in this discussion so that

$$\begin{aligned} &\int (p + q \cosh(ax))^{-1} dx \\ &= \frac{2}{a} \int (q + 2p\xi + q\xi^2)^{-1} d\xi \\ &= \frac{2}{aq} \int \left[ \left( \xi + \frac{p}{q} + \frac{\sqrt{p^2 - q^2}}{q} \right) \left( \xi + \frac{p}{q} - \frac{\sqrt{p^2 - q^2}}{q} \right) \right]^{-1} d\xi \\ &= \frac{1}{aq\sqrt{p^2 - q^2}} \int \left( \frac{1}{\xi + \frac{p}{q} - \frac{\sqrt{p^2 - q^2}}{q}} - \frac{1}{\xi + \frac{p}{q} + \frac{\sqrt{p^2 - q^2}}{q}} \right) d\xi \\ &= \frac{1}{aq\sqrt{p^2 - q^2}} \log \left( \frac{\xi + \frac{p}{q} - \frac{\sqrt{p^2 - q^2}}{q}}{\xi + \frac{p}{q} + \frac{\sqrt{p^2 - q^2}}{q}} \right) \\ &= \frac{1}{a\sqrt{p^2 - q^2}} \log \left( \frac{q e^{ax} + p - \sqrt{p^2 - q^2}}{q e^{ax} + p + \sqrt{p^2 - q^2}} \right) . \end{aligned}$$

In our case, we have  $p = \cosh\left(\frac{\Delta t}{\tau}\right)$  and  $q = 1$ . Thus,  $p > q$  if  $\Delta t \neq 0$  and  $\sqrt{p^2 - q^2} = \sinh\left(\frac{\Delta t}{\tau}\right)$ . We then obtain with  $a = 2/\tau$

$$\begin{aligned} \mathcal{G}(\Delta t) &= \frac{2I_0\tau}{\sinh\left(\frac{\Delta t}{\tau}\right)} \log\left(\frac{1 + \cosh\left(\frac{\Delta t}{\tau}\right) + \sinh\left(\frac{\Delta t}{\tau}\right)}{1 + \cosh\left(\frac{\Delta t}{\tau}\right) - \sinh\left(\frac{\Delta t}{\tau}\right)}\right) \\ &= \frac{2I_0\tau}{\sinh\left(\frac{\Delta t}{2\tau}\right)} \log\left(\frac{1 + \frac{\sinh\left(\frac{\Delta t}{\tau}\right)}{1 + \cosh\left(\frac{\Delta t}{\tau}\right)}}{1 - \frac{\sinh\left(\frac{\Delta t}{\tau}\right)}{1 + \cosh\left(\frac{\Delta t}{\tau}\right)}}\right) \\ &= \frac{4I_0\tau}{\sinh\left(\frac{\Delta t}{\tau}\right)} \frac{1}{2} \log\left(\frac{1 + \tanh\left(\frac{\Delta t}{2\tau}\right)}{1 - \tanh\left(\frac{\Delta t}{2\tau}\right)}\right). \end{aligned}$$

In the last step, we used the relation in Eq. (AP.18). Using Eq. (AP.20), we finally write

$$\begin{aligned} \mathcal{G}(\Delta t) &= \frac{2I_0 \Delta t}{\sinh\left(\frac{\Delta t}{\tau}\right)} \\ &= 2I_0\tau \frac{\Delta t/\tau}{\sinh\left(\frac{\Delta t}{\tau}\right)} \\ &= 2I_0 \frac{\Delta t}{\sinh\left(\frac{\Delta t}{\tau}\right)}. \end{aligned}$$

For the calculation of the spectral density, we may use an integral table, as provided in standard mathematical literature. With the Fourier transform of the field

$$\begin{aligned} \tilde{E}(\omega) &= \int_{-\infty}^{\infty} E(t) e^{-i\omega t} dt \\ &= \int_{-\infty}^{\infty} \sqrt{I_0} \operatorname{sech}\left(\frac{t}{\tau}\right) e^{-i\omega t} dt \\ &= 2\sqrt{I_0} \int_0^{\infty} \frac{\cos(\omega t)}{\cosh(t/\tau)} dt \\ &= \frac{\pi\tau\sqrt{I_0}}{\cosh\left(\frac{\pi}{2}\tau\omega\right)}, \end{aligned}$$

we directly obtain the spectral density (see also Appendix 4)

$$\sigma(\omega) = (\tilde{E}(\omega))^2 = I_0 \left(\frac{\pi\tau}{\cosh(\pi\tau\omega/2)}\right)^2.$$

**Appendix 4:**

**Alternative calculation of the spectral density  $\sigma(\omega)$  directly from the Fourier transform of the field  $E(t)$**

For the sake of simplicity, we write

$$\tilde{E}(\omega) = \mathcal{F}\{E\} \left( \frac{\omega}{2\pi} \right)$$

and separate the field in an even and an odd component according to

$$E_{\text{even}}(t) = \frac{E(t) + E(-t)}{2} ,$$

$$E_{\text{odd}}(t) = \frac{E(t) - E(-t)}{2} ,$$

respectively. We then have  $E = E_{\text{even}} + E_{\text{odd}}$  and  $\tilde{E} = \tilde{E}_{\text{even}} + \tilde{E}_{\text{odd}}$ , in which  $\tilde{E}_{\text{even}}$  has a real and  $\tilde{E}_{\text{odd}}$  a purely imaginary value. Hence, it follows that

$$(\tilde{E}_{\text{even}}(\omega))^2 = |\tilde{E}_{\text{even}}(\omega)|^2 ,$$

$$(\tilde{E}_{\text{odd}}(\omega))^2 = -|\tilde{E}_{\text{odd}}(\omega)|^2 ,$$

or

$$\tilde{E}_{\text{even}}(\omega) = \text{Re}(\tilde{E}(\omega)) , \tag{AP.21}$$

$$\tilde{E}_{\text{odd}}(\omega) = i \text{Im}(\tilde{E}(\omega)) . \tag{AP.22}$$

With the symbol  $\otimes$  for the correlation and  $*$  for the convolution, we have

$$\begin{aligned} \mathcal{G}(\Delta t) &= E \otimes E \\ &= \int_{-\infty}^{\infty} E(t)E(t + \Delta t) dt \\ &= \int_{-\infty}^{\infty} E(t - \Delta t)E(t) dt \\ &= \int_{-\infty}^{\infty} (E_{\text{even}}(t - \Delta t) + E_{\text{odd}}(t - \Delta t)) (E_{\text{even}}(t) + E_{\text{odd}}(t)) dt \\ &= \int_{-\infty}^{\infty} (E_{\text{even}}(\Delta t - t) - E_{\text{odd}}(\Delta t - t)) (E_{\text{even}}(t) + E_{\text{odd}}(t)) dt \\ &= E_{\text{even}} * E_{\text{even}} - E_{\text{odd}} * E_{\text{odd}} + \underbrace{E_{\text{even}} * E_{\text{odd}} - E_{\text{odd}} * E_{\text{even}}}_{=0, \text{ as the convolution is commutative}} . \end{aligned}$$

Using the convolution theorem as well as Eqs. (AP.21) and (AP.22), we find

$$\mathcal{F}\{\mathcal{G}\} = \tilde{E}_{\text{even}}^2 - \tilde{E}_{\text{odd}}^2 = |\tilde{E}_{\text{even}}|^2 + |\tilde{E}_{\text{odd}}|^2$$

and finally

$$\sigma(\omega) = |\tilde{E}(\omega)|^2 . \quad (\text{AP.23})$$

In Appendix 1,  $\sigma$  was calculated via the Fourier transform of the autocorrelation function. An alternative approach is given by Eq. (AP.23). From Eq. (AP.1), we derive

$$\begin{aligned} \tilde{E}(\omega) &= E_0 \int_{-\frac{\Delta\tau_{\text{FWHM}}}{2}}^{\frac{\Delta\tau_{\text{FWHM}}}{2}} e^{-i\omega t} dt \\ &= E_0 \frac{e^{-i\omega\Delta\tau_{\text{FWHM}}/2} - e^{i\omega\Delta\tau_{\text{FWHM}}/2}}{-i\omega} \\ &= E_0 \Delta\tau_{\text{FWHM}} \frac{-2i \sin\left(\omega \frac{\Delta\tau_{\text{FWHM}}}{2}\right)}{-2i\omega \frac{\Delta\tau_{\text{FWHM}}}{2}} \\ &= E_0 \Delta\tau_{\text{FWHM}} \operatorname{sinc}\left(\frac{\omega\Delta\tau_{\text{FWHM}}}{2\pi}\right) , \end{aligned}$$

which leads directly to Eq. (AP.7) by taking the square. The above considerations are valid for real functions  $E(t)$  of any symmetry. Additionally, it can be shown that Eq. (AP.23) also holds for complex functions.

Let us now consider some further symmetry properties by defining

$$E^{(-)} \equiv E(-t) .$$

Then, we have

$$\begin{aligned} \tilde{E}^{(-)*}(\omega) &= \int_{-\infty}^{\infty} E^*(-t) e^{-i\omega t} dt \\ &= \left( \int_{-\infty}^{\infty} E(-t) e^{+i\omega t} dt \right)^* \\ &= \left( \int_{-\infty}^{\infty} E(t) e^{-i\omega t} dt \right)^* \\ &= \tilde{E}^*(\omega) . \end{aligned}$$

By introducing another complex function  $F$ , we can further write

$$\begin{aligned}
 (E \otimes F)(\Delta t) &= \int_{-\infty}^{\infty} E^*(t) F(t + \Delta t) dt \\
 &= \int_{-\infty}^{\infty} E^*(-t) F(\Delta t - t) dt \\
 &= \int_{-\infty}^{\infty} E^{(-)*}(t) F(\Delta t - t) dt \\
 &= (E^{(-)*} * F)(\Delta t) .
 \end{aligned}$$

With the convolution theorem, it follows that

$$\widetilde{E \otimes F} = \widetilde{E^{(-)*} * F} = \widetilde{E^{(-)*}} \cdot \widetilde{F} = \tilde{E}^* \cdot \tilde{F} = |\tilde{E}|^2$$

if  $E = F$ .

## Appendix 5:

### Relation between autocorrelation and intensity correlation function

In literature, we often find a confusion between autocorrelation and intensity correlation function. Here, we would like to clarify this issue by using the following denominations:

$$\mathcal{G}_E(\Delta t) = \int_{-\infty}^{\infty} E(t)E(t + \Delta t) dt , \quad (\text{AP.24})$$

$$\mathcal{G}_I(\Delta t) = \int_{-\infty}^{\infty} I(t)I(t + \Delta t) dt , \quad (\text{AP.25})$$

with  $I(t) = |E(t)|^2$ . As an example, we compare the autocorrelation and the intensity correlation for the sech pulse shape. In Appendix 3, we calculated

$$\mathcal{G}_E(\Delta t) = \frac{2I_0 \Delta t}{\sinh(\Delta t/\tau)}$$

for

$$E(t) = \frac{\sqrt{I_0}}{\cosh(t/\tau)} \quad \text{and} \quad \tau = \frac{\Delta\tau_{\text{FWHM}}}{1.7627} .$$

In analogy to the derivation of Eq. (AP.14), we can write

$$\mathcal{G}_I(\Delta t) = 8I_0^2 \int_0^{\infty} \left( \cosh\left(\frac{2t}{\tau}\right) + \cosh\left(\frac{\Delta t}{\tau}\right) \right)^{-2} dt .$$

The integral  $\int (p + q \cosh(ax))^{-1} dx$  is already known from Appendix 3, so we use a linear combination of

$$\frac{1}{(p + q \cosh(ax))^2} + \frac{p}{q^2 - p^2} \frac{1}{p + q \cosh(ax)},$$

which can be re-written as

$$\begin{aligned} & \frac{(q^2 - p^2) + (p^2 + pq \cosh(ax))}{(q^2 - p^2)(p + q \cosh(ax))^2} \\ &= \frac{q}{q^2 - p^2} \frac{q + p \cosh(ax)}{(p + q \cosh(ax))^2} \\ &= \frac{q}{q^2 - p^2} \frac{p \cosh(ax) + q (\cosh^2(ax) - \sinh^2(ax))}{(p + q \cosh(ax))^2} \\ &= \frac{q}{q^2 - p^2} \frac{(p + q \cosh(ax)) \cosh(ax) + q \sinh^2(ax)}{(p + q \cosh(ax))^2} \\ &= \frac{q}{a(q^2 - p^2)} \left( \frac{a \cosh(ax)}{p + q \cosh(ax)} - \frac{\sinh(ax) a q \sinh(ax)}{(p + q \cosh(ax))^2} \right) \\ &= \frac{q}{a(q^2 - p^2)} \frac{d}{dx} \frac{\sinh(ax)}{p + q \cosh(ax)} \end{aligned}$$

so that

$$\frac{1}{(p + q \cosh(ax))^2} = \frac{1}{q^2 - p^2} \left( \frac{q}{a} \frac{d}{dx} \frac{\sinh(ax)}{p + q \cosh(ax)} - \frac{p}{p + q \cosh(ax)} \right).$$

with  $p = \cosh(\Delta t/\tau)$ ,  $q = 1$ ,  $q^2 - p^2 = -\sinh^2(\Delta t/\tau)$ , and  $a = 2/\tau$ . We now obtain for the intensity correlation

$$\begin{aligned} \mathcal{G}_I(\Delta t) &= \frac{-8I_0^2}{\sinh^2(\Delta t/\tau)} \left( \frac{\tau}{2} \frac{\sinh(2t/\tau)}{p + q \cosh(2t/\tau)} \Big|_0^\infty - \cosh\left(\frac{\Delta t}{\tau}\right) \frac{\mathcal{G}_E(\Delta t)}{4I_0} \right) \\ &= \frac{4I_0^2 \tau}{\sinh^2(\Delta t/\tau)} \left( \cosh\left(\frac{\Delta t}{\tau}\right) \frac{\Delta t/\tau}{\sinh(\Delta t/\tau)} - 1 \right) \\ &= \left( \frac{2I_0}{\sinh(\Delta t/\tau)} \right)^2 \left( \frac{\Delta t/\tau}{\tanh(\Delta t/\tau)} - 1 \right) \tau. \end{aligned}$$

Since  $\tanh(x) = 1 - x^3/3 + \mathcal{O}(x^5)$  and  $\sinh(x) = x + \mathcal{O}(x^3)$ , we finally find

$$\begin{aligned} \lim_{\Delta t \rightarrow 0} \mathcal{G}_I(\Delta t) &= \frac{4I_0^2 \tau}{3}, \\ \mathcal{G}_I(\Delta t) &= \frac{3\mathcal{G}_I(0)}{\sinh^2(\Delta t/\tau)} \left( \frac{\Delta t/\tau}{\tanh(\Delta t/\tau)} - 1 \right). \end{aligned}$$

The significant difference between the autocorrelation (which correlates the fields) and intensity correlation becomes not only obvious from the pure mathematics, but also if we plot the corresponding functions.

---

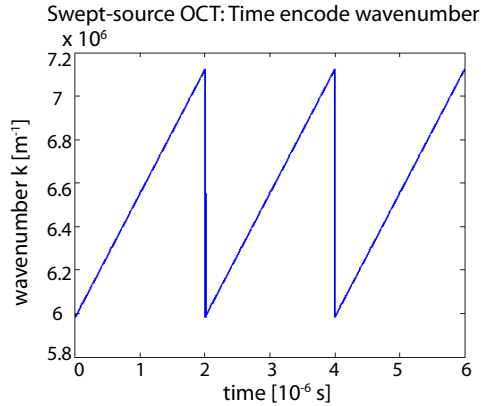


**Figure S7.9** Time-encoded wave number over time for a center wavelength of 1050 nm of a swept-source OCT.

### P7.3 Swept-source OCT

How would you design a 1050 nm swept-source OCT with variable sweep rates up to 500 kHz and a tunable range of 100 nm for the various applications?:

1. High speed/high resolution/small “imaging” depth (e.g., used for retinal scans)
2. Medium speed/medium resolution/medium “imaging” depth (e.g., used for scans in the anterior chamber)
3. Low speed/medium resolution/ultra-deep “imaging” depth (e.g., used for whole-eye scans)

Determine relevant parameters for sweep rate, bandwidth, SNR, measuring time per axial scan, and so on.

#### **Solution:**

The saw-tooth profile of the swept light source (Figure S7.9) is obtained as function of time  $t$  by

$$k(t) = k_0 + \frac{\Delta k}{\Delta t} t, \quad (\text{S7.9})$$

where  $k$ ,  $k_0 = 2\pi/\lambda_0$ ,  $\Delta k$ , and  $\Delta t$  are the instantaneous optical wave number, the wave number at the central wavelength ( $\lambda_0$ ), the optical bandwidth in  $k$ -space, and the sweep or A-scan time, respectively. In swept-source OCT (SS-OCT), the acquired signal ideally has values at “ $N$ ” evenly spaced wave numbers  $K = \{k_1, \dots, k_N\}$  with spacing  $\delta k = \Delta k/N$ . The maximum A-scan depth  $z_{\max}$  is given by the spectral

resolution of the “spectrometer”, that is, the number of channels per sweep range  $\Delta k$  and can be derived from the Fourier transformation theory via

$$\begin{aligned} z_{\max} &= \frac{\pi}{2n_s \delta k} \\ &= \frac{\pi}{2} \frac{N}{n_s \Delta k} \\ &= \frac{\pi N}{2n_s \Delta t \sigma_{\text{SS-OCT}}} \\ &= \frac{\pi f_s}{2n_s \sigma_{\text{SS-OCT}}} \end{aligned}$$

where  $\sigma_{\text{SS-OCT}} = \Delta k / \Delta t$ ,  $n_s$ , and  $f_s = N / \Delta t$  are the sweep rate, the average refractive index of the sample, and the analog-to-digital sampling frequency of the photodetector, respectively. These relations show that the wave number range, the sampling rate, and the sweep rate all affect the depth range  $z_{\max}$ . It should be noted that the “back-sweep” is often not much shorter than the “forward-sweep”, but cannot be used for acquisition. In this case, the A-scan time is double the sweep rate. Typically, one does not design a source but selects one for a given task and designs the appropriate acquisition system. As a consequence, we discuss a selection of three typical example sources with (each with a tunable range of 100 nm)

- a)  $1/\Delta t = 200$  kHz;  $f_s = 100$  MHz,
- b)  $1/\Delta t = 100$  kHz;  $f_s = 250$  MHz,
- c)  $1/\Delta t = 50$  kHz;  $f_s = 500$  MHz,

where  $1/\Delta t$  denotes the scan rate and  $f_s$  the sampling frequency. The appropriate SS-OCT source and the acquisition parameters for the various envisioned application ranges can now be easily selected<sup>9)</sup>. Note that if one chooses the sweep and the sampling rates freely and keeps the sweep range  $\Delta k$  fixed, the number of channels (because of  $N = \Delta k f_s / \sigma_{\text{SS-OCT}}$ ) and thus the signal-to-noise ratio (SNR) as well as the resolution vary. For the three applications to be considered, we thus conclude:

### 1. High resolution/high speed:

*Source A:* sampling rate of  $f_s = 100$  MHz, scan rate of  $1/\Delta t = 200$  kHz for an imaging range of  $z_{\max} = 1$  mm.

- Large wave number range, that is,  $\Delta k$  is maximum or  $\Delta \lambda$  is maximum, and the A-scan time ( $\Delta t$ ) is minimal.
- Bandwidth needs to be high as well as the analog-digital (A/D) sampling frequency ( $f_s$ ).
- A-scan depth is small.

### 2. Medium speed/low resolution/medium “imaging” depth:

*Source B:* sampling rate of  $f_s = 250$  MHz, scan rate of  $1/\Delta t = 100$  kHz for an imaging range of  $z_{\max} = 5.1$  mm.

9) In all cases, we assume a refractive index of  $n_s = 1.35$

### 3. Low speed/medium resolution/“ultra-deep imaging” depth:

*Source C:* sampling rate of  $f_s = 500$  MHz, scan rate of  $1/\Delta t = 50$  kHz for an imaging range of  $z_{\max} = 20$  mm. Such a light source can be used to scan the entire eye.

- Longest scan time  $\Delta t$ .
- A-scan depth is maximal.

For illustration, we determined the numerical values for the three cases above in Table S7.2.

**Table S7.2** Numerical values for the three sample applications discussed in Problem 7.3.

For all cases, we assumed an average refractive index of the sample of  $n_s = 1.35$ , a central frequency of  $\lambda_0 = 1050$  nm, a bandwidth of  $\Delta\lambda = 100$  nm,  $\lambda_{\min} = 1000$  nm,  $\lambda_{\max} = 1100$  nm,  $k_0 = 0.00598399/\text{nm}$ ,  $k_{\max} = 0.00628319/\text{nm}$ ,  $k_{\min} = 0.00571199/\text{nm}$ , and  $\Delta k = 0.0005712/\text{nm}$ .

Parameter	Application 1	Application 2	Application 3
Sampling rate $f_s$ (1/s)	$1 \times 10^8$	$2.5 \times 10^8$	$5 \times 10^8$
Scan rate $1/\Delta t$ (1/s)	$2 \times 10^5$	$1 \times 10^5$	$5 \times 10^4$
Scan time $\Delta t$ (ms)	$5 \times 10^{-3}$	$1 \times 10^{-2}$	$2 \times 10^{-2}$
Sweep rate $\sigma_{\text{SS-OCT}}$ (1/(nm s))	114	57.1	28.6
Number of channels	500	2,500	10,000
Scan depth $z_{\max}$ (mm)	1.0	5.1	20.4

## P7.4

### Group velocity delay

Calculate the group velocity delay in a Michelson interferometer for various broadband light sources:

1. SLD with  $\lambda_0 = 850$  nm and 50 nm bandwidth
2. Titanium–sapphire laser with  $\lambda_0 = 800$  nm and 70 nm bandwidth
3. SLD with  $\lambda_0 = 1050$  nm and 100 nm bandwidth

Assume the anterior chamber of the human eye to be the object (sample). Use as material the data from the Gullstrand Eye (Section 2.2.1) and treat the chamber as one slab.

### Solution:

For the calculation, we use the slab thickness of the anterior chamber from Table 2.1 of  $3.1$  mm =  $3100$   $\mu\text{m}$ . For the refractive index, we assume the values for water as obtained from the measurement data for the optical dispersion of water<sup>10</sup>. The

10) Masahiko, D. and Masumura, A. (2007) Measurement of the refractive index of distilled water from the near-infrared region to the ultraviolet region. *Appl. Opt.*, **46**, 3811–3820.

**Table S7.3** Light source parameters resulting from calculations discussed in Problem 7.4.

	Case 1: SLD	Case 2: Ti-Sapphire	Case 3: SLD
$\lambda$ ( $\mu\text{m}$ )	0.850	0.800	1.050
$\Delta\lambda$ (nm)	50	70	100
$dn/d\lambda$ ( $1/\mu\text{m}$ )	-0.008367	-0.010081	-0.004386
$\Delta t_g$ (fs)	2765	2768	2757
$\Delta\omega$ (1/fs)	0.055	0.087	0.072
$\Delta z_{\text{OCT}}$ ( $\mu\text{m}$ )	6.38	4.03	4.86

parameters to be inserted to the Sellmeier equation (6.81)

$$n(\lambda) = \sqrt{1 + \sum_{j=1}^3 \frac{B_j \cdot \lambda^2}{\lambda^2 - C_j}}$$

are at temperature of 20°C given by  $B_1 = 0.5684027565$ ,  $B_2 = 0.1726177391$ ,  $B_3 = 2.086189578 \times 10^{-2}$ ,  $C_1 = 5.101829712 \times 10^{-3}$ ,  $C_2 = 1.821153936 \times 10^{-2}$ , and  $C_3 = 2.620722293 \times 10^{-2}$ . The values for the derivatives  $dn/d\lambda$  can be obtained by calculating the model curve of refractive index  $n(\lambda)$  and numerically differentiating it on a sufficiently dense  $\lambda$ -grid. Here,  $\lambda$  must be inserted in micrometers.

We now calculate the round-trip group delay in femtoseconds (fs) via Eq. (7.32) which follows as

$$\Delta t_g = \frac{2 \cdot \Delta z}{c} \left( n - \lambda \cdot \frac{dn}{d\lambda} \right) = \frac{2 \cdot \Delta z}{c} \frac{1}{c_g}, \quad (\text{S7.10})$$

the bandwidth  $\Delta\omega$  via Eq. (7.36) in 1/fs, and the OCT resolution  $\Delta z_{\text{OCT}}$  in  $\mu\text{m}$  via Eq. (7.40). The corresponding results are listed in Table S7.3. Although the round-trip group delay is very similar in all cases, the different bandwidths lead to quite deviating OCT resolutions.

**P7.5**  
**Theory of TD-OCT**

Derive in detail Eqs. (7.34) and (7.37) from Eq. (7.28). Why is the resolution in TD-OCT half the coherence length and not the coherence length itself (Figure 7.6)?

**Solution:**

**a) Derivation of Eq. (7.34):**

We start from Eq. (7.28) in Section 7.4.1 which reads

$$I_{TD}(\Delta\xi) = R_S \operatorname{Re} \left( \int_{-\infty}^{+\infty} S(\omega) e^{-i\Delta\xi(\omega)} d\omega \right) \quad (7.28)$$

and want to derive in detail

$$I_{TD}(\Delta z) = R_S \cos(\omega_0 \Delta t_p) \int_{-\infty}^{+\infty} S(\omega) e^{-i(\omega - \omega_0) \Delta t_g} d\omega \quad (7.34)$$

For this purpose, we use from Eq. (7.32)

$$\Delta\xi = \omega_0 \Delta t_p + (\omega - \omega_0) \Delta t_g \quad (7.32)$$

in which

$$\Delta t_p = \frac{2\Delta z}{c_p} \quad \text{and} \quad \Delta t_g = \frac{2\Delta z}{c_g(\omega_0)} .$$

Therefore, we have

$$\begin{aligned} I_{TD}(\Delta z) &= R_S \operatorname{Re} \left( \int_{-\infty}^{+\infty} S(\omega) e^{-i\omega_0 \Delta t_p - i(\omega - \omega_0) \Delta t_g} d\omega \right) \\ &= R_S \operatorname{Re} \left( e^{-i\omega_0 \Delta t_p} \int_{-\infty}^{+\infty} S(\omega) e^{-i(\omega - \omega_0) \Delta t_g} d\omega \right) \\ &= R_S \operatorname{Re} \left( e^{-i\omega_0 \Delta t_p} \int_{-\infty}^{+\infty} S(\omega) [\cos((\omega - \omega_0) \Delta t_g) + i \sin((\omega - \omega_0) \Delta t_g)] d\omega \right) \\ &= R_S \operatorname{Re} \left( e^{-i\omega_0 \Delta t_p} \int_{-\infty}^{+\infty} S(\omega) \cos((\omega - \omega_0) \Delta t_g) d\omega \right) \\ &\quad + R_S \operatorname{Re} \left( i e^{-i\omega_0 \Delta t_p} \int_{-\infty}^{+\infty} S(\omega) \sin((\omega - \omega_0) \Delta t_g) d\omega \right) . \end{aligned}$$

The spectrum  $S(\omega)$  is a positive quantity and, hence, the second integrand is an odd function so that

$$\int_{-\infty}^{+\infty} S(\omega) \sin((\omega - \omega_0)\Delta t_g) d\omega = 0 .$$

The interference term therefore reduces to

$$\begin{aligned} I_{\text{TD}}(\Delta z) &= R_S \operatorname{Re} \left( e^{-i\omega_0\Delta t_p} \int_{-\infty}^{+\infty} S(\omega) \cos((\omega - \omega_0)\Delta t_g) d\omega \right) \\ &= R_S \cos(\omega_0\Delta t_p) \int_{-\infty}^{+\infty} S(\omega) \cos((\omega - \omega_0)\Delta t_g) d\omega \\ &\quad \cdot \left( \int_{-\infty}^{+\infty} S(\omega) \cos((\omega - \omega_0)\Delta t_g) d\omega + i \int_{-\infty}^{+\infty} S(\omega) \sin((\omega - \omega_0)\Delta t_g) d\omega \right) \end{aligned}$$

which finally leads to

$$I_{\text{TD}}(\Delta z) = R_S \cos(\omega_0\Delta t_p) \int_{-\infty}^{+\infty} S(\omega) e^{-i(\omega - \omega_0)\Delta t_g} d\omega . \quad (\text{S7.11})$$

**b) Derivation of Eq. (7.37):**

We assume a light source with a Gaussian spectral distribution given by

$$S(\omega) = S_0 e^{-\frac{1}{2} \left( \frac{\omega - \omega_0}{\Delta\omega_{\text{FWHM}}} \right)^2} .$$

The interference term then reads

$$\begin{aligned} I_{\text{TD}}(\Delta z) &= R_S \cos(\omega_0\Delta t_p) \int_{-\infty}^{+\infty} S_0 e^{-\frac{1}{2} \left( \frac{\omega - \omega_0}{\Delta\omega_{\text{FWHM}}} \right)^2} e^{-i(\omega - \omega_0)\Delta t_g} d\omega \\ &= R_S \cos(\omega_0\Delta t_p) \int_{-\infty}^{+\infty} S_0 e^{-\frac{1}{2} \left( \frac{\omega - \omega_0}{\Delta\omega_{\text{FWHM}}} \right)^2 - i(\omega - \omega_0)\Delta t_g} d\omega \\ &= R_S \cos(\omega_0\Delta t_p) \int_{-\infty}^{+\infty} S_0 e^{-\frac{1}{2} \left( \frac{\chi}{\Delta\omega_{\text{FWHM}}} \right)^2 - i\chi\Delta t_g} d\chi \end{aligned}$$

with  $\chi = \omega - \omega_0$ . As derived in the Problem P7.1, the final interference signal is

$$I_{\text{TD}}(\Delta z) = 4\sqrt{\pi} \Delta\omega_{\text{FWHM}} S_0 R_S \cos(\omega_0\Delta t_p) \exp\left(-\frac{\Delta\omega_{\text{FWHM}}^2 \Delta t_g^2}{2}\right) . \quad (\text{S7.12})$$

Consequently, in Michelson interferometry, the optical path difference between the two is  $OPD = 2 \Delta z$  due to the round-trip distance traveled by the wave. The axial resolution is then given by  $\Delta z = \frac{1}{2} OPD$ . On the other hand, we have

$$\Delta t_g = \frac{2\Delta z}{c_g} = t_c = \frac{L_c}{c_g}$$

from which we conclude that  $\Delta z = L_c/2$ .

## P7.6 Theory of FD-OCT

Derive in detail Eq. (7.49) from Eq. (7.47).

### Solution:

We start from Eq. (7.47) which is given by

$$I_{FD} = S(k)R_R^2 + S(k)R_R \underbrace{\int_{-\infty}^{+\infty} \hat{R}_S(z_S) e^{2ik(n_S z_S)} dz_S}_{\text{cross-correlation term}} + \frac{1}{4} S(k) \left| \int_{-\infty}^{+\infty} \hat{R}_S(z_S) e^{2ik(n_S z_S)} dz_S \right|^2. \quad (7.47)$$

At first, we normalize the coordinates according to

$$\begin{aligned} z_S &= \frac{\hat{z}_S}{2n_S}, \\ \hat{z}_S &= 2n_S z_S, \\ dz_S &= \frac{d\hat{z}_S}{2n_S} \end{aligned}$$

and only consider the evolution of the cross-correlation term.

$$\begin{aligned} I_{FD,cc}(k) &= S(k) R_R \int_{-\infty}^{+\infty} \hat{R}_S(z_S) e^{ikz_S 2n_S} dz_S \\ &= S(k) R_R \int_{-\infty}^{+\infty} \hat{R}_S \left( \frac{\hat{z}_S}{2n_S} \right) e^{ik\hat{z}_S} \frac{d\hat{z}_S}{2n_S} \\ &= \frac{S(k)R_R}{2n_S} \int_{-\infty}^{+\infty} \hat{R}_S \left( \frac{\hat{z}_S}{2n_S} \right) e^{ik\hat{z}_S} d\hat{z}_S. \end{aligned} \quad (S7.13)$$

By using the Fourier transform (A104), we obtain

$$\mathcal{F}_k\{\hat{R}_S(\hat{z}_S)\} = \int_{-\infty}^{+\infty} \hat{R}_S(\hat{z}_S) e^{ik\hat{z}_S} d\hat{z}_S .$$

Finally, the cross-correlation term in Eq. (S7.13) can be written as

$$\begin{aligned} I_{\text{FD,cc}}(k) &= \frac{S(k)R_R}{2n_S} \cdot \mathcal{F}_k \left\{ \hat{R}_S \left( \frac{\hat{z}_S}{2n_S} \right) \right\} \\ &= \frac{R_R}{2n_S} \cdot S(k) \cdot \mathcal{F}_k \left\{ \hat{R}_S \left( \frac{\hat{z}_S}{2n_S} \right) \right\} . \end{aligned} \quad (\text{S7.14})$$

The inverse Fourier transform (defined in Eq. (A105)) of a product of two functions of  $k$  is the convolution of the inverse of each of the functions (inverse convolution theorem). Hence, we derive

$$\begin{aligned} \mathcal{F}_k^{-1} \{I_{\text{FD,cc}}(k)\} &= \frac{R_R}{2n_S} \cdot \mathcal{F}_k^{-1} \left\{ S(k) \cdot \mathcal{F}_k \left\{ \hat{R}_S \left( \frac{\hat{z}_S}{2n_S} \right) \right\} \right\} \\ &= \frac{R_R}{2n_S} \cdot \mathcal{F}_k^{-1} \{S(k)\} \otimes \mathcal{F}_k^{-1} \left\{ \mathcal{F}_k \left\{ \hat{R}_S \left( \frac{\hat{z}_S}{2n_S} \right) \right\} \right\} \\ &= \frac{R_R}{2n_S} \cdot \mathcal{F}_k^{-1} \{S(k)\} \otimes \left\{ \hat{R}_S \left( \frac{\hat{z}_S}{2n_S} \right) \right\} . \end{aligned} \quad (\text{S7.15})$$

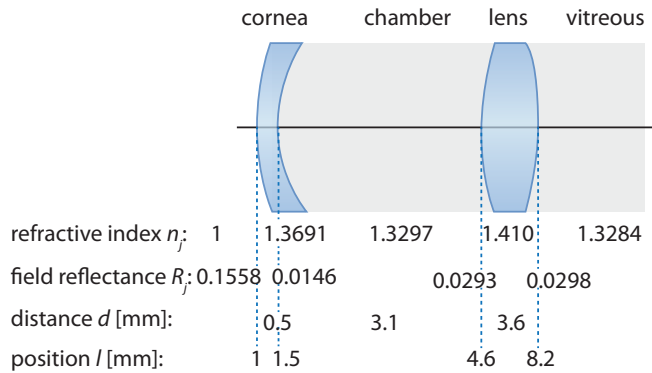


Figure S7.10 Geometry of a simplified eye model for the anterior segment.

**P7.7**

**Theory of FD-OCT**

1. Use a mathematical software tool (e.g., MATLAB or MathCad) to simulate an FD-OCT spectrum resulting from the reflections of the 4 major interfaces of the anterior segment of the eye (assumed to be  $\delta$  functions in space). Assume a Gaussian pulse of spectral bandwidth for various broadband light sources, for example, SLD with  $\lambda_0 = 1300$  nm and 200 nm bandwidth, titanium:sapphire laser with  $\lambda_0 = 800$  nm and 70 nm bandwidth, and/or SLD with  $\lambda_0 = 1050$  nm and 100 nm bandwidth. What can you say about the required resolution of the spectrometer and the dynamic range?
2. Overlay on the simulated spectra a simulated white noise spectrum. Then, Fourier transform the simulated results to obtain an A-scan of the anterior eye segment. What do you observe?

**Solution:**<sup>11)</sup>

1. The relevant geometry of the anterior segment of the eye is shown in Figure S7.10. The reflectances at the interfaces are calculated according to the Fresnel equation (A4) which reads in general

$$R_j = \left| \frac{n_j - n'_j}{n_j + n'_j} \right|^2,$$

where  $j$  denotes the position of the reflective layer. Note that, contrary to Eq. (A4), we have to take here the square root of the reflectance, since we work with field

<sup>11)</sup> Support by Rudolf von Buena (Carl Zeiss Meditec AG, Jena, Germany) greatly acknowledged.

**Table S7.3** Optical parameters of a simplified eye model for the anterior segment.

	$n_\infty$	$K$ ( $\mu\text{m}$ )	$\lambda_0$ (nm)	$\lambda$ (nm)	$n_j$	$R_j$
Cornea	1.3610	7.4147	130.0	1300	1.3673	0.1552
Anterior chamber	1.3221	7.0096	130.0	1300	1.3281	0.0146
Lens	1.3999	9.2492	130.0	1300	1.4078	0.0291
Vitreous	1.3208	6.9806	130.0	1300	1.3268	0.0296
Cornea				1050	1.3691	0.1558
Anterior chamber				1050	1.3297	0.0146
Lens				1050	1.4100	0.0293
Vitreous				1050	1.3284	0.0298
Cornea				800	1.3721	0.1569
Anterior chamber				800	1.3326	0.0146
Lens				800	1.4137	0.0295
Vitreous				800	1.3312	0.0301

amplitudes in the following formulas. Furthermore, we have to take into account that, for the various wavelengths of 1300 nm, 1050 nm, and 800 nm, the refractive indices and thus the reflectances are quite different. As an approximation, we therefore use the so-called Cornu dispersion equation given by

$$n(\lambda) = n_\infty + \frac{K}{\lambda - \lambda_0} . \quad (\text{S7.16})$$

The parameters for the simplified eye model can be found in Atchinson *et al.*<sup>12)</sup> and are presented in Table S7.3. As we can see, the variation of the refractive index with the wavelength is relatively small, as are the differences in reflectances. However, in an exact calculation, these differences would have to be taken into account. For our purposes, we use the values for 1050 nm in the following considerations. For a Gaussian pulse, the spectrum in  $k$  representation can be given by

$$S(k) = S_0 \cdot \exp \left( -4 \ln(2) \cdot \left( \frac{k - k_0}{\Delta k} \right)^2 \right) .$$

For  $\lambda_0 = 1050$  nm, there follows a mean wave number of

$$k_0 = \frac{2\pi}{\lambda_0} = 5984/\text{mm} .$$

12) Atchinson, D.A. and Smith, G. (2006) *Optics of the Human Eye*, Butterworth–Heinemann.

With a bandwidth of  $\Delta\lambda = 100$  nm (for other sources use corresponding values), this leads to

$$\Delta k = \frac{2\pi}{\lambda_0^2} \Delta\lambda = 569.9/\text{mm} .$$

The FD-OCT signal is calculated in accordance with Eq. (7.45) via

$$\begin{aligned} I(k) = & S(k) R_R^2 + 2S(k) R_R \int_{-\infty}^{+\infty} R_S(z_S) \cos(2k(n_S z_S - z_R)) dz_S \\ & + S(k) \left| \int_{-\infty}^{+\infty} R_S(z_S) e^{2ik \cdot n_S z_S} dz_S \right|^2 . \end{aligned} \quad (\text{S7.17})$$

In the derivation of Eq. (7.45), we disregarded dispersion and strong refractive index changes (compare assumption in Eq. (7.43)). Hence, in our case, Eq. (S7.17) would only be approximately correct, as in our sample the refractive index strongly varies (e.g., the index jump at the corneal surface). As a consequence, the exponent must be changed to correctly display the optical path length in the sample arm. This means that the terms  $\exp(2ik n_S z_S)$  and  $\cos[2k(n_S z_S - z_R)]$  become

$$\begin{aligned} & \exp\left(2ik \int_0^{z_S} n_S(z') dz'\right) \text{ and} \\ & \cos\left[2k \left(\int_0^{z_S} n_S(z') dz' - z_R\right)\right] , \end{aligned}$$

respectively. For our simplified anterior segment eye model, we assume the OCT “reflection” (backscattering) planes to be approximated by Dirac delta functions at positions  $z_{Sj}$  so that we have

$$R_S(z_S) = \sum_{j=1}^4 R_{Sj} \delta(z_S - z_{Sj}) . \quad (\text{S7.18})$$

Here, the index  $j$  counts the interfaces and the corresponding positions  $z_{Sj}$ . The optical path integral now becomes a sum of  $n_{Sj} z_{Sj}$  over the homogeneous layers for the 4-layer sample, that is,

$$\begin{aligned} I(k) = & S(k) R_R^2 + 2S(k) R_R \int_{-\infty}^{\infty} R_S(z_S) \cos(2k(\tilde{z}_S - z_R)) dz_S \\ & + S(k) \left| \int_{-\infty}^{\infty} R_S(z_S) e^{2ik \tilde{z}_S} dz_S \right|^2 , \end{aligned} \quad (\text{S7.19})$$

where

$$\tilde{z}_S = \int_0^{z_S} n_S(z') dz'$$

is the optical path length in the signal arm. With Eq. (S7.18), we obtain from Eq. (S7.19)

$$\begin{aligned} I(k) &= S(k)R_R^2 + 2S(k)R_R \sum_{j=1}^4 R_{Sj} \int_{-\infty}^{\infty} \delta(z_S - z_{Sj}) \cos(2k(\tilde{z}_S - z_R)) dz_S \\ &\quad + S(k) \left| \sum_{j=1}^4 R_{Sj} \int_{-\infty}^{\infty} \delta(z_S - z_{Sj}) e^{2ik\tilde{z}_S} dz_S \right|^2 \\ &= S(k)R_R^2 + 2S(k)R_R \sum_{j=1}^4 R_{Sj} \cos(2k(\tilde{z}_{Sj} - z_R)) + S(k) \left| \sum_{j=1}^4 R_{Sj} e^{2ik\tilde{z}_{Sj}} \right|^2 \end{aligned}$$

where

$$\tilde{z}_{Sj} = \int_0^{z_S} n_S(z_S) dz_S = \sum_{m=1}^j n_m(z_{Sm} - z_{S(m-1)})$$

is the optical path length for the various layers. If  $R_R = 1$  and  $z_R = 0$  are assumed, it follows that

$$\begin{aligned} I(k) &= S(k) \left( 1 + 2 \sum_{j=1}^4 R_{Sj} \cos(2k\tilde{z}_{Sj}) + \left| \sum_{j=1}^4 R_{Sj} e^{2ik\tilde{z}_{Sj}} \right|^2 \right) \\ &= S(k) \left( 1 + 2 \sum_{j=1}^4 R_{Sj} \cos \left( 2k \sum_{m=1}^j n_m(z_{Sm} - z_{S(m-1)}) \right) \right) \\ &\quad + \left| \sum_{j=1}^4 R_{Sj} \exp \left( 2ik \sum_{m=1}^j n_m(z_{Sm} - z_{S(m-1)}) \right) \right|^2 \cdot \quad (S7.20) \end{aligned}$$

Equation (S7.20) is easily programmable in MATLAB, as shown in the following script. Like in the derivation of Eq. (S7.20), the reflectance of the reference arm has been set to  $R_R = 1$  and its length to  $z_R = 0$ . A finite value of  $z_R$  only leads to a phase shift of the oscillations.

---

```
% define light source center wavelength (mm) and
bandwidth (mm)
w10 = 1050e-6; Dw1 = 100e-6;
% calculate center wave number (1/mm) and bandwidth in k
-space (1/mm)
```

```

k0 = 2*pi/wl0;
Dk = 2*pi*Dwl/(wl0^2);
% define k-grid with 20,001 points over a k-interval of
% +/- 1000/mm
Nk = 20001;
kmax = Dk;
k = k0+(-kmax:kmax/((Nk-1)/2):kmax);
komark=0:0.01:2;
% define sample interface distances, refractive indices,
% reflectances
zs = [1 1.5 4.6 8.2];
ns = [1 1.3691 1.3297 1.41006];
Rs = [0.1558 0.0146 0.0293 0.0298];
% calculate optical path length to each sample interface
opl = ns.*diff([0 zs]);
for m = 1:4; zz(m) = sum(opl(1:m)); end
% calculate spectral density function of the light
% source
S = exp(-4*log(2)*((k-k0)/Dk).^2);
% calculate simulated spectrometer signal
I1 = S.*(ones(size(k'))+2*cos(2*k'*zz)*Rs'+abs(exp(2*i*k
'*zz)*Rs')).^2);
% calculate envelope of the spectrometer signal
Imax = S*(1+2*sum(Rs)+sum(Rs)^2);
Imin = S*(1-2*sum(Rs)+sum(Rs.*[1 -1 -1 -1])^2);
% plot Figure
figure();
plot(k, I1, k, Imax, 'g', k, Imin, 'g', k, S, 'r', k0, komark, 'r');
ylim([0 1.6]);
grid on;
title('Simulated FD-OCT spectrometer signal')
xlabel('wavenumber (1/mm)')

```

Figure S7.11 shows the calculated spectrum in the  $k$ -range of 4000/mm to 5800/mm. For a better illustration, a green envelope is plotted in the diagram. The envelope of all three terms of Eq. (S7.20) is determined by

$$I(k)_{\pm} = S(k) \left( 1 \pm 2 \sum_{j=1}^4 R_{Sj} + R_{Sj}^2 + \left( R_{Sj} \pm \sum_{j=2}^4 R_{Sj} \right)^2 \right).$$

When we consider the second term of Eq. (S7.20) for the available numeric values, it becomes obvious that the term produces oscillations with  $k$ -periods of

$$k_j = \frac{\pi}{n_j z_j} = 3.14/\text{mm}, 1.52/\text{mm}, 0.51/\text{mm}, 0.27/\text{mm}.$$

Due to the different reflectances, the amplitudes of these oscillations are different. Zooming into the above signal (Figures S7.12 and S7.13) can be done via

```

figure();
plot(k, I1, k, Imax, 'g', k, Imin, 'g', k, S, 'r', k0, komark, 'r');
ylim([0 1.6]);
xlim([k0-0.001*k0 k0+0.001*k0]);

```

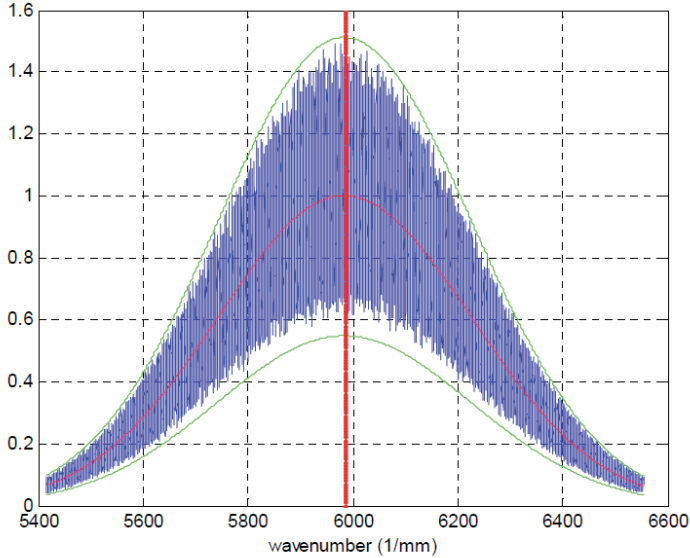


**Figure S7.11** Simulated FD-OCT spectrometer signal.

```

grid on;
title ('High resolution simulated FD-OCT spectrometer
signal')
xlabel ('wavenumber (1/mm)')
figure ();
plot(k, I1, k, I_max, 'g', k, I_min, 'g', k, S, 'r', k0, k_0mark, 'r');
ylim([0 1.6]);
xlim([k0-0.01*k0 k0+0.01*k0]);
grid on;
title ('Zoom into simulated FD-OCT spectrometer signal')
xlabel ('wave number (1/mm)')

```

In Figure S7.12, at least two periods belonging to the first and last system surfaces are evident. The large period with the large amplitude belongs to the front surface of the cornea. The third term in the signal term of Eq. (S7.20) describes the auto-interference of the surfaces. As  $R_{Sj} \ll R_R$  and reflectance  $R_{Sj}$  is squared, these signal contributions are relatively small. The superposition of signals at system surfaces 2 to 4 is shown here only as a disturbance of the oscillation of the dominant reflection at the front of the cornea.

According to the sampling theorem, the signal detector in the spectrometer must have a resolution of

$$\Delta k = \frac{k_4}{2} = 0.13/\text{mm} \text{ or}$$

$$\Delta \lambda = \frac{\lambda_0^2}{2\pi} \cdot \Delta k = 0.035 \text{ nm} .$$

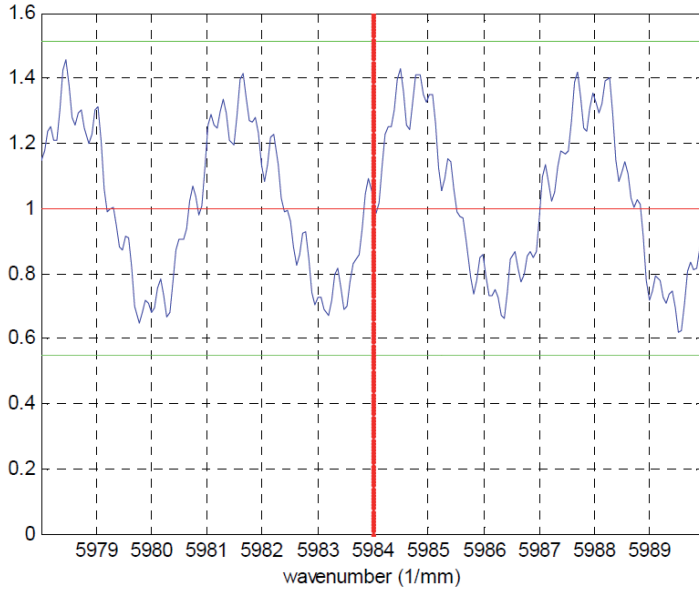


**Figure S7.12** Zoom-in into spectrum within a  $k$ -range of 5978/mm to 5990/mm.

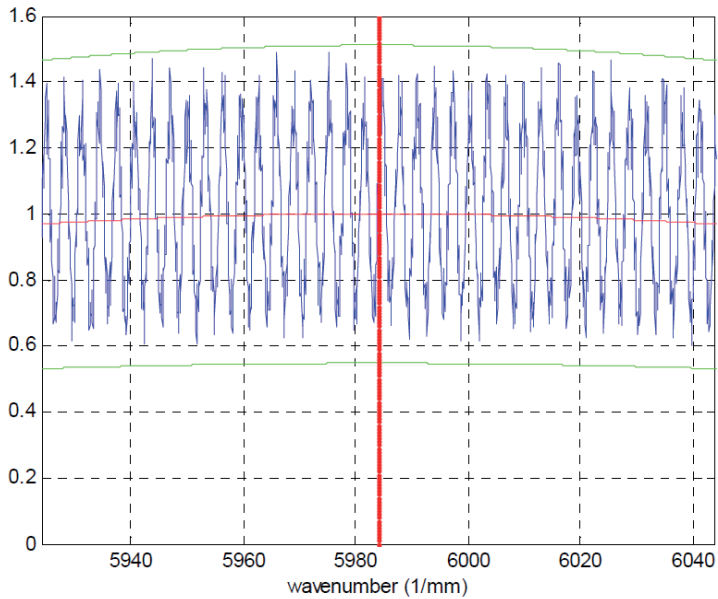


**Figure S7.13** Spectrum within a  $k$ -range of 5920/mm to 6040/mm.

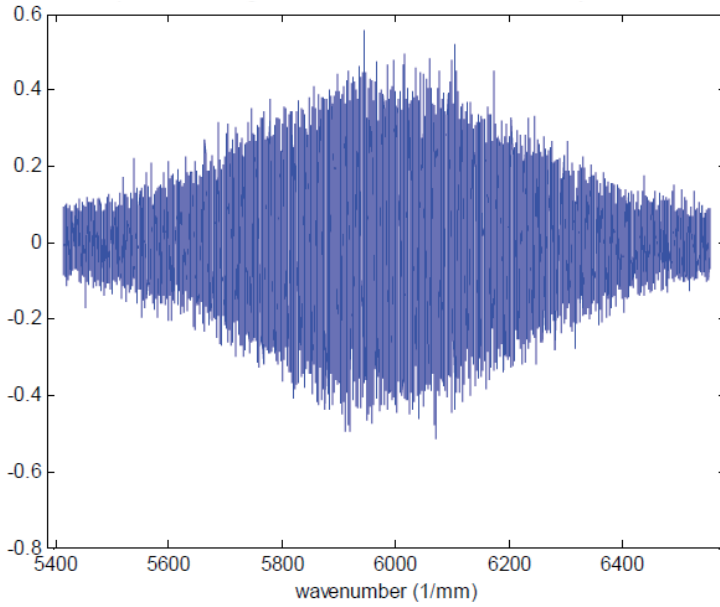


**Figure S7.14** Simulated spectrometer signal of the interference cross-term overlaid with white noise.

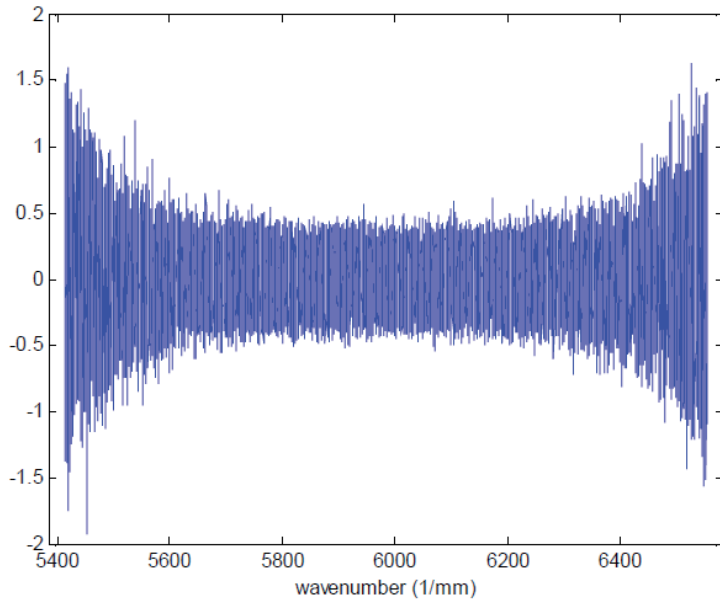


**Figure S7.15** Cross-term normalized by the source spectrum.

If, in accordance with Figure S7.11, the entire signal ( $k$ -range of  $\approx 1500/\text{mm}$ ) is to be sampled, the pixel number of the spectrometer is approximately  $1500/0.13 = 11500$ , which can normally not be realized with CCDs. Therefore, only a partial area (and thus  $z$ -distance) will be recorded. With regard to the amplitude dynamics, the measurement conditions are rather relaxed. With a 12-bit camera and 4096 levels, there are 33 levels available to sample the smallest signal amplitude of 0.0147.

- To overlay the noise, we first simulate the measured spectrometer signal with and without a  $180^\circ$  phase shift between the reference and the sample arm. After adding Gaussian white noise to each, we take the difference in order to obtain the cross-term and normalize it by the spectral density function of the source. The following MATLAB code performs a corresponding simulation (Figures S7.14 and S7.15):

---

```
% calculate simulated spectrometer signal with and
without 180° phase shift
I1 = S.*(ones(size(k'))+2*cos(2*k'*zz)*Rs'+abs(exp(2*i*k
'*zz)*Rs')).^2)';
I2 = S.*(ones(size(k'))-2*cos(2*k'*zz)*Rs'+abs(exp(2*i*k
'*zz)*Rs')).^2)';
% add white noise to both spectrometer signals
I1n = imnoise(I1/2,'gaussian',0,1e-3);
I2n = imnoise(I2/2,'gaussian',0,1e-3);
% extract intensity cross-term, normalize, and take
Fourier transform
I = (I1n-I2n);
%plot Figure
figure();
plot(k,I);
title('Simulated spectrometer signal of interference
cross-term overlaid with white noise')
xlabel('wave number (1/mm)');
xlim([k0-0.1*k0 k0+0.1*k0]);
In = I./S;
figure();
plot(k,In);
title('Cross-term signal normalized by source spectrum')
xlabel('wave number (1/mm)');
xlim([k0-0.1*k0 k0+0.1*k0]);
```

---

Note that noise dominates at the upper and lower ends of the normalized spectrometer signal. Finally, Figure S7.16 shows the resulting A-scan which clearly exhibits the four peaks from the front and back surfaces of the cornea and the front and back surfaces of the lens.

The corneal and lens thicknesses and the anterior chamber appear “stretched” by the refractive index of each layer, as the optical path length and not the biometric path length is obtained from the OCT measurement. We can assume an average index of the eye components between cornea and vitreous of  $n_{av} = 1.36$  and obtain by this calibration the approximate biometric A-scan. In Figure S7.17, the red curves show the optical path length plot as directly obtained from the Fast Fourier

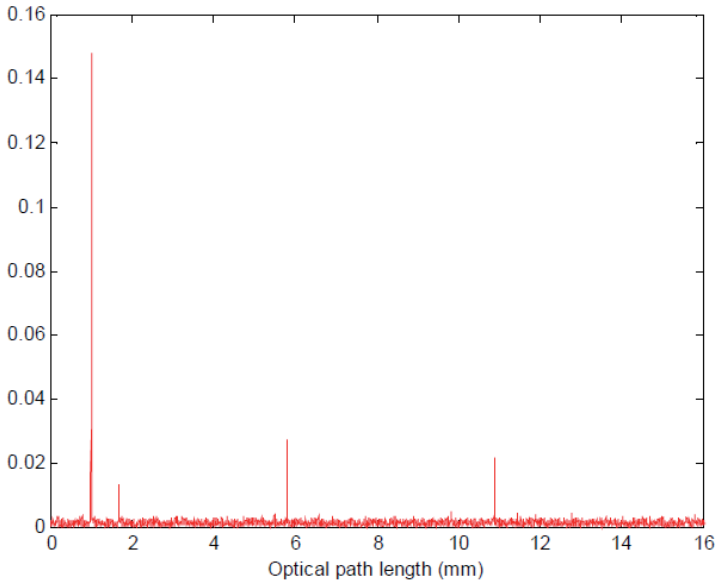


**Figure S7.16** A-Scan along the optical path length of the anterior segment of the eye.

Transform (FFT) of the spectrum and the green curve (for clarity shifted in the  $y$ -direction) an approximate “biometric” scan.

## P7.8

### Theory of SS-OCT

Let us consider an SS-OCT with 1050 nm center wavelength and a sawtooth-like sweep.

1. Simulate the detector signal for a typical sweep rate of 200 kHz and various arm length mismatches (100  $\mu\text{m}$ , 1 mm, 10 mm).
2. How does the result changes when the direction of the sweep is reversed? How, if the sweep rate is reduced to 50 kHz?
3. Use a mathematical software tool (e.g., MATLAB or MathCad) to simulate the SS-OCT spectrum resulting from the reflections of the 4 major interfaces of the anterior eye segment (assumed to be  $\delta$  functions in space). Use 1050 nm as a center wavelength and a sawtooth-like sweep with 200 kHz. Then, Fourier transform the simulated results to obtain an A-scan of the anterior segment of the eye.

Compare with the results of Problem P7.7.

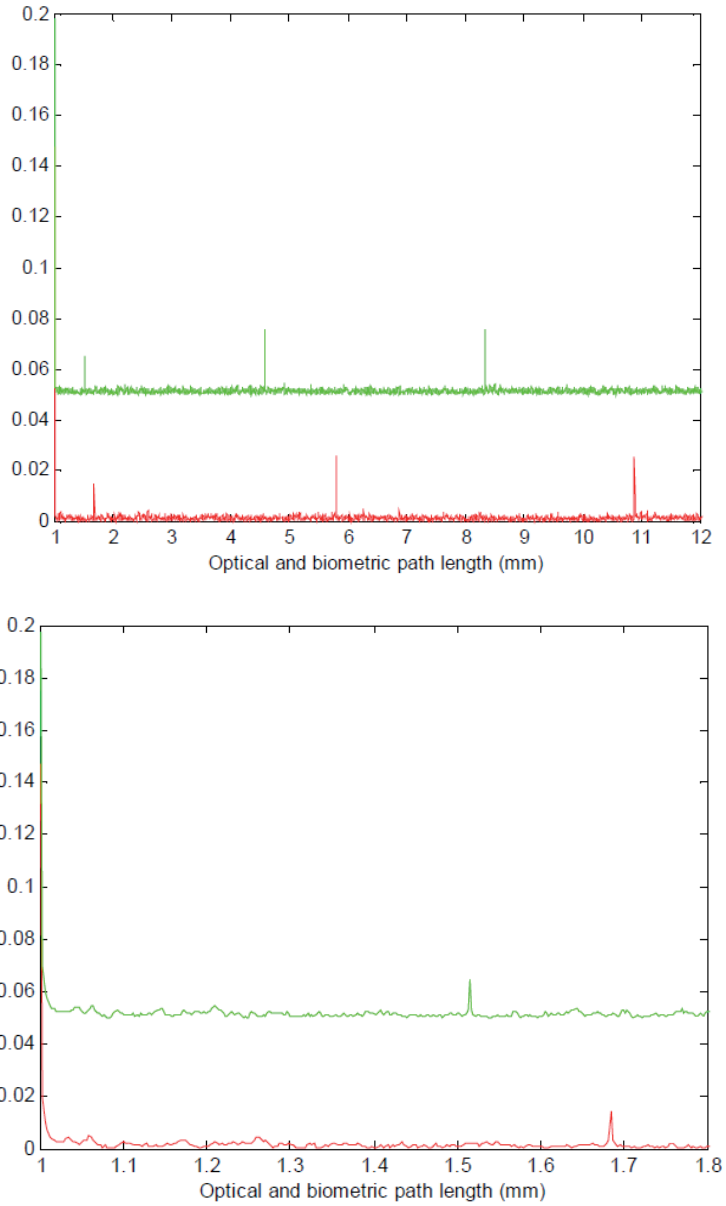


**Figure S7.17** Comparison of the (a) optical and (b) the “approximate” biometric path length, for which we assumed an average refractive index of 1.36.

**Solution:**<sup>13)</sup>

1. For comparability with Problem P7.7, we assume the swept-source tuning spectrum to have a Gaussian shape with a source bandwidth of  $\Delta\lambda_s = 100$  nm and a wavelength tuning range of  $\Delta\lambda_t = 200$  nm. In practice, this spectral “envelope” can also have a rectangular or some other shape, depending on the type of swept laser design. The resulting range of wave numbers is then  $\Delta k_t \approx 2\pi\Delta\lambda_t/\lambda_0^2 = 1140/\text{mm}$ , that is, the sweep goes from  $k_{\min} = k_0 - \Delta k_t/2 = 5414/\text{mm}$  to  $k_{\max} = k_0 + \Delta k_t/2 = 6554/\text{mm}$  with  $k_0 = 5984/\text{mm}$ .

For an anterior scan of the eye, the maximum path length difference will be in the order of  $\Delta\tilde{z} = 2n\Delta z \approx 2 \cdot 1.35 \cdot 10 \text{ mm} \approx 27 \text{ mm}$ . The required minimum number of sample points per sweep is thus  $N_{\min} = 2/\pi\Delta\tilde{z}\Delta k = 19.595$ . If we choose  $N = 20,000$  samples, the step size in  $k$ -space becomes  $\delta k = \Delta k/N = 0.057/\text{mm}$ . At 200 kHz sweep rate, we have  $\kappa = \Delta k/\Delta t = 1140 \text{ mm}^{-1}/5 \mu\text{s} = 2.28 \times 10^8/\text{mm s}$ .

The following MATLAB code simulates the corresponding  $k$ -sweep:

---

```
% define time (ms) and wave number (1/mm) axes for k-
sweep
Nk = 20000;
kmin = 5414; kmax = 6554; k0 = 5984;
Dk = kmax-kmin;
dk = Dk/Nk;
k = kmin:dk:kmax;
tmax = 0.025; dt = 0.005/Nk; tt = 0:dt:tmax;
% calculate saw-tooth k-sweep
kd = dk/dt; kk = kmin + mod(kd*tt, Dk);
% plot saw-tooth k-sweep
figure();
plot(tt*1000, kk, 'blue');
grid;
xlabel('time (microseconds)');
ylabel('wave number (1/mm)');
title('Sawtooth k-sweep')
```

---

The sawtooth wave number output is shown over 5 consecutive sweeps in Figure 1. The source spectrum is generated by the following MATLAB code and shown in Figure 2.

---

```
% define swept source tuning spectrum
l0 = 1050; D1 = 100;
Dks = 2*pi*D1/(l0)^2*1e6;
S = exp(-4*log(2).*((k-k0)/Dks).^2);
% plot swept source tuning spectrum
figure();
plot(k, S, 'blue');
xlabel('wave number (1/mm)');
ylabel('spectral density');
title('Swept-source tuning spectrum');
```

---

13) Support by Rudolf von Buena (Carl Zeiss Meditec AG, Jena, Germany) greatly acknowledged.

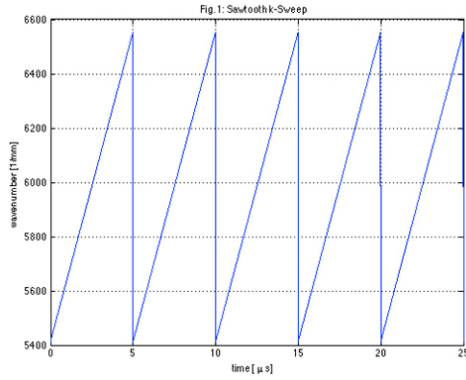


Figure S7.18 Sawtooth  $k$ -sweep of a swept-source OCT

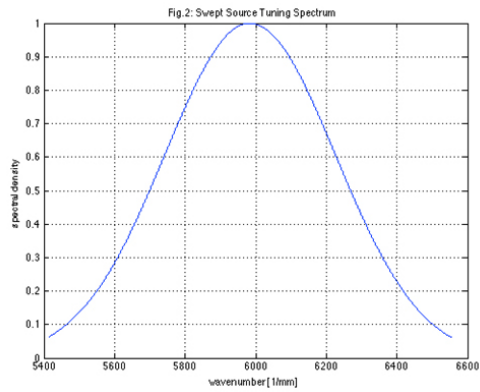


Figure S7.19 Swept-source OCT tuning spectrum

In order to derive the interference signal in a SS-OCT Michelson interferometer, we need to understand that the emitted signal at the source is “chirped”. According to Figure 1, it thus has a frequency and a wave number which varies in time like

$$\begin{aligned}\omega_i(t) &= \omega_0 + \kappa ct = \kappa c(t - t_0) \ , \\ k_i(t) &= k_0 + \kappa t = \kappa(t - t_0) \ .\end{aligned}$$

To simplify the calculation, we choose  $k_0$  and  $\omega_0$  to be zero at time  $t_0 = 0$ . We then have  $k(t) = \kappa t$  and  $\omega_i(t) = \kappa ct$ . The phase of the signal originating at  $z = 0$  at time  $t$  is then given by

$$\psi(0, t) \propto e^{i\varphi(t)}$$

with

$$\varphi(t) = \int_0^t \omega_i(t') dt' = \int_0^t \kappa ct' dt' = \kappa c \frac{t^2}{2} \ .$$

However, if we measure the signal with a detector located at some path distance  $\tilde{z}$  from the source, the amplitude of the signal  $\psi(\tilde{z}, t)$  is equal to  $\psi(0, t - \tilde{z}/c)$ , as this point on the wave train left the source at time  $t - \tilde{z}/c$ . It thus follows that

$$\psi(\tilde{z}, t) \propto e^{i\varphi(\tilde{z}, t)} = e^{i(\kappa/(2c))(\tilde{z}-ct)^2} \ . \quad (S7.21)$$

In analogy to Eqs. (7.41) and (7.42) of Chapter 7, we can re-write the wavefunctions of Eq. (S7.21) for the reference arm wave with total optical path length  $2n_R z_R$  and the sample arm wave with total optical path length  $2n_S z_S$ , which are assumed to interfere at a chosen time  $t$  at the detector via

$$\begin{aligned}\psi_R(t) &= \psi_{R,0}(k_R) R_R e^{-i\frac{\kappa}{2c}(2n_R z_R - ct)^2} \\ \psi_S(t) &= \psi_{S,0}(k_S) \int_{-\infty}^{\infty} R_S(z_S) e^{-i\frac{\kappa}{2c}(2n_S z_S - ct)^2} dz_S \ ,\end{aligned}$$

where  $R_R$  and  $R_S(z_S)$  are the reflection coefficients in the reference arm and sample arm, respectively. Note that the instantaneous angular frequencies  $\omega_R(t)$  and  $\omega_S(t)$  of the reference and sample arm waves at time  $t$  are not equal. Both waves traveled different distances and left the source at different times. This leads to the “beating” phenomenon discussed in Section 7.3.5. In analogy with Eqs. (7.44) and (7.45), we can express the detector intensity for a swept-source OCT as

$$\begin{aligned}I_{SS} &= |\psi_R(t) + \psi_S(t)|^2 \\ &\approx S(k)R_R^2 + 2S(k)R_R \int_{-\infty}^{\infty} R_S(z_S) \cos(2\kappa t(n_S z_S - n_R z_R) - \varphi_2(z_S)) dz_S \\ &\quad + S(k) \left| \int_{-\infty}^{\infty} R_S(z_S) \exp(2i\kappa t n_S z_S - \varphi_3(z_S)) dz_S \right|^2 \ .\end{aligned}$$

Here, we assumed that

$$S(k) \approx |\psi_R(\kappa_R(t))|^2 \approx |\psi_S(\kappa_S(t))|^2,$$

as  $S(k)$  is slowly varying. The time-constant phase terms  $\varphi_2(z_S)$  and  $\varphi_3(z_S)$  can be disregarded as long as we are only interested in the image amplitude  $|R_S(z_S)|$ . According to Problem 7.7, we use the simplification  $R_R = 1$  and  $z_R = 0$  to obtain

$$I_{SS}(t) = S(k) + 2S(k) \int_{-\infty}^{\infty} R_S(z_S) \cos(2\kappa t n_S z_S) dz_S + S(k) \left| \int_{-\infty}^{\infty} R_S(z_S) \exp(2i\kappa t n_S z_S) dz_S \right|^2. \quad (S7.22)$$

The following MATLAB code calculates the detector signal in Eq. (S7.22) for  $R_S = \delta(z_S - z_{Sj})$  and  $n_S = 1$  with arm length mismatches of  $z_{Sj} = 100 \mu\text{m}$ , 1 mm, and 10 mm:

---

```
% calculate detector signal for z_S = 100 microns, 1mm,
    10mm
zs = [0.1 1 10];
zoom = 0.1;
tz = tt (Nk/2*(1-zoom):Nk/2*(1+zoom)+1);
kz = k (Nk/2*(1-zoom):Nk/2*(1+zoom)+1);
Sz = S (Nk/2*(1-zoom):Nk/2*(1+zoom)+1);
Iz = (ones(3,1)*Sz) .* (1+2*cos(2*kz'*zs)+abs(exp(2*i*kz'*
    zs)).^2)';
% plot detector signal for z_S = 100 microns, 1mm, 10mm
figure();
subplot(3,1,1);
plot(tz*1000,Iz(1,:)); axis tight; grid;
title('Fig.3: Zoom into central part of detected signal
    for z_S=');
xlabel('time (\mus)'); ylabel('100 \mum');
subplot(3,1,2);
plot(tz*1000,Iz(2,:)); axis tight; grid;
xlabel('time (\mus)'); ylabel('1 mm');
subplot(3,1,3);
plot(tz*1000,Iz(3,:)); axis tight; grid;
xlabel('time (\mus)'); ylabel('10 mm');
```

---

The resulting zoom into the central range ( $0.5 \mu\text{s}$ ) of one sweep is shown in Figure S7.20.

- Reversing the direction of the frequency sweep will produce the reversed detector output, that is, the signal is “mirrored” at the center of one sweep period. Nevertheless, taking the direction of the sweep into account, the measured spectrum as a function of the wave number will be the same. If the sweep rate is slowed down from 200 kHz to 50 kHz, the detector output will be “stretched” 4-fold in time. But with proper scaling, the measured spectrum will remain the same.

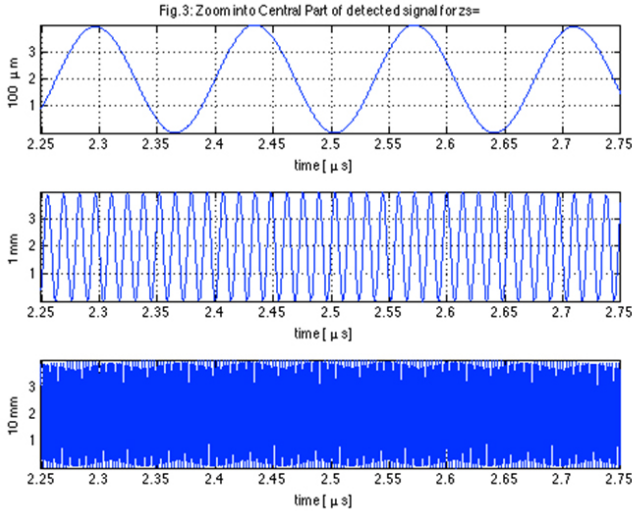


**Figure S7.20** Zoom into SS-OCT detector signal for various arm length differences  $z_{Sj} = 100 \mu\text{m}$ ,  $1 \text{ mm}$ , and  $10 \text{ mm}$ .

The reversed and stretched sweeps can be visualized with MATLAB in the following manner:

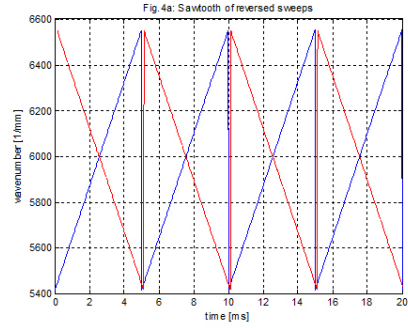
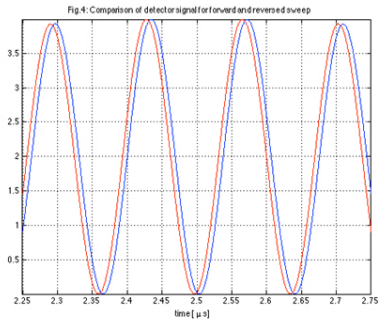
---

```
% calculate detector signal for reversed k-sweep
kr = fliplr(kz);
Ir = (ones(3,1)*Sz) .* (1+2*cos(2*kr'*zs)+abs(exp(2*i*kr'*zs)).^2)';
% calculate detector signal for stretched k-sweep
ks = kmin:dk/4:kmin+Dk/4;
kzs = ks(Nk/2*(1-zoom):Nk/2*(1+zoom)+1);
Is = (ones(3,1)*Sz) .* (1+2*cos(2*kzs'*zs)+abs(exp(2*i*kzs'*zs)).^2)';
```

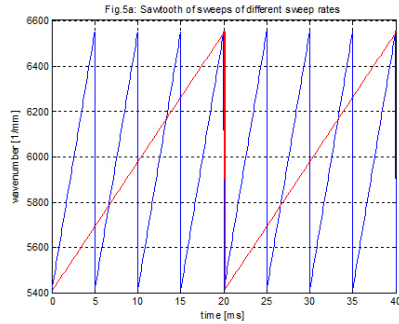
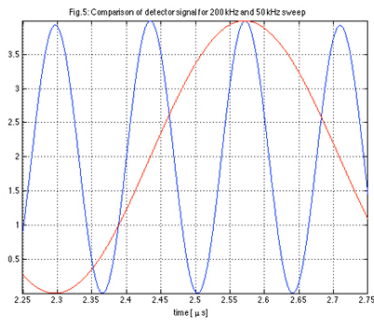
---

Figure S7.21 shows the central part of a 200 kHz sweep for  $z_{Sj} = 100 \mu\text{m}$  (blue curve) and the sawtooth of the reversed sweep at 200 kHz (red curve). Similarly, Figure S7.22 shows the comparison of a 200 kHz sweep (blue curve) for  $z_{Sj} = 100 \mu\text{m}$  and a “stretched” 50 kHz sweep (red curve).

- As in Problem P7.7, we have to replace  $n_S z_S$  in the expression for the detected signal by the path length integral over the sample arm  $\tilde{z}_S \equiv \int_0^{z_S} n_S(z) dz$  for a sample with strong refractive index variations such as the anterior segment of the



**Figure S7.21** Comparison of SS-OCT signals with forward and reverse sweep.



**Figure S7.22** Comparison of SS-OCT signals for 200 kHz and 50 kHz sweeps

eye. We have

$$I_{SS}(t) = S(k) + 2S(k) \int_{-\infty}^{\infty} R_S(z_S) \cos(2\kappa t \tilde{z}_S) dz_S + S(k) \left| \int_{-\infty}^{\infty} R_S(z_S) \exp(2i\kappa t \tilde{z}_S) dz_S \right|^2 .$$

For the first four backscattering interfaces at positions  $z_{Sj}$ , we can express the reflection coefficient via

$$R_S(z_S) = \sum_{j=1}^4 R_{Sj} \delta(z_S - z_{Sj}) .$$

The integrals in the signal intensity then become summations over these four interfaces so that

$$I_{SS}(t) = S(k) \cdot \left( 1 + 2S \sum_{j=1}^4 R_{Sj} \cos(2\kappa t \tilde{z}_{Sj}) + \left| \sum_{j=1}^4 R_{Sj} \exp(2i\kappa t \tilde{z}_{Sj}) \right|^2 \right)$$

and the path length integral can be written in terms of the four homogeneous segments

$$\tilde{z}_{Sj} = \sum_{m=1}^j n_m (z_{Sm} - z_{S(m-1)}) .$$

The final expression for the signal intensity then becomes

$$I_{SS}(t) = S(k) + 2S S(k) \sum_{j=1}^4 R_{Sj} \cos \left( 2\kappa t \sum_{m=1}^j n_m (z_{Sm} - z_{S(m-1)}) \right) + S(k) \left| \sum_{j=1}^4 R_{Sj} \exp \left( 2i\kappa t \sum_{m=1}^j n_m (z_{Sm} - z_{S(m-1)}) \right) \right|^2 . \quad (S7.23)$$

The following MATLAB code computes this signal for the distances, refractive indices, and reflection coefficients given in Problem P7.7:

---

```
% define ocular distances , refractive indices ,
    reflectivities
zs = [1 1.5 4.6 8.2];
ns = [1 1.3691 1.3297 1.4100];
Rs = [0.1558 0.0146 0.0293 0.0298];
% calculate optical path length to each ocular interface
opl = ns.*diff([0 zs]);
for m = 1:4; zz(m) = sum(opl(1:m)); end
% calculate simulated detector signal
I1 = S.*(1+2*cos(2*k'*zz)*Rs'+abs(exp(2*i*k'*zz)*Rs')
    .^2)';
% calculate envelope of the detector signal
Imax = S*(1+2*sum(Rs)+sum(Rs)^2);
Imin = S*(1-2*sum(Rs)+sum(Rs.*[1 -1 -1 -1])^2);
% plot detector signal as a function of time
figure();
t = 1000*tt(1:Nk+1);
plot(t, I1, 'blue', t, S, 'red', t, Imin, 'green', t, Imax, 'green'
)
axis([0 5 0 1.6]); grid
xlabel('time (\mus)')
title('Simulated SS-OCT detector signal as a function of
    time')
```

---

Figure S7.23a shows the simulated detector signal as a function of time over one sweep together with its envelope (green) and the source spectrum envelope (red).

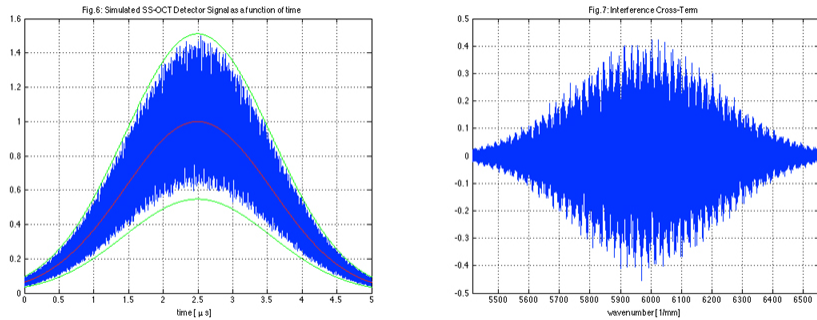


**Figure S7.23** (a) Simulated SS-OCT detector signal as a function of time. (b) Interference cross-term of SS-OCT as a function of the wave number  $k$ .

Like for frequency-domain OCT (FD-OCT), the interference cross-term can be extracted by subtracting a second detector signal with a  $180^\circ$  phase shift between the two arms of the interferometer. The resulting difference signal is then normalized by the source spectrum as shown in the following section of MATLAB code:

---

```
% calculate simulated detector signal with 180° phase
shift
I2 = S .* (1 - 2 * cos(2 * k' * z z) * Rs' + abs(exp(2 * i * k' * z z) * Rs')
.^2)';
% extract cross-term and normalize by the source
spectrum
I = (I1 - I2) / 2;
In = I ./ S;
% plot interference cross-term as a function of wave
number
figure();
plot(k(1:5:Nk), I(1:5:Nk)); axis([min(k) max(k) -.5 .5]);
grid
xlabel('wave number (1/mm)')
title('Interference cross-term')
```

---

The cross-term is plotted as a function of the wave number in Figure S7.23b. Note that by moving from Figure S7.23a to Figure S7.23b, the  $x$ -axis is converted from time to wave number taking the functionality displayed in Figure S7.18 into account.

Taking the Fourier transform of the normalized cross-term yields the A-scan as a function of path length, whereas the spatial coordinate has to be scaled properly. This is accomplished with the following MATLAB commands, which create the A-scan plotted in Figure S7.24:

---

```
% take Fourier transform and determine z-scaling
FT = abs(iff( In ));
dz = pi / Dk; zn = 0 : dz : dz * Nk;
% plot A-scan obtained by Fourier transform
```

---

```
figure ();
plot (zn, FT, 'red'); grid; axis ([0 16 0 0.16]);
xlabel ('optical path length (mm)')
title ('A-Scan obtained by Fourier transformation')
```

We note the agreement with the A-scan obtained in Problem P7.7.

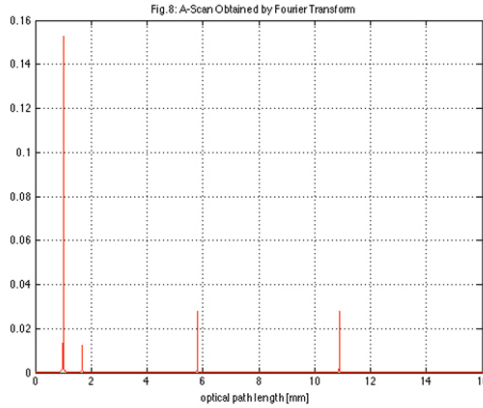


**Figure S7.24** A-scan derived from simulated SS-OCT signal.

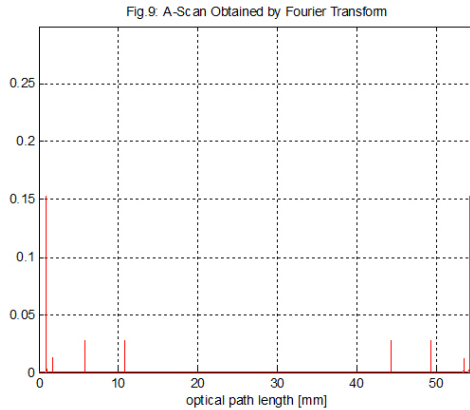


**Figure S7.25** A-scan from simulated SS-OCT signal with mirror image.

Let us compare this with the results of Problem P7.7. We observe that the equations describing the FD-OCT and SS-OCT cases share the same general form, where  $k(t) = \kappa t$  replaces the (time-)constant wave number  $k$ . In Figure S7.25, we have also plotted the absolute magnitude of the Fast Fourier Transform (FFT) for the entire  $z$ -range. As expected from the FFT formalism, we see the so-called mirror-image of the reflections along  $z$ . This is due to the fact that the FFT of a real signal is conjugate symmetric.

**P7.9****Group velocity dispersion in OCT**

We assume Gaussian pulses of spectral bandwidths for various broadband light sources (e.g., those considered in Problem P7.4.).

1. One of the arms of the OCT Michelson interferometer contains glass (type BK7) with a (geometric) length of 10 cm. What axial loss in resolution results from the group velocity dispersion (GVD) as compared to an “empty” OCT?
2. Use the results of 1.) to estimate how much BK7 glass you must place into the reference arm of the OCT to compensate for the GVD of the eye in the signal arm. What would be even better than BK7? As an approximate model of the human eye, we assume as slab with a length of 24.4 mm having the same dispersion as water (aqueous humor).

**Solution:**

1. If material with a group velocity dispersion (GVD, see Section 7.4.3) is present in one arm of the OCT’s Michelson interferometer, the axial resolution decreases. This is due to the fact that the GVD causes frequency-dependent phase delays which in TD-OCT broaden the pulse and/or lead to destructive interference in FD-OCT. Let us consider a TD-OCT setup that contains glass (BK7) with a length of 10 cm in its signal arm. The reference arm is assumed to be “empty”, that is  $n = 1$ .

**a) Pulse and spectral parameters:**

A bandwidth of  $\Delta\lambda = 200$  nm leads to

$$\Delta\omega = \frac{2\pi c}{\lambda_0^2} \Delta\lambda .$$

For a Gaussian-shaped pulse, the power spectral density is given by (see also Problem P7.2)

$$\sigma(\omega) = \sigma_0 \cdot \exp\left(-4 \ln(2) \left(\frac{\omega - \omega_0}{\Delta\omega_{\text{FWHM}}}\right)^2\right) . \quad (\text{S7.24})$$

**b) Taylor expansion of the propagation constant up to the quadratic term:**

The Taylor expansion of the wave number dispersion up to the quadratic term in the signal arm reads

$$\begin{aligned} k_{\text{S}}(\omega) &= k(\omega_0) + \left. \frac{\partial k(\omega)}{\partial \omega} \right|_{\omega=\omega_0} \cdot (\omega - \omega_0) + \left. \frac{1}{2} \frac{\partial^2 k(\omega)}{\partial \omega^2} \right|_{\omega=\omega_0} \cdot (\omega - \omega_0)^2 \\ &= k(\omega_0) + k'(\omega_0) \cdot (\omega - \omega_0) + \frac{1}{2} k''(\omega_0) \cdot (\omega - \omega_0)^2 \end{aligned} \quad (\text{S7.25})$$

with

$$\begin{aligned}
 k_0 &= k(\omega) , \\
 k'(\omega_0) &= \left. \frac{\partial k(\omega)}{\partial \omega} \right|_{\omega=\omega_0} , \text{ and} \\
 k''(\omega_0) &= \left. \frac{\partial^2 k(\omega)}{\partial \omega^2} \right|_{\omega=\omega_0} .
 \end{aligned}$$

In the empty reference arm ( $n = 1$ ), we have

$$k_R(\omega) = k_0 + \frac{(\omega - \omega_0)}{c} . \quad (\text{S7.26})$$

**c) Auxiliary calculation:  $k$ -derivatives from the wavelength dependence of the refractive index:**

We start from

$$k_0 = k(\omega_0) = \frac{2\pi \cdot n(\lambda_0)}{\lambda_0} . \quad (\text{S7.27})$$

Thus, for the first derivative, we obtain

$$\begin{aligned}
 k'(\omega_0) &= \left. \frac{\partial k(\omega)}{\partial \omega} \right|_{\omega=\omega_0} \\
 \frac{dk}{d\omega} &= \frac{d\lambda}{d\omega} \cdot \frac{dk}{d\lambda} = -\frac{2\pi c}{\omega^2} \cdot \frac{dk}{d\lambda} = -\frac{\lambda^2}{c} \cdot \frac{d\left(\frac{n(\lambda)}{\lambda}\right)}{d\lambda} \\
 &= -\frac{\lambda^2}{c} \left( \frac{1}{\lambda} \cdot \frac{dn}{d\lambda} - \frac{n}{\lambda^2} \right) \\
 &= \frac{1}{c} \left( n - \lambda \cdot \frac{dn}{d\lambda} \right) = \frac{1}{c_g} . \quad (\text{S7.28})
 \end{aligned}$$

From this follows the second derivative according to

$$\begin{aligned}
 k''(\omega_0) &= \left. \frac{\partial k'(\omega)}{\partial \omega} \right|_{\omega=\omega_0} \\
 \frac{d^2k}{d\omega^2} &= \frac{d\lambda}{d\omega} \cdot \frac{dk'}{d\lambda} = -\frac{2\pi c}{\omega^2} \cdot \frac{dk'}{d\lambda} = -\frac{\lambda^2}{c} \cdot \frac{1}{2\pi c} \cdot \frac{d\left(n - \lambda \cdot \frac{dn}{d\lambda}\right)}{d\lambda} \\
 &= -\frac{\lambda^2}{2\pi c^2} \left( \frac{dn}{d\lambda} - \frac{dn}{d\lambda} - \lambda \cdot \frac{d^2n}{d\lambda^2} \right) \\
 &= \frac{\lambda^3}{2\pi c^2} \cdot \frac{d^2n}{d\lambda^2} \quad (\text{S7.29})
 \end{aligned}$$

To determine the derivatives of the refractive indices for BK7 at a wavelength of  $\lambda = 1300$  nm, the Sellmeier dispersion formula (see also Problem P6.5)

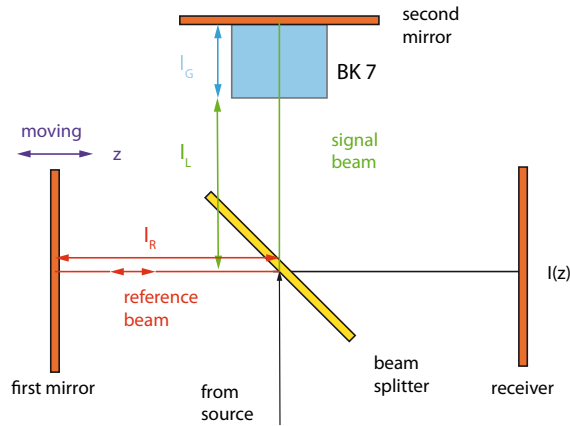


**Figure S7.26** Setup of a Michelson interferometer consisting of a reference and a signal arm. In the signal arm, a block of BK7 glass is placed.

with three terms

$$n(\lambda) = \sqrt{1 + \sum_{j=1}^3 \frac{B_j \lambda^2}{\lambda^2 - C_j}} \quad (\text{S7.30})$$

can be used for calculation of the refractive indices of glass in the visible and infrared ranges. This leads to the constants ( $\lambda$  to be inserted in  $\mu\text{m}$ )  $B_1 = 1.03961212$ ,  $B_2 = 0.231792344$ ,  $B_3 = 1.01046945$ ,  $C_1 = 6.00069867$ ,  $C_2 = 2.00179144 \times 10^{-2}$ , and  $C_3 = 1.03560653 \times 10^2$ . The values for the derivatives  $dn/d\lambda$  and  $d^2n/d\lambda^2$  can be obtained by calculating the model curve of the refractive index  $n(\lambda)$  and numerically differentiating once and twice on an accordingly dense  $\lambda$ -grid, respectively.

**d) Calculation of the phase difference between signal arm and reference arm:**

The dispersion-related phase difference between signal and reference arm is given by

$$\Delta\xi(\omega) = k_L(\omega) \cdot 2z_L + k_G(\omega) \cdot 2z_G - k_R(\omega) \cdot 2z_R, \quad (\text{S7.31})$$

where the index  $G$  stands for “glass” and  $L$  for “left empty”. Using the expansions from Eqs. (S7.25) and (S7.26) leads to

$$\begin{aligned} \Delta\xi(\omega) &= k_L(\omega_0) \cdot 2z_L + k_G(\omega_0) \cdot 2z_G - k_R(\omega) \cdot 2z_R \\ &\quad + k'_G(\omega_0) \cdot (\omega - \omega_0) \cdot 2z_G - \frac{1}{c} \cdot (\omega - \omega_0) \cdot 2z_R \\ &\quad + \frac{1}{2} k''_G(\omega_0) \cdot (\omega - \omega_0)^2 \cdot 2z_G. \end{aligned} \quad (\text{S7.32})$$

Due to the free choice of  $z_R$  and  $z_L$ , Eq. (S7.32) expressing the phase delay between both arms can be simplified via

$$\Delta\xi(\omega) = \omega_0 \Delta t_p + (\omega - \omega_0) \cdot \Delta t_g + \frac{1}{2} k_G''(\omega_0) \cdot (\omega - \omega_0)^2 \cdot 2z_G . \quad (\text{S7.33})$$

The parameters  $\Delta t_p$  and  $\Delta t_g$  can now be calculated according to Eq. (7.32), that is,

$$\Delta t_p = \frac{k_L(\omega_0) \cdot 2z_L + k_G(\omega_0) \cdot 2z_G - k_R(\omega_0) \cdot 2z_R}{\omega_0} ,$$

$$\Delta t_g = k_G'(\omega_0) \cdot 2z_G - \frac{1}{2\pi c} \cdot 2z_R .$$

If we compare this result with Eq. (7.32), there is a component in the phase response between both arms which is not linear with  $\omega$  and thus changes the interference signal for  $\Delta\phi = 0$ , as compared to the case of two arms with disappearing GVD or equal GVD (expressed by  $k''$ ). Let us now calculate the effect of this asymmetry in the GVD on the OCT signal.

#### e) Calculation of the OCT signal in the presence of GVD:

As shown in Section 7.4.1, the OCT signal is given by

$$I_{\text{TD}}(\Delta\xi) = R_S \text{Re} \left( \int_{-\infty}^{+\infty} S(\omega) e^{-i\Delta\xi(\omega)} d\omega \right) . \quad (\text{7.28})$$

Insertion of Eqs. (S7.33) and (S7.24) into Eq. (7.28) yields

$$I_{\text{TD}}(\Delta\xi) = S R_S \text{Re} \left( e^{-i\omega_0 \Delta t_p} \int_{-\infty}^{+\infty} \exp \left( -4 \ln(2) \left( \frac{\omega - \omega_0}{\Delta\omega_{\text{FWHM}}} \right)^2 - i(\omega - \omega_0) \Delta t_g - i \frac{k_G''}{2} (\omega - \omega_0)^2 \cdot 2z_G \right) d\omega \right) .$$

With the transformation  $\omega - \omega_0 \rightarrow \omega$ , completing the square in the exponent, and  $k'' = k_G''$ , we deduce

$$I_{\text{TD}}(\Delta\xi) = S R_S \text{Re} \left( e^{-i\omega_0 t_p} \int_{-\infty}^{+\infty} \exp \left( -4 \ln(2) \left( \frac{\omega}{\Delta\omega_{\text{FWHM}}} \right)^2 - i\omega \cdot \Delta t_g - i k'' \omega^2 z_G \right) d\omega \right)$$

$$= S R_S \text{Re} \left( e^{-i\omega_0 t_p} \exp \left( -\frac{1}{4} \frac{\Delta t_g^2}{\beta^2} \right) \int_{-\infty}^{+\infty} \exp \left( -\beta^2 \left( \omega + \frac{i\Delta t_g}{2\beta^2} \right)^2 \right) d\omega \right) , \quad (\text{S7.34})$$

where

$$\beta^2 = \frac{4 \ln(2)}{\Delta\omega_{\text{FWHM}}^2} + ik''l_G .$$

With the integral relation

$$\int_{-\infty}^{+\infty} e^{-\beta^2 x^2} dx = \frac{\sqrt{x}}{\beta} ,$$

Eq. (S7.34) can be written as

$$I_{\text{TD}}(\Delta\xi) = S R_S \text{Re} \left( e^{-i\omega_0 t_P} \underbrace{\frac{\sqrt{\pi}}{\sqrt{4 \ln(2)/\Delta\omega_{\text{FWHM}}^2 + ik''z_G}}}_{\text{term I}} \cdot \underbrace{\exp\left(-\frac{1}{4} \frac{\Delta t_g^2}{4 \ln(2)/\Delta\omega_{\text{FWHM}}^2 + ik''z_G}\right)}_{\text{term II}} \right) . \quad (\text{S7.35})$$

Equation (S7.35) represents the OCT signal in the presence of GVD in the signal arm. Term I describes the damping of the signal amplitude, while term II describes the envelope of the axial PSF of the OCT in accordance with Eq. (7.37) for the “empty” interferometer. Evidently, the signal is broadened as compared to the “empty” Michelson. The envelope of Eq. (7.37) given by

$$\exp\left(-\frac{1}{2} \frac{\Delta t_g^2}{8 \ln(2)/\Delta\omega_{\text{FWHM}}^2}\right)$$

turns into

$$\exp\left(-\frac{1}{2} \frac{\Delta t_g^2}{8 \ln(2)/\Delta\omega_{\text{FWHM}}^2 + 2ik''z_G}\right) .$$

In addition to broadening, the complex denominator also generates frequency modulation (chirp). For  $\sigma_\tau^2 = 8 \ln(2)/\Delta\omega^2$  and  $\tau_{\text{GVD}}^2 = 2k''z_G$ , the broadening is determined by

$$\begin{aligned} \frac{1}{\sigma_\tau^2 + i\tau_{\text{GVD}}^2} &\stackrel{!}{=} \frac{\sigma_\tau^2}{\sigma_\tau^4 + \tau_{\text{GVD}}^4} - i \frac{\tau_{\text{GVD}}^2}{\sigma_\tau^4 + \tau_{\text{GVD}}^4} , \\ \tilde{\sigma}_\tau &= \sigma_\tau \cdot \sqrt{1 + \left(\frac{\tau_{\text{GVD}}^2}{\sigma_\tau^2}\right)^2} \\ &= \frac{2\sqrt{2 \ln(2)}}{\Delta\omega} \cdot \sqrt{1 + \left(\frac{k''z_G \Delta\omega_{\text{FWHM}}^2}{4 \ln 2}\right)^2} . \end{aligned} \quad (\text{S7.36})$$

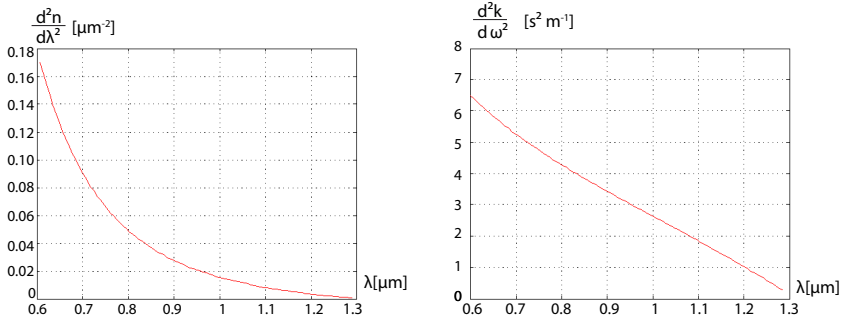


**Figure S7.26** Numerically calculated dispersion of BK 7.

**Table S7.4** Numerically calculated parameters for typical OCT wavelengths.

Wavelength (nm)	$d^2n/d\lambda^2$ ( $\mu\text{m}^{-2}$ )	$k''$ ( $\text{s}^2\text{m}^{-1}$ )	Resolution $\Delta z$ without GVD ( $\mu\text{m}$ )	Loss is resolution $\delta z$ with GVD ( $\mu\text{m}$ )
850	0.036651	$3.980 \times 10^{-26}$	2.71	1051.0
1000	0.015464	$2.735 \times 10^{-26}$	3.75	519.0
1300	0.005598	$2.165 \times 10^{-27}$	6.32	19.1

Conversion to coherence lengths leads to

$$c\Delta t_g = \Delta L_c \stackrel{!}{=} 2c\sigma_\tau, \\ \Delta \tilde{L}_c \stackrel{!}{=} 2c \cdot \tilde{\sigma}_\tau.$$

According to Eq. (S7.36), the loss in axial resolution of the OCT thus yields

$$\delta L_c = \Delta \tilde{L}_c - \Delta L_c \\ = 4c \frac{\sqrt{2 \ln(2)}}{\Delta \omega_{\text{FWHM}}} \cdot \left( \sqrt{1 + \left( \frac{k'' \cdot \Delta \omega_{\text{FWHM}}^2 z_G}{4 \ln(2)} \right)^2} - 1 \right). \quad (\text{S7.37})$$

**f) Numerical calculation:**

Equation (S7.29) provides to the constant  $k''$  for the various wavelengths. In Figure S7.26,  $d^2n/d\lambda^2$  is specified in  $\mu\text{m}^{-2}$  and  $k'' = d^2k/d\omega^2$  in  $\text{s}^2\text{m}^{-1}$ . For the various wavelengths, we obtain the results listed in Table S7.4. Figure S7.27 shows the broadening of the axial PSF  $\delta l - c$  versus the wavelength according to Eq. (S7.37). It is evident that the GVD almost disappears at  $\lambda = 1300$  nm, but is not negligible in the visible range. Consequently, at around 1300 nm, we find no noticeable pulse broadening.

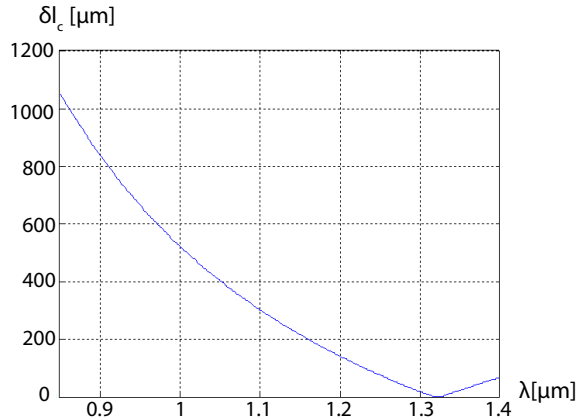


Figure S7.27 Broadening of the axial PSF according to Eq. (S7.37).

## 2. The parameters for the Sellmeier equation

$$n(\lambda) = \sqrt{1 + \sum_{j=1}^3 \frac{B_j \lambda^2}{\lambda^2 - C_j}}$$

for the refractive index the values can be obtained from the measurement data for the optical dispersion of water<sup>14</sup>. They read  $B_1 = 0.5684027565$ ,  $B_2 = 0.1726177391$ ,  $B_3 = 2.086189578 \times 10^{-2}$ ,  $C_1 = 5.101829712 \times 10^{-3}$ ,  $C_2 = 1.821153936 \times 10^{-2}$ , and  $C_3 = 2.620722293 \times 10^{-2}$ .

The values for the derivatives  $dn/d\lambda$  can be obtained by calculating the model curve of refractive index  $n(\lambda)$  and numerically differentiating it on a sufficiently dense  $\lambda$ -grid. The diagram in Figure S7.28a shows the wavelength-dependence of the refractive index of water and the various operating wavelengths of typical OCT systems.

The second derivative of the refractive index with respect to  $\lambda$  (Figure S7.28b, left graph) – which corresponds to the curvature of  $n(\lambda)$  – is responsible for the GVD effects. The right graph in Figure S7.28b shows the constant  $k'' = d^2k/d\omega^2$  in units of  $10^{-27} \text{ s}^2 \text{ m}^{-1}$  for BK7 (red) and water/eye tissue (blue). According to Eq. (S7.32), GVD compensation occurs if a material is inserted into the reference arm such that the product  $k''_A z_A = k''_G z_G$  remains constant. It is evident that the different signs of  $k''$  at 1300 nm make compensation impossible for BK7 (Table S7.5). In this case, the best solution is to use a water cuvette. At the other wavelengths, good compensation is possible. Of course, the calculations are only approximations, since ocular tissue has not been taken into account.

14) Masahiko, D. and Masumura, A. (2007) Measurement of the refractive index of distilled water from the near-infrared region to the ultraviolet region. *Appl. Opt.*, **46**, 3811–3827.

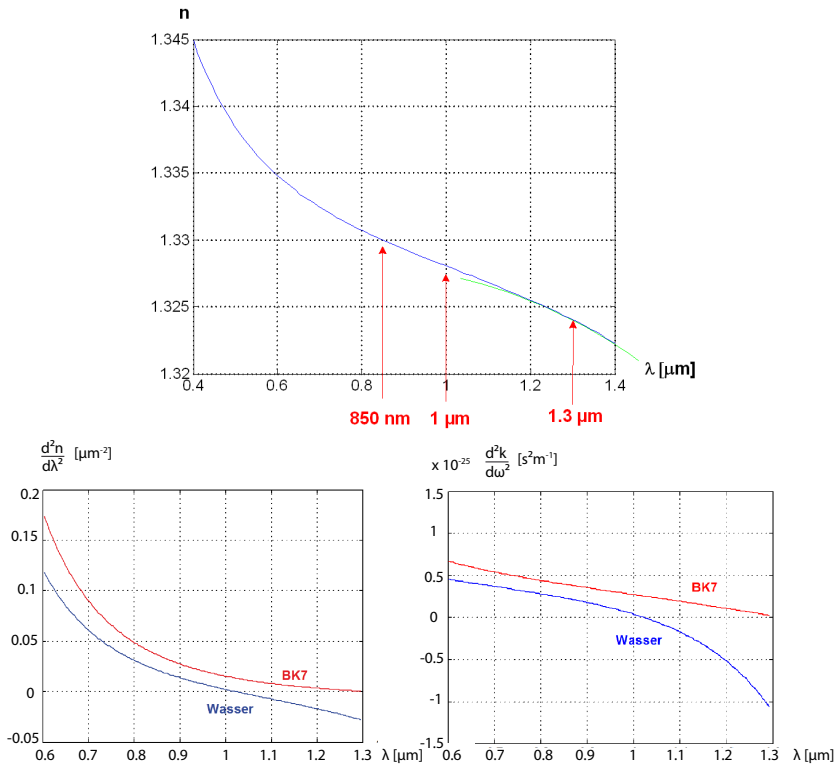


Figure S7.28 (a) Refractive index profile  $n(\lambda)$  of water. (b) Dispersion of water in comparison to BK7.

Table S7.5 Dispersion for typical OCT wavelengths.

Wavelength (nm)	$k''_A$	$k''_G$	$z_G/z_A$	$z_G$ (mm)
850	2.342	3.980	0.588	14.4
1000	0.417	2.735	0.152	3.72
1300	-10.879	0.217	impossible	impossible

**P7.10****Signal-to-noise ratio**

Calculate the SNR for TD-OCT, FD-OCT, and SS-OCT for shot-noise limited detection (see Eqs. (7.58) and (7.59)).

**Solution:**<sup>15)</sup>

We define the signal-to-noise ratio (SNR) as the signal power divided by the noise process variance. As the autocorrelation function of a signal and its frequency spectrum are linked via the Wiener-Khinchin theorem (Section A.2.4.2), an analogous relationship also applies in optics for the optical spectrum and the wave function. This means that we can expand our TD-OCT theory to an appropriate FD-OCT theory and vice versa.

**a) Time Domain:**

We start with

$$\psi_R(\omega) = \psi_{R,0}(\omega) R_R e^{2ik_R(\omega)z_R - i\omega t} , \quad (7.41)$$

$$\psi_S(\omega) = \psi_{S,0}(\omega) \int_{-\infty}^{+\infty} R_S(z_S) e^{2ik_S(\omega)z_S - i\omega t} dz_S . \quad (7.42)$$

The variables  $R_R$  and  $R_S$  denote the reflectance in the reference and sample arms, respectively. In the following, we describe the backscattering planes (indicated by  $i$ ) in the sample by sequence of planes with backscattering coefficients  $R_S(z_S)$  at position  $z_{S_i}$ , that is,  $R_S(z_S) = \sum_i R_S(z_{S_i})\delta(z_S - z_{S_i})$ . Therefore, the backscattered field is given by

$$\psi_S(\omega) = \psi_{S,0}(\omega) \sum_i R_S(z_{S_i}) e^{2ik_S(\omega)z_{S_i} - i\omega t} . \quad (S7.38)$$

The detector photocurrent is defined as

$$I_D(\omega) = \frac{e\eta}{h\nu_0} \langle |\psi_R(kc) + \psi_S(kc)|^2 \rangle , \quad (S7.39)$$

where the angular brackets denote integration over the response time of the detector,  $k = 2\pi/\lambda = \omega/c$  the wave number,  $e$  the electric charge,  $\eta$  the detector quantum efficiency,  $h$  Planck's constant and  $\nu_0$  the mean frequency of the power

<sup>15)</sup> Support by Herbert Gross (Friedrich Schiller Universitaet Jena, Germany) greatly acknowledged.

spectrum. Inserting Eq. (S7.38) into Eq. (S7.39) leads to

$$\begin{aligned}
 I_D(k) = & \frac{e\eta}{h\nu_0} \left[ S(k)(R_R^2 + R_{S1}^2 + R_{S2}^2 + \dots) \right] \\
 & + \frac{e\eta}{h\nu_0} \left[ S(k) \sum_i R_R R_S(z_{Si}) [2 \cos(2k(n_S z_{Si} - z_R))] \right] \\
 & + \frac{e\eta}{h\nu_0} \left[ S(k) \sum_i R_S(z_{Sj}) R_S(z_{Si}) [2 \cos(2k(n_S z_{Si} - n_S z_{Sj}))] \right]
 \end{aligned} \tag{S7.40}$$

$S(k) = \langle |\psi_{S,0}(\omega)|^2 \rangle = \langle |\psi_{R,0}(\omega)|^2 \rangle$  is the power spectral density of the light source. Here, a Gaussian spectrum is considered so that

$$S(k) = \exp \left( -4 \ln(2) \left( \frac{k - k_0}{\Delta k_{\text{FWHM}}} \right)^2 \right). \tag{S7.41}$$

In TD-OCT, the wave number-dependent detector current  $I_D(k)$  is captured on a single receiver while the reference delay  $z_R$  is scanned to reconstruct an approximation for the internal sample reflectance profile  $R_S(z_S)$ . The A-scan is obtained by summing Eq. (S7.40) over all wave numbers  $k$ . Hence, we have

$$\begin{aligned}
 I_D(z_R) = & \frac{e\eta}{h\nu_0} \underbrace{S(k)(R_R^2 + R_{S1}^2 + R_{S2}^2 + \dots) \int_0^\infty S(k) dk}_{\text{term I}} \\
 & + \frac{e\eta}{h\nu_0} \underbrace{\int_0^\infty S(k) \sum_i R_R R_S(z_{Si}) [2 \cos(2k(n_S z_{Si} - z_R))] dk}_{\text{term II}} \\
 & + \frac{e\eta}{h\nu_0} \underbrace{\int_0^\infty S(k) \sum_{i \neq j} R_S(z_{Sj}) R_S(z_{Si}) [2 \cos(2k(n_S z_{Si} - n_S z_{Sj}))] dk}_{\text{term III}}.
 \end{aligned} \tag{S7.42}$$

Term II in Eq. (S7.42) contains all the information about the backscattering. It is also called the interference or cross-correlation term. Let us first evaluate the

integral of this second term:

$$\begin{aligned}
 & \frac{e\eta}{h\nu_0} \int_0^\infty S(k) \sum_i R_R R_S(z_{S_i}) [2 \cos(2k(n_S z_{S_i} - z_R))] dk \\
 &= 2 \frac{e\eta}{h\nu_0} \sum_i R_R R_S(z_{S_i}) \int_0^\infty S(k) \cos(2k(n_S z_{S_i} - z_R)) dk \\
 &= 2 \frac{e\eta}{h\nu_0} \sum_i R_R R_S(z_{S_i}) \int_0^\infty \exp\left(-4 \ln(2) \left(\frac{k - k_0}{\Delta k_{\text{FWHM}}}\right)^2\right) \\
 & \quad \cdot \cos(2k(n_S z_{S_i} - z_R)) dk .
 \end{aligned}$$

Here, we have substituted  $S(k)$  by its expression in Eq. (S7.41). The integral can be further evaluated via

$$\begin{aligned}
 & \int_0^\infty \exp\left(-4 \ln(2) \left(\frac{k - k_0}{\Delta k_{\text{FWHM}}}\right)^2\right) \cos(2k(n_S z_{S_i} - z_R)) dk \\
 &= \frac{1}{2} \int_0^\infty \exp\left(-4 \ln(2) \left(\frac{k - k_0}{\Delta k_{\text{FWHM}}}\right)^2\right) \left(e^{ik\Delta z_{S_i}} + e^{-ik\Delta z_{S_i}}\right) dk \\
 &= \frac{1}{4} \int_{-\infty}^{+\infty} \exp\left(-4 \ln(2) \left(\frac{k - k_0}{\Delta k_{\text{FWHM}}}\right)^2\right) \left(e^{ik\Delta z_{S_i}} + e^{-ik\Delta z_{S_i}}\right) dk \\
 &= \frac{1}{4} \sqrt{\frac{\pi}{\ln(2)}} \frac{\Delta k_{\text{FWHM}}}{2} \exp\left(-\frac{\Delta k_{\text{FWHM}}^2}{4 \ln(2)} \Delta z_{S_i}^2\right) \cdot \left(e^{ik_0 \Delta z_{S_i}} + e^{-ik_0 \Delta z_{S_i}}\right) \\
 &= \frac{1}{2} S_0 \exp\left(-\frac{\Delta k_{\text{FWHM}}^2}{4 \ln(2)} \Delta z_{S_i}^2\right) \cos(k_0 \Delta z_{S_i}) ,
 \end{aligned}$$

where

$$\Delta z_{S_i} = 2(n_S z_{S_i} - z_R)$$

and

$$S_0 = \sqrt{\frac{\pi}{\ln(2)}} \frac{\Delta k_{\text{FWHM}}}{2} = \int_0^\infty S(k) dk .$$

$S_0$  represents the spectrally integrated power emitted by the light source. Finally, we thus obtain

$$\begin{aligned}
 I_{\text{TD}}(z_R) &= \frac{e\eta}{h\nu_0} (R_R^2 + R_{S_1}^2 + R_{S_2}^2 + \dots) S_0 \\
 & \quad + \frac{e\eta}{h\nu_0} \sum_i R_R R_S(z_{S_i}) S_0 \exp\left(-\frac{\Delta k_{\text{FWHM}}^2}{2 \ln(2)} (n_S z_{S_i} - z_R)^2\right) \\
 & \quad \cdot \cos(2k_0(n_S z_{S_i} - z_R)) .
 \end{aligned}$$

Next, we assume a single sample reflector at the position  $z_S$ . The photocurrent then becomes

$$I_{\text{TD}}(z_R) = \frac{e\eta}{h\nu_0} (T_R T_S) (R_R^2 + R_{S1}^2 + R_{S2}^2 + \dots) S_0 \\ + \frac{e\eta}{h\nu_0} (T_R T_S) R_R R_S S_0 \exp\left(-\frac{\Delta k_{\text{FWHM}}^2}{2 \ln(2)} (n_S z_{Si} - z_R)^2\right) \\ \cdot \cos[2k_0(n_S z_S - z_R)] .$$

Here, we have now taken into account that the sample and reference arms have different overall transmittances (losses and different beam splitter reflectances) which we describe again by field transmittances. The instantaneous power incident in the sample and reference arms is  $P_0 = S_0/2$ . The mean square peak power occurs at  $n_S z_S = z_R$  and equals

$$\langle I_{\text{TD}} \rangle^2 = \left(\frac{e\eta}{h\nu_0}\right)^2 (T_R T_S)^2 P_0^2 R_R^2 R_S^2 .$$

For shot noise-limited detection, the noise variance in an optical receiver is given by

$$\sigma_{\text{sh}}^2 = e \langle I_{\text{TD}} \rangle B = \frac{e^2 \eta}{h\nu_0} (T_R T_S) P_0 R_R^2 B$$

in which  $e$  is the electric charge,  $\langle I_{\text{TD}} \rangle$  the mean photo detector photocurrent, and  $B$  the electronic detection bandwidth. The signal-to-noise ratio for shot-limited detection is

$$\text{SNR}_{\text{TD-OCT}} = \frac{\langle I_{\text{TD}} \rangle^2}{\sigma_{\text{sh}}^2} = (T_R T_S) \frac{\eta}{h\nu_0 B} P_0 R_S^2 . \quad (\text{S7.43})$$

If we use intensity and transmittance quantities  $\mathcal{T} = T_R T_S$  and  $\mathcal{R}_S = R_S^2$  and a perfect 50:50 beam splitter, that is,  $\mathcal{T} = 1/4$ , we find

$$\text{SNR}_{\text{TD-OCT}} = \frac{\langle I_{\text{TD}} \rangle^2}{\sigma_{\text{sh}}^2} = \frac{\mathcal{T} \eta \mathcal{R}_S}{h\nu_0 B} P_0$$

#### b) Frequency-Domain OCT (FD-OCT):

The sample version of the spectral interferogram in FD-OCT systems is (cross-correlation term in Eq. (S7.40))

$$I_{\text{FD}}[k_n] = \frac{1}{2} \frac{e\eta}{h\nu_0} P[k_n] \\ \cdot \left[ R_R^2 + R_{S1}^2 + \dots + \sum_i R_R R_S(z_{Si}) [2 \cos(2k_n(n_S z_{Si} - z_R))] \right] . \quad (\text{S7.44})$$

Here,  $P[k_n] = S(k)|_{k=k_n}/2$  is that portion of the instantaneous power incident on the sample that corresponds to the  $n$ -th spectral channel of the spectrometer.

In this case, with discrete spectrometer channels, the inverse Fourier transform (IFT) operation is implemented as an inverse Discrete Fourier Transform (DFT) which reads

$$i_D[z_n] = \sum_{n=1}^N I_{FD}[k_n] e^{-ik_n z_n/N} .$$

In the case of a single sample reflector at the position  $z_S$  and a source with a Gaussian intensity spectrum, the peak value of  $I_{FD}[k_n]$  occurs when  $z_n = n_S z_S - z_R = 0$ . Therefore, we have

$$i_D[z_n = 0] = \frac{e\eta}{h\nu_0} R_R R_S \sum_{n=1}^N P[k_n] .$$

As we assume that each channel has equal power in it, we finally obtain

$$i_D[z_n = 0] = \frac{e\eta}{h\nu_0} R_R R_S N P[k_n] ,$$

where  $N$  is the maximum spectral channel number of the spectrometer. The sinusoidal spectral interference pattern in each separated detection channel from a single reflector adds coherently to give a peak signal power much greater than the signal power in each channel alone. The mean peak power is then

$$\langle i_D \rangle^2 = (i_D[z_n = 0])^2 = \left( \frac{e\eta}{h\nu_0} R_R R_S N P[k_n] \right)^2 .$$

In order to evaluate the SNR in FD-OCT, we have to generalize our interferogram signal described by Eq.(S7.44) by adding an uncorrelated Gaussian white noise term  $\alpha[k_n]$ .  $\alpha[k_n]$  has a zero mean value and a standard deviation  $\sigma[k_n]$ . Assuming  $R_R \gg R_S$  in the shot noise-limited detection, it follows that

$$\sigma^2[k_n] = \frac{e^2\eta}{h\nu_0} P[k_n] R_R^2 B_{FD} .$$

The noise in each spectral channel is uncorrelated. Thus, the noise variances add incoherently in the IFT to give

$$\sigma^2[z_n] = \sum_{n=1}^N \sigma^2[k_n] = \frac{e^2\eta}{h\nu_0} P[k_n] R_R^2 B_{FD} N .$$

Hence, we finally obtain the SNR of a FD-OCT

$$\text{SNR}_{FD-OCT} = \frac{\langle i_D \rangle^2}{\sigma^2[z_n]} = \frac{\eta}{h\nu_0} \frac{R_S}{B_{FD}} P[k_n] N . \quad (\text{S7.45})$$

**c) Evaluation of bandwidths  $B_{TD-OCT}$ ,  $B_{FD-OCT}$ , and  $B_{SS-OCT}$  :**

In *TD-OCT*, the reference arm scans over a depth range of  $z_{\max}$  during the A-scan

acquisition time  $\Delta t$  with velocity  $v = z_{\max}/\Delta t$ . The reference light frequency is Doppler shifted by

$$f_D = \frac{2v}{\lambda_0} = \frac{k_0 z_{\max}}{\pi \Delta t} .$$

The FWHM signal power bandwidth is  $\Delta f_D = \Delta k_{\text{FWHM}} z_{\max}/(\pi \Delta t)$ , and the optical detection bandwidth is thus

$$B_{\text{TD-OCT}} \approx 2 \frac{\Delta f_{\text{FWHM}} z_{\max}}{\pi \Delta t} . \quad (\text{S7.46})$$

For an *FD-OCT* system, where all spectral channels are illuminated and detected simultaneously, the power per spectral channel is the total power divided by the number of channels  $N$ , that is,  $I_{\text{FD}}[k_n] = P_0/N$ . This also holds for the detection bandwidth determined by

$$B_{\text{FD-OCT}} = \frac{B_{\text{TD-OCT}}}{N} \approx 2 \frac{\Delta f_{\text{FWHM}} z_{\max}}{N \pi \Delta t} . \quad (\text{S7.48})$$

This can also be understood by the fact that in *FD-OCT* the signals from each channel are integrated over the entire *A-scan* time. For an *SS-OCT* system, the allowable sample illumination power for each spectral channel is the same as the total illumination power in *TD-OCT*, since only one channel is illuminated at a given point in time. Thus,  $P_{\text{SS-OCT}}[k_n] = P_0$ . The detection bandwidth is *SS-OCT* is limited by an analog-to-digital sampling frequency

$$f_s = \frac{N}{\Delta t} = 2 \frac{\Delta f_{\text{FWHM}} z_{\max}}{\Delta t} .$$

When we assume a scanning range of  $\Delta k = 2\Delta k_{\text{FWHM}}$  and a detection bandwidth of  $B_{\text{SS-OCT}} = f_s/2$ , we find

$$B_{\text{SS-OCT}} = B_{\text{TD-OCT}} = 2 \frac{\Delta k_{\text{FWHM}} z_{\max}}{\pi \Delta t} . \quad (\text{S7.49})$$

From this, we find for the SNR of an *SS-OCT*

$$\text{SNR}_{\text{SS-OCT}} = \text{SNR}_{\text{FD-OCT}} = \frac{\eta}{h\nu_0} \frac{\mathcal{R}_S}{B_{\text{TD}}} P_0 N \quad (\text{S7.50})$$

After all, we find the simple relationship

$$\text{SNR}_{\text{FD-OCT}} = \text{SNR}_{\text{SS-OCT}} = \text{SNR}_{\text{TD-OCT}} ,$$

as discussed in Section 7.4.4. Please note that Eqs. (7.58) and (7.59) suggest an improvement of sensitivity by a factor of  $N$ . Due to the nature of the FFT, *FD-OCT* produces redundant data for positive and negative frequencies. Thus, the real improvement is only  $N/2$ . However, even a factor of  $N/2$  is too optimistic, as this would assume that the power is equal in each spectral channel (rectangular power spectrum). A more realistic Gaussian spectrum would reduce the sensitivity advantage by approximately another factor of 2.

**P7.11****Light sources for OCT**

1. What can be done to avoid any optical feedback from the Fresnel reflection of the fiber into which the SLD light should be coupled in?
2. Calculate from the spectrum in Table 7.4 the autocorrelation function and the OCT interference signal. Do a best fit to the spectrum by assuming a sum of two spectrally shifted Gaussian beams. What is the effect of the trough? How do the autocorrelation function and interference signal change if the trough becomes deeper? What can you say about the coherence length? Alternatively you may use numerical methods (FFT) to simulate the influence of the shape of the spectrum on autocorrelation function and interference signal.
3. Calculate numerically and assume as Gaussian fit from the spectra in Figure 7.20 the autocorrelation functions and the OCT interference signals. What is the difference between the numerical result and the Gaussian approximation? Why does the autocorrelation function of the SLD exhibit side lobes?

**Solution:**

1. The geometry of the SLD has to be chosen such that one can avoid any optical feedback from the Fresnel reflection of the fiber end facets. We distinguish between two main options:

- “Angled” SLD, where the active waveguide is tilted versus the SLD crystal facet.
- “Ends” SLD, where the ends of the SLD active region are followed by a relatively long “transparent window” region and/or “integrated” absorbing region on the backside of SLD waveguide.

All modern SLDs are based either on the “angled” or “transparent window” or “integrated absorber” approach, or on their combination.

2. Let us simulate the autocorrelation function and the OCT interference spectrum. For this purpose, we assume the intensity spectrum to be the sum of two shifted Gaussian-shaped spectra. The total intensity spectrum is defined as

$$\sigma(\omega) = \sigma_{01} \exp\left(-4 \ln(2) \left(\frac{\omega - \omega_{01}}{\Delta\omega_1}\right)^2\right) + \sigma_{02} \exp\left(-4 \ln(2) \left(\frac{\omega - \omega_{02}}{\Delta\omega_2}\right)^2\right) \quad (\text{S7.51})$$

in which  $\omega = 2\pi c/\lambda$  is the angular frequency. The simulated spectrum shown in Figure S7.29 has been obtained by applying the following MATLAB code:

---

```
% unit lengths are in millimeter
c = 3e14; % Speed of light (mm/s)
Npoints = 2^10; % Number of channels
```

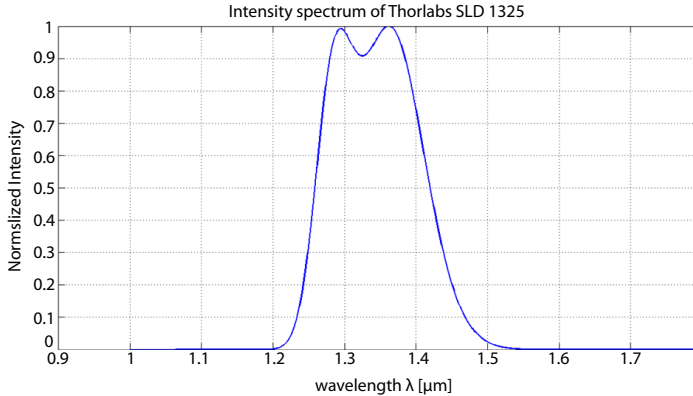


Figure S7.29 Intensity spectrum of the Thorlabs SLD 1325

```

wl_min = 1.0; % Minimum wavelength value
wl_max = 1.9; % Maximum wavelength value
wl_range = (wl_min:(wl_max-wl_min)/(Npoints - 1):wl_max)
; % Wavelength range
Omega_range = 2*pi*c./wl_range; wlo = 1.325; % Angular
frequency range: omega
delwl_01 = 65e-3; % FWHM of the first Gaussian fitting
spectrum
wl_o1 = wlo - 40e-3; % Centred angular frequency of the
first fitting
delwl_02 = 100e-3; % FWHM of the second Gaussian fitting
spectrum
wl_o2 = wlo + 40e-3; % Centred angular frequency of the
second fitting
Z2max = Npoints/2*wlo^2/(wl_max - wl_min); % Maximum Z
depth: 2*Zmax
delay_range = -Z2max:2*Z2max/(Npoints-1):Z2max; % Depth
range -2Zmax - 2Zmax
delomg_01 = 2*pi*c./wlo^2*delwl_01; % First angular
frequency FWHM range
Omega_o1 = 2*pi*c./wl_o1; % First centred angular
frequency
delomg_02 = 2*pi*c./wlo^2*delwl_02; % Second angular
frequency FWHM range
Omega_o2 = 2*pi*c./wl_o2; % Second centred angular
frequency
S1 = exp(-4*log(2)/delomg_01^2.*(Omega_range - Omega_o1)
.^2);
S2 = 1.25*exp(-4*log(2)/delomg_02^2.*(Omega_range -
Omega_o2).^2);
S = (S1+S2);
plot(wl_range, S/(max(S)-min(S)));

```

The autocorrelation function is defined as the inverse Fourier transform of the intensity spectrum, that is,

$$\begin{aligned} \mathcal{G}(\Delta t) &= \int_{-\infty}^{+\infty} \sigma(\omega) e^{-i\omega\Delta t} d\omega \\ &= \sigma_{01} \int \exp\left(-4 \ln(2) \left(\frac{\omega - \omega_{01}}{\Delta\omega_1}\right)^2\right) e^{-i\omega\Delta t} d\omega \\ &\quad + \sigma_{02} \int_{-\infty}^{+\infty} \exp\left(-4 \ln(2) \left(\frac{\omega - \omega_{02}}{\Delta\omega_2}\right)^2\right) e^{-i\omega\Delta t} d\omega . \end{aligned} \quad (\text{S7.52})$$

We now evaluate the first integral of Eq.(S7.52):

$$\begin{aligned} &\int_{-\infty}^{+\infty} \exp\left(-4 \ln(2) \left(\frac{\omega - \omega_{01}}{\Delta\omega_1}\right)^2\right) e^{-i\omega\Delta t} d\omega \\ &= e^{-i\omega_{01}\Delta t} \exp\left(-\frac{\Delta\omega_{01}^2}{16 \ln(2)} \Delta t^2\right) \int_{-\infty}^{+\infty} \exp\left(-\frac{4 \ln(2)}{\Delta\omega_{01}^2} \left(\chi + \frac{i\Delta t}{\sin(2)} \Delta\omega_{01}^2\right)^2\right) d\chi \\ &= \sqrt{\frac{\pi}{\ln(2)}} \frac{\Delta\omega_{01}}{2} e^{-i\omega_{01}\Delta t} \exp\left(-\frac{\Delta\omega_{01}^2}{16 \ln(2)} \Delta t^2\right) . \end{aligned} \quad (\text{S7.53})$$

By substituting Eq. (S7.53) into Eq. (S7.52), we obtain the autocorrelation function

$$\begin{aligned} \mathcal{G}(\Delta t) &= \sigma_{01} \sqrt{\frac{\pi}{\ln(2)}} \frac{\Delta\omega_{01}}{2} e^{-i\omega_{01}\Delta t} \exp\left(-\frac{\Delta\omega_{01}^2}{16 \ln(2)} \Delta t^2\right) \\ &\quad + \sigma_{02} \sqrt{\frac{\pi}{\ln(2)}} \frac{\Delta\omega_{02}}{2} e^{-i\omega_{02}\Delta t} \exp\left(-\frac{\Delta\omega_{02}^2}{16 \ln(2)} \Delta t^2\right) , \end{aligned} \quad (\text{S7.54})$$

which has a complex value. As a consequence, it can be written as

$$\mathcal{G}(\Delta t) = a + ib$$

The envelope of  $\mathcal{G}(\Delta t)$  is known as the autocorrelation function, that is,  $\text{ENV} = |\mathcal{G}(\Delta t)|$ . The interference spectrum is then given by

$$\text{INT} = \text{ENV} \cdot \cos\left[\arctan\left(\frac{b}{a}\right)\right] . \quad (\text{S7.55})$$

The following MATLAB code illustrates the corresponding evaluations:

---

```
% Autocorrelation function and interference spectrum
IFT_S = fftshift( ifft(S) ); % SLD 1325
Envelop_g = abs(IFT_S); % autocorrelation function
The_phase = angle(IFT_S); % phase of the interference
          signal
Interf_signal = (Envelop_g / (max(Envelop_g) - min(Envelop_g)
          )) .* cos(The_phase); % interference spectrum
```

---

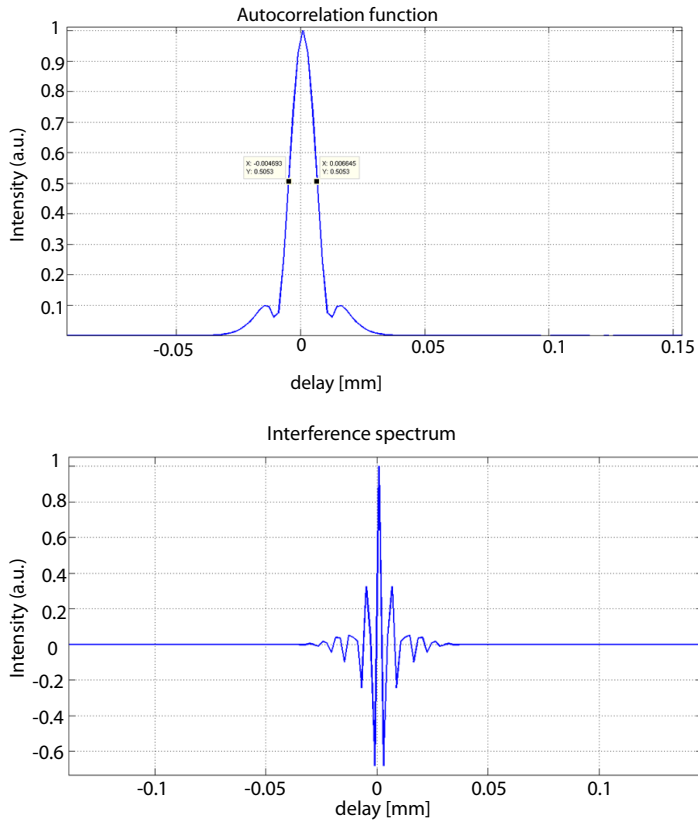


**Figure S7.30** (a) Autocorrelation envelope. (b) Intensity spectrum.

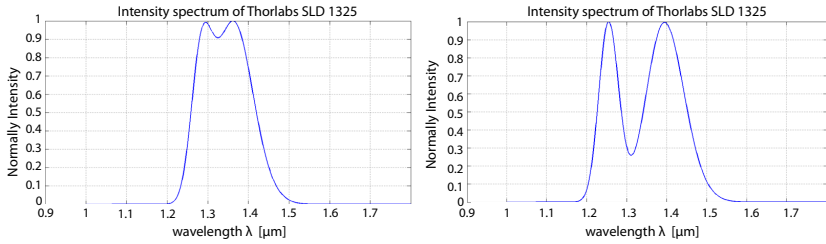


**Figure S7.31** Comparison of two intensity spectra. (a) Small trough with  $\sigma_{01} = 1.0$  and  $\sigma_{02} = 1.25$ . (b) Large trough with  $\sigma_{01} = \sigma_{02} = 1$ . Here, the following data were used:  $\text{delwl\_01} = 65\text{e-}3$ ,  $\text{delwl\_02} = 100\text{e-}3$ ,  $\text{wl\_01} = \text{wlo} - 70\text{e-}3$ , and  $\text{wl\_02} = \text{wlo} + 70\text{e-}3$ .

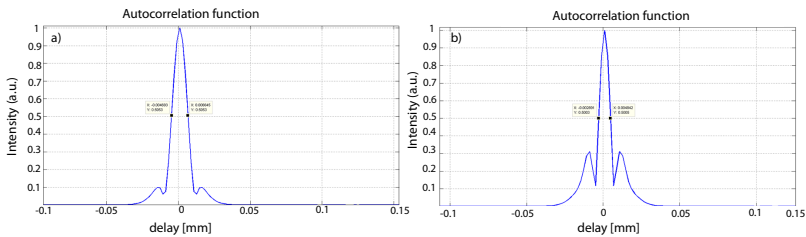


**Figure S7.32** Envelopes for (a) a small and (b) a large trough.

In Figures (S7.30) and (S7.31), the autocorrelation envelope and the intensity spectrum are shown, respectively. Figures (S7.31) – (S7.33) compare the intensity spectra, envelopes, and interference spectra for small and large troughs. In conclusion, the autocorrelation function sidelobes become larger for an increasing trough. In addition, the interference spectrum presents more sidelobes in the case of a large trough. Due to the overall broadened spectrum, however, the coherence length decreases. Thus, the overall broadening compensates “the trough effect”, which means that it is useful to use such diodes in OCT applications.

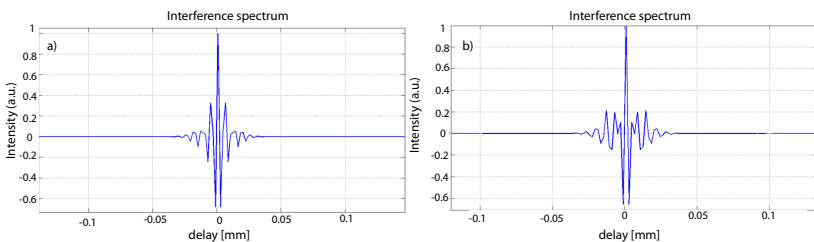


**Figure S7.33** Interference spectra for (a) a small and (b) a large trough.

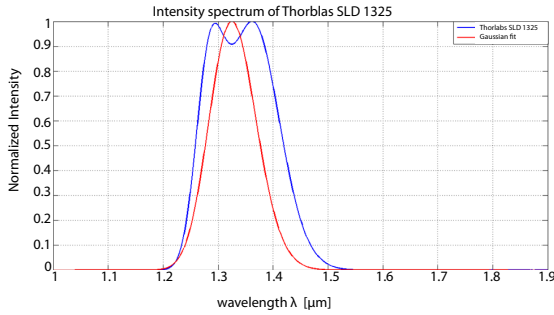


**Figure S7.34** Intensity spectrum of the Thorlabs SLD 1325 (blue) and a Gaussian shape fit (red).

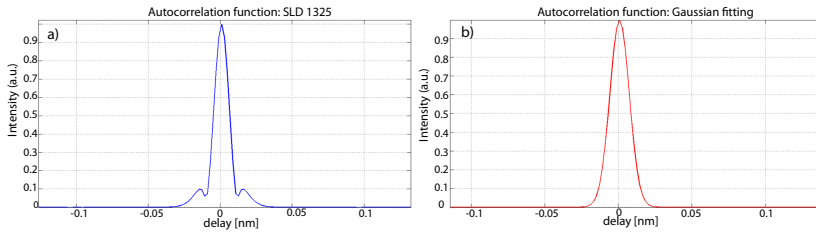


**Figure S7.35** Autocorrelation function of (a) the Thorlabs 1325 SLD and (b) a Gaussian function.

3. Now we want to compare the Thorlabs SLD 1325 (spectrum shown in Figure S7.34) with a Gaussian-shaped spectrum. From Figures (S7.35) and (S7.36) we can conclude that the autocorrelation function of the Thorlabs 1325 exhibits pronounced sidelobes due to its non-Gaussian spectrum.

**P7.12**  
**Optical and acoustic biometry**

Show that the correlation displayed in Figure 7.36b follows directly from Figure 7.36a. Estimate the slope of the correlation curve.

**Solution:**

From Figure S7.37, we can derive the relationship between  $L'_{eye,opt}$  and  $L_{eye,ac}$ . We have

$$L'_{eye,opt} = \frac{L_{eye,ac}}{\cos \kappa} .$$

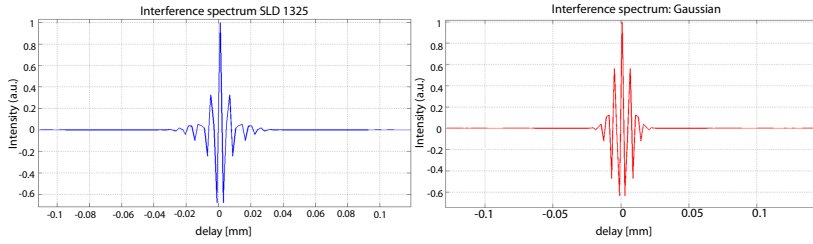


**Figure S7.36** Interference spectrum of (a) the Thorlabs 1325 SLD and (b) the Gaussian spectrum for comparison.

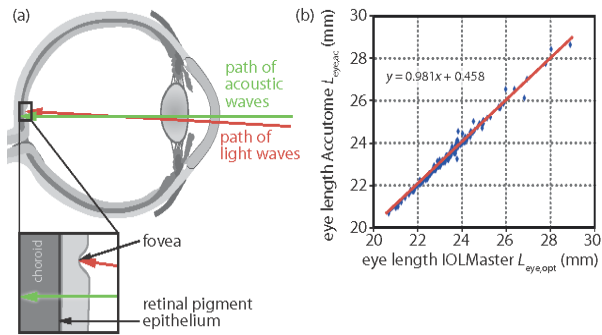


**Figure 7.36** (a) Axial eye lengths as measured by optical and acoustical biometry and (b) their correlation.

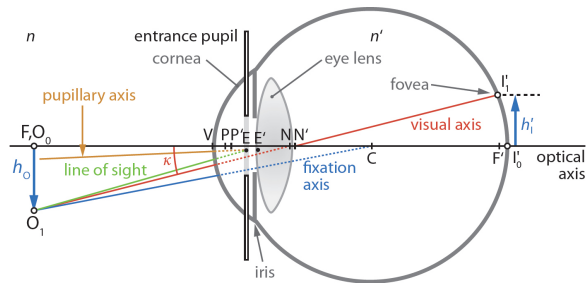


**Figure S7.37** Axis and cardinal points of the eye.

With  $\kappa = 5^\circ$ , we find

$$L_{\text{eye,ac}} = 0.996 \cdot L'_{\text{eye,opt}} .$$

The actual value of  $L_{\text{eye,opt}}$  measured by an optical biometer is even larger than the distance displayed in Figure 7.36b because of two reasons:

1. The optical A-scan is aligned to the fovea, adding the depth of the retinal pit to the measured length.
2. The strongest optical backscattering signal comes from the retinal pigment epithelium (RPE), whereas an ultrasound A-scan detects the inner limiting membrane (ILM). This adds the retinal distance at the center of the fovea to the optically measured length.

When the axial length of the simplified Gullstrand eye are used and a total contribution of  $250 \mu\text{m}$  from both effects is assumed, we can introduce a corresponding correction factor

$$L'_{\text{eye,opt}} = \frac{23.896}{24.146} L_{\text{eye,opt}} .$$

In summary, we thus find

$$L_{\text{eye,ac}} = 0.986 L_{\text{eye,opt}} .$$

As discussed in Section 7.7.2, optical biometers are typically calibrated to agree with high-precision ultrasound measurements<sup>16)</sup>. Hence, the output of a commercial optical biometer would ideally yield the same result as a perfectly calibrated ultrasound device. Systematic differences such as the one shown between the commercial biometry devices ZEISS IOLMaster and Accutome A-Scan Plus can be attributed to a number of factors:

- Ultrasound biometers have to be calibrated against a reference normal. Not all commercial ultrasound devices agree perfectly with each other when measured versus the same normal.
- The retinal shape and thickness vary as a function of axial length. Differences in the relative lengths of the axial segments (cornea, aqueous humor, lens, vitreous) also affect the average refractive index (and velocity of sound). A linear fit between optical and ultrasound axial length measurements is thus only an empirical approximation.
- For a given axial length, retinal shape and thickness vary between subjects, depending, e.g., on age and ethnicity and thus show a distribution about a mean value. In addition, they can be affected by conditions such as staphyloma or macular edema. The result of any calibration can thereby depend on the subject population of the clinical study.

16) Haigis, W., Lege, B., Miller, N., and Schneider, B. (2000) Comparison of immersion ultrasound biometry and partial coherence interferometry for intraocular lens calculation according to Haigis, *Graefe's Arch. Clin. Exp. Ophthalmol.*, **238**, 765–773.

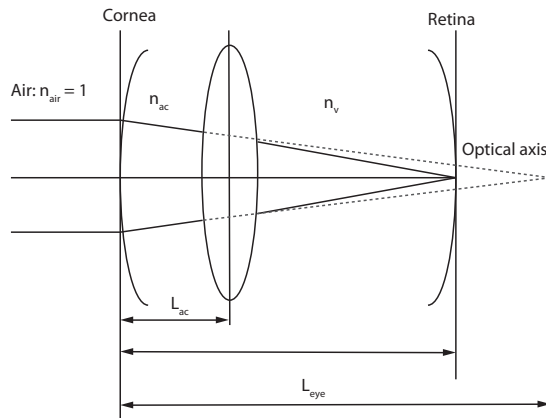


Figure S7.38 Simplified eye model used in Problem P7.13.

### P7.13

#### Intraocular lens formula

Derive the IOL formula (7.64) from the model shown in Figure 7.39. How does the calculation change if we use a more elaborated model, in particular, if both cornea and lens are treated as thick lenses.

#### Solution:

For the derivation of the intraocular lens (IOL) formula, we use the simplified eye model shown in Figure S7.38.

#### Step 1:

Determination of the image formation of an object at optical infinity which is imaged by the cornea. The cornea is assumed to be a thin lens. Equation (A14) yields

$$\frac{n_{\text{air}}}{s} + \mathcal{D}'_{c1} = \frac{n_{\text{ac}}}{s'}$$

where  $s$  and  $s'$  are the object distances from the first and back corneal surface, respectively.  $\mathcal{D}'_{c1}$  denotes the corneal optical power.  $n_{\text{air}}$  and  $n_{\text{ac}}$  are the refractive indices of air and the anterior chamber, respectively. In the case of emmetropia,  $s$  tends to infinity. Therefore,  $s' = n_{\text{ac}}/\mathcal{D}'_{c1}$ .

#### Step 2:

Next, we determine the effect of the IOL power. As the image location is known

(location on the retina), we can use Eq. (A14) once again and obtain

$$\frac{n_{ac}}{s' - L_{ac}} + \mathcal{D}'_1 = \frac{n_v}{L_{eye} - L_{ac}} .$$

Here,  $n_v$  is the refractive index of the vitreous. After re-arranging this equation, the IOL power necessary to achieve emmetropia follows to

$$\mathcal{D}'_1 = \frac{n_v}{L_{eye} - L_{ac}} - \frac{n_{ac}}{n_{ac}/\mathcal{D}'_{ac} - L_{ac}} . \quad (S7.56)$$

In the case of a “thick” cornea, the corneal total refractive power is given by Eq. (2.20), that is,

$$\mathcal{D}'_c = \mathcal{D}'_a + \mathcal{D}'_p - \frac{L_c}{n_c} \mathcal{D}'_a \mathcal{D}'_p ,$$

where  $\mathcal{D}'_a$  and  $\mathcal{D}'_p$  denote the refractive power of the corneal front and back surfaces, respectively.  $n_c$  and  $L_c$  are the refractive index and the thickness of the cornea. Hence, Eq. (S7.56) will be modified by replacing  $\mathcal{D}'_{c1}$  by the total corneal total refractive power  $\mathcal{D}'_c$ .

## P7.14

### Intraocular lens power determination with biometry

Estimate the uncertainties in the determination of the IOL power which result from uncertainties in the measurement of the biometric parameters:

1. eye length uncertainty: 10  $\mu\text{m}$  and 50  $\mu\text{m}$
2. uncertainty of the anterior chamber depth: 10  $\mu\text{m}$  and 50  $\mu\text{m}$
3. corneal radius

Which other factors influence the calculated power of an IOL?

### Solution:

1. In Problem P7.13, we derived

$$\mathcal{D}'_1(L_{eye}) = \frac{n_v}{L_{eye} - L_{ac}} - \frac{n_{ac}}{n_{ac}/\mathcal{D}'_{c1} - L_{ac}} .$$

The uncertainty to be considered is the eye length  $L_{eye}$ . Therefore, the uncertainty formula is obtained by differentiation with respect to  $L_{eye}$ . We have

$$\begin{aligned} \Delta \mathcal{D}'_1 &= \left| \frac{d\mathcal{D}'_1}{dL_{eye}} \right| \Delta L_{eye} , \text{ with} \\ \frac{d\mathcal{D}'_1}{dL_{eye}} &= -\frac{n_v}{(L_{eye} - L_{ac})^2} \text{ and} \\ \Delta \mathcal{D}'_1 &= \frac{n_v}{(L_{eye} - L_{ac})^2} \Delta L_{eye} . \end{aligned}$$

For the parameters of the Gullstrand Eye #1 for relaxed vision (Table 2.1) and  $\Delta L_{eye} = 10 \mu\text{m}$ ,  $50 \mu\text{m}$ , we obtain

$$\Delta \mathcal{D}'_1 = 0.03 \dots 0.16 \text{ D} .$$

2. Now, the IOL power is a function of  $L_{ac}$ , and the corresponding uncertainty is

$$\Delta \mathcal{D}'_1 = \left| \frac{d\Delta \mathcal{D}'_1}{dL_{ac}} \right| \Delta L_{ac} = \left| \frac{n_v}{(L_{eye} - L_{ac})^2} - \frac{n_{ac}}{(n_{ac}/\mathcal{D}'_1 - L_{ac})^2} \right| \Delta L_{ac} .$$

For the parameters of the Gullstrand Eye #1 for relaxed vision (Table 2.1) and  $\Delta L_{ac} = 10 \mu\text{m}$ ,  $50 \mu\text{m}$ , we find

$$\Delta \mathcal{D}'_1 = 0.013 \dots 0.066 \text{ D} .$$

3. We assume the corneal refractive power given by Eq. (7.62), that is,

$$\mathcal{D}'_{c1} = \frac{0.3315}{r_{c1}} .$$

This yields

$$\mathcal{D}'_1(r_{c1}) = \frac{n_v}{L_{eye} - L_{ac}} - \frac{n_{ac}}{\frac{n_{ac}}{0.3315} r_{c1} - L_{ac}} .$$

The uncertainty in  $\mathcal{D}'_1$  is then obtained by applying the same concept as before, but now with respect to  $r_{c1}$ . We then obtain

$$\Delta \mathcal{D}'_1 = \left| \frac{d\mathcal{D}'_1}{dr_{c1}} \right| \Delta r_{c1} = \left| \frac{n_{ac}}{0.3315} \cdot \frac{n_{ac}}{\left(\frac{n_{ac}}{0.3315} r_{c1} - L_{ac}\right)^2} \right| \Delta r_{c1} .$$

For the parameters of the Gullstrand Eye # 1 for relaxed vision (Table 2.1) and  $\Delta r_{c1} = 0.02r_{c1}$ ,  $0.1r_{c1}$ , we get

$$\Delta \mathcal{D}'_1 = 1.1 \dots 5.5 \text{ D} .$$

This error seems to be the right order of magnitude, given a corneal power in the Gullstrand model of 43 D. It is quite significant, which demonstrates that the corneal radius measurement accuracy has a significant influence on the overall accuracy of the IOL power measurement. Additional factors which influence the calculated power of an IOL are

- the difference between measured anterior chamber depth before surgery and effective lens position (ELP) of the implanted IOL after surgery. A number of factors contribute to this, that is,
  - the axial location of the lens equator of the (cataractous) crystalline lens relative to its anterior apex,
  - the location of the IOL after surgery relative to the equator of the capsular bag (depends, e.g., on IOL haptic design and capsular bag shrinkage), and
  - the location of the IOL's principal planes relative to its equator (depends on the lens design and even varies with IOL power for a given IOL type).
- the uncertainty in the corneal thickness.
- the individual deviations from the (population) mean in the corneal front and back surface radii (i.e., individual deviation from the ideal Gullstrand ratio).

**P7.15****Polarization-sensitive OCT**

Describe the measurement concept of PS-OCT and sketch the calculation (simulation) of an FD-signal as a function of the depolarization of a sample. Assume a simple model for the retinal pigment epithelium consisting of two layers with different depolarization behavior.

**Solution:**

In polarization-sensitive OCT (Figure 7.41), we have basically two OCT signals coming back from the signal arm, namely one for each polarization state. The general theories for TD-OCT or FD-OCT thus apply for each polarization state separately. For the simulation, we refer to Problem P7.7. The algorithm presented there can be used without any changes. One just has to calculate the spectrum and the Fast Fourier Transform (FFT) for each polarization channel separately.

**P7.16****Doppler OCT**

Describe the measurement principle of DOCT and calculate (simulate) the FD-signal as a function of the blood flow of a sample. Assume a simple model consisting of a layer in which blood flows at an angle of  $45^\circ$  with a velocity of  $v$  below a layer of scattering tissue.

**Solution:**

Doppler OCT is based on OCT combined with laser Doppler flowmetry (LDF) and permits the quantitative imaging of fluid flow in highly scattering media, such as monitoring *in-vivo* blood beneath the skin. When light from a moving particle interferes with the reference beam, a Doppler frequency shift occurs in the interference fringe which is given by

$$\Delta\nu_{\text{Doppler}} = \frac{1}{2\pi}(\mathbf{k}_s - \mathbf{k}_i) \cdot \mathbf{v} . \quad (\text{S7.57})$$

$\mathbf{k}_i$  and  $\mathbf{k}_s$  are the wave vectors of the incoming and scattered light, respectively.  $\mathbf{v}$  is the velocity vector of the moving particle. Since Doppler OCT measures the backscattered light, we assume the angle between the flow and sampling beams to be  $\theta$ . The Doppler shift equation (S7.57) is then simplified by

$$\Delta\nu_{\text{Doppler}} = \frac{2v \cos \theta}{\lambda_0} .$$

The optical system of Doppler OCT is similar to that of OCT. However, the signal processing is different. Following the FD-OCT calculation in Section 7.4, the component optical field at the detector after reflection from the reference arm is

$$\psi_R(\omega, k) = \psi_{R,0}(\omega) R_R e^{2ik(z_R+z_d)} e^{-i\omega t} .$$

The component optical field at the detector after reflection/backscattering from the sample arm is

$$\psi_S(\omega, k) = \psi_{S,0}(\omega) \int_{-\infty}^{+\infty} R_S(z_S) e^{2ik(z_S+z_d)} e^{-i\omega t} dz_S ,$$

where  $z_R$ ,  $z_S$ , and  $z_d$  are the geometrical length of the reference, sample, and detector arms, respectively.  $R_R$  and  $R_S$  are the amplitude reflection coefficients of light which is reflected/backscattered from the reference and sample arms, respectively. The FD-OCT intensity is calculated according to

$$\begin{aligned} I_{FD}(k) = S(k)R_R^2 + S(k) \left| \int_{-\infty}^{+\infty} R_S(z_S) e^{2ik(n_S z_S)} dz_S \right|^2 \\ + 2S(k)R_R \int_{-\infty}^{+\infty} R_S(z_S) \cos(2k \Delta z) dz_S , \end{aligned} \quad (7.45)$$

where  $S(k) = |\psi_{0,R}(\omega)|^2 = |\psi_{0,S}(\omega)|^2$  is the power spectral density of the low coherent light source and  $\Delta z = n_S z_S - z_R$  the optical path difference between the light in the sample and reference arms. The last term of Eq. (7.45) encodes the backscattering amplitude information of the sample.

When a moving object passes through the sample volume, an additional phase  $2\pi \Delta \nu_{\text{Doppler}} t = 2\pi n_S (k_S - k_i) vt = 2n_S k v t \cos \theta$  exists which adds to the stationary phase shift  $\Delta z$ . Here,  $n_S$  and  $v$  denote the refractive index of the sample and the speed of the moving object, respectively. Therefore, the spectral domain interference fringe signal, which is the third term in the above Eq.(7.45), becomes

$$I_{\text{DOCT}}(k) = 2S(k)R_R \int_{-\infty}^{+\infty} R_S(z_S) \cos(2k(\Delta z + 2n_S v \cos \theta t)) dz_S . \quad (S7.58)$$

Let us now assume a simple model of the sample which has a single layer beneath which the blood flows at an angle of  $\theta = 45^\circ$  with a velocity  $v$ . We also assume  $R_S(z_S) = R_S \delta(z_{S,0} - z_S)$ . Therefore, we have

$$I_{\text{DOCT}}(k) = 2S(k)R_R R_S \cos(2k(\Delta z + 2n_S v \cos \theta t)) . \quad (S7.59)$$

With  $\Delta z = n_S z_{S,0} - z_R$ , an inverse Fourier transform of the term in the brackets in Eq. (S7.59) gives a complex signal  $I(\Delta z)$ , containing the amplitude and phase

information of the interference signal in time domain, that is,

$$I(\Delta z) = |I(\Delta z)| e^{i\varphi(\Delta z) + 2\pi i \Delta\nu_{\text{Doppler}} t} .$$

The equivalent phase shift due to the moving object will introduce a phase change  $2\pi \Delta\nu_{\text{Doppler}} t$ , on  $I(\Delta z)$ , which is the Doppler effect. The corresponding Doppler shift can be determined by comparing the phases between two complex signals  $I(\Delta z)$  during two exposures at a same location, namely the phase change is recorded by the product of  $I_{j,T}(\Delta z)$  and  $I_{(j+1),T}^*(\Delta z)$ , where  $*$  denotes the conjugate operation and  $T$  is the time interval between two exposures and determines the A-line scanning rate. With these definitions, it follows that

$$\begin{aligned} I_{j,T}(\Delta z) &= |I(\Delta z)| e^{i\varphi(\Delta z) + 2\pi i \Delta\nu_{\text{Doppler}} jT} , \\ I_{(j+1),T}(\Delta z) &= |I(\Delta z)| e^{i\varphi(\Delta z) + 2\pi i \Delta\nu_{\text{Doppler}} (j+1)T} \\ &= I_{j,T}(\Delta z) e^{2\pi i \Delta\nu_{\text{Doppler}} T} , \\ I_{j,T}(\Delta z) \cdot I_{(j+1),T}^*(\Delta z) &= |I(\Delta z)|^2 e^{-2\pi i \Delta\nu_{\text{Doppler}} T} . \end{aligned}$$

The Doppler shift is obtained using

$$\Delta\nu_{\text{Doppler}} = \frac{\Delta\varphi}{2\pi T} = \frac{1}{2\pi T} \arg \left[ \frac{1}{N-1} \sum_{j=1}^{N-1} I_{j,T}(\Delta z) \cdot I_{(j+1),T}^*(\Delta z) \right] , \quad (\text{S7.60})$$

with the number of A-scan measurements used for averaging  $N$ .  $T$  is the time duration between A-scans, that is, it determines the imaging speed and the Doppler frequency shift range, namely the velocity dynamic range because  $\Delta\varphi$  can only be correctly traced between  $-\pi$  and  $\pi$ .

## P7.17

### Spectroscopic OCT

Describe the idea of a measurement concept for spectroscopic OCT and sketch the calculation of the corresponding FD-signal as a function of the diameter of a strongly absorbing pigment sphere located inside scattering tissue of approximately the same refractive index and with equal backscattering properties.

#### Solution:

For spectroscopic OCT (wavelength-dependent OCT), the general theory as outlined in Section 7.4.2. has to be modified. In Eq. (7.45), we have assumed that  $R_S(z_S)$  is independent of  $\omega$  or  $k$  which allowed the spectral density function of the light source

to factor from the depth-dependent integral over the backscattering function  $R_S(z_S)$ . In a backscattering geometry with spectral dependence (absorption, scattering), both amplitude and phase changes of the backscattering function  $R_S(z_S, \omega)$  depend on the depth. Thus,  $R_S(z, \omega)$  becomes complex, and we have to write

$$R_S(z, \omega) = |R_S(z, \omega)| e^{i\theta(z, \omega)} .$$

From literature ([2] in Chapter 7), we find

$$|R_S(z, \omega)| = \frac{\sigma_b(z, \omega)}{z^2} \exp \left( -2 \int_0^z \mu_a(z', \omega') dz' \right) \quad (\text{S7.61})$$

and

$$\theta(z, \omega) = 2k_0 \int_0^z (n(z', \omega) - 1) dz' = 2 \int_0^z (k(\omega) - k_0) dz' . \quad (\text{S7.62})$$

In most applications, Eq. (S7.62) is a nearly constant term with respect to  $\omega$  in tissue so that it is sufficient to consider Eq. (S7.61).